# Metallothionein expression in tissues of rotenone-treated rats

By

**JUDEY PRETORIUS, B.Sc. HONS.**

Dissertation submitted for the degree Magister Scientiae (M.Sc.) in Biochemistry at the North-West University

**Supervisor:** **Professor Francois van der Westhuizen**
School for Biochemistry, North-West University
(Potchefstroom Campus)

**Co-Supervisor:** **Professor Antonel Olckers**
Centre for Genome Research, North-West University
(Potchefstroom Campus)

**2006**
**Potchefstroom**

# Metallothionein uitdrukking in weefsel van rotenoon-behandelde rotte

Deur

**JUDEY PRETORIUS, B.Sc. HONS.**

Verhandeling voorgelê vir die graad Magister Scientiae (M.Sc.) in Biochemie aan die Noordwes-Universiteit

**Studieleier:** **Professor Francois van der Westhuizen**
Skool vir Biochemie, Noordwes-Universiteit
(Potchefstroom Kampus)

**Medestudieleier:** **Professor Antonel Olckers**
Sentrum vir Genomiese Navorsing, Noordwes-Universiteit
(Potchefstroom Kampus)

**2006**
**Potchefstroom**

This dissertation is dedicated to God, Who has been gracious, loving, sovereign and in ultimate control throughout my whole life!

*Do not believe in anything simply because you have heard it.*
*Do not believe in anything simply because it is spoken and rumoured by many.*
*Do not believe in anything simply because it is found written in your religious books.*
*Do not believe in anything merely on the authority of your teachers and elders.*
*Do not believe in traditions because they have been handed down for many generations.*
*But after observation and analysis, when you find that anything agrees with reason and is conducive to the good and benefit of one and all, then accept it and live up to it.*
*- Buddha*

# Abstract

Mitochondrial NADH:ubiquinone oxidoreductase (complex I) carries out a number of well defined functions required for cell physiology. Deficiencies of complex I lead to multi-system disorders that include several well-known phenotypes such as type 2 diabetes mellitus, Alzheimer's disease as well as less known phenotypes such as MELAS, Leigh syndrome and MERRF. It was recently identified that ROS sensitive proteins known as metallothioneins (MTs), are over-expressed in complex I deficient cell lines and that these proteins have a protective effect against ROS related pathologies. It is still not clear if isoform-specific MT expression occurs in this disease and if it plays a significant role *in vivo*. This study investigated the expression of different MT isoforms in rotenone-treated Sprague Dawley rats, an *in vivo* model that has been used to study cellular biological responses of mitochondrial complex I deficiency.

The hypothesis of this study states that a rotenone-induced complex I deficiency would lead to an increase of MT mRNA expression *in vivo*. The specific aim was to determine the relative mRNA expression levels of the three main MT isoforms in rotenone-treated rat tissues. Real-time PCR was used to achieve this aim. In this dissertation the differential expression of MT-1, MT-2 and the brain specific isoform, MT-3 in brain, liver, heart- and skeletal muscle tissues of rotenone-treated Sprague Dawley rats is described.

The results indicate that MT-1 expression is significantly increased in the liver as well as, but to a lesser extent, in the brain and heart muscle. MT-1 expression in skeletal muscle was not detected. In contrast, significant increases in expression were observed for MT-2 in all the tissue types with an approximate two-fold increase at the highest rotenone dosage in liver, brain and heart muscle. Skeletal muscle had the smallest increase. For MT-3, no detectable levels of expression could be observed in skeletal and heart muscle. Surprisingly, levels of expression occurred in the liver which slightly (43%), but significantly increased at the highest rotenone dose. As expected, much higher relative levels of MT-3 expression were observed in brain

tissue with a more pronounced increase (almost two-fold) at the highest rotenone dose.

As the hypothesis of this study proposed, the *in vivo* data generated from this study supports the published *in vitro* data which showed that a rotenone-induced complex I deficiency results in MT expression. This over expression may contribute to a protected effect on the pathology of this disease although this still needs to be established. Furthermore, the results of this study show that the expression of the various MT isoforms in rotenone-treated rat tissues is not expressed in a similar way to the induced deficiency which may point to a differential regulation and response of the three MT isoforms to such a deficiency.

# Uittreksel

Mitochondriale NADH:ubikinoon oksidoreduktase (kompleks I) is verantwoodelik vir verskeie gespesialiseerde funksies wat vir selfisiologie noodsaaklik is. Defekte van kompleks I lei tot multi-sisteem defekte wat verskeie bekende fenotipes insluit, soos byvoorbeeld tipe 2 diabetes mellitus, Alzheimer se siekte asook minder bekende fenotipes soos MELAS, Leigh sindroom en MERFF. Dit is onlangs geïdentifiseer dat ooruitdrukking van ROS-sensitiewe proteïene, metallothioneine (MT), in kompleks I defektiewe sel lyne plaasvind en 'n beskermende effek teen ROS-verwante patologie tot gevolg het. Dit is nog onduidelik of isoform-spesifieke uitdrukking van MT in hierdie siekte voorkom en of dit 'n beduidende rol speel *in vivo*. In hierdie studie is die uitdrukking van verkillende MT-isoforme in rotenoon-behandelde Sprague Dawley rotte ondersoek. Hierdie model is 'n *in vivo* model wat gebruik kan word om selbiologiese response van mitochondriale kompleks I-defekte te bestudeer.

Die hipotese van die studie stel dat 'n rotenoon-geïnduseerde kompleks I-defek tot 'n verhoging van MT mRNA uitdrukking *in vivo* sal lei. Die spesifieke doel was om die relatiewe vlakke van mRNA uitdrukking van die drie MT-isoforme in weefsel van rotenoon-behandelde rotte te bepaal. Om dit te bereik, is van 'n kwantitatiewe polimerase ketting reaksie gebruik gemaak. In hierdie verhandeling word die weefsel-verskillende uitdrukking van MT-1 en MT-2, en die breinspesifieke isoform MT-3, in rotenoon behandelde brein, lewer, hart- en skeletspierweefsel van Sprague Dawley rotte beskryf.

Die resultate toon dat MT-1 beduidend uitgedruk word in die lewer asook maar tot in 'n mindere mate in die brein en hartspier. Geen uitdrukking van MT-1 was in die skeletspier waargeneem nie. Daarteenoor is MT-2 in alle weefseltipes uitgedruk, met ongeveer 'n tweevoud verhoging in die uitdrukkingsvlakke by die hoogste rotenoonkonsentrasie in die lewer, brein en hartspierweefsel. Die skeletspier het minder verhoging getoon. Vir MT-3 was daar geen waarneembare vlakke van uitdrukking in die skelet- en hartspierweefsel nie. Verbasend genoeg is 'n geringe betekenisvolle verhoging (43%) in die lewer met ooreenstemmende verhoging in die

hoogste rotenoon behandeling waargeneem. In die breinweefsel is heelwat hoër vlakke van MT-3 uitdrukking waargeneem, wat beduidend verhoog het (ongeveer tweevoud) by die hoogste rotenoonkonsentrasies .

Soos die hipotese van die studie voorstel ondersteun die *in vivo* data wat uit hierdie studie verkry is, die gepubliseerde *in vitro* data, wat getoon het dat rotenoon geïnduseerde kompleks I defekte lei tot MT uitdrukking. Die ooruitdrukking, van MT kan moontlik bydrae tot die patologie van die siekte, alhoewel dit nog ondersoek moet word. Die resultate van die studie toon ook dat die uitdrukking van die onderskeie MT-isoforme in rotenoonbehandelde rotweefsel nie op dieselfde manier as die geïnduseerde defek uitgedruk word nie. Hierdie waarneming kan moontlik dui op 'n verskil in die regulering en respons van die drie MT-isoforme op so 'n defek.

# TABLE OF CONTENTS

# LIST OF TABLES

# LIST OF FIGURES

# LIST OF EQUATIONS

# LIST OF SYMBOLS AND ABBREVIATIONS

## LIST OF SYMBOLS

| | |
|---|---|
| **α** | alpha |
| **β** | beta |
| **λ** | lambda |
| **Δψ** | Electrochemical gradient, membrane potential |
| **I** | complex I, NADH:ubiquinone oxidoreductase |
| **II** | complex II, succinate:ubiquinone oxidoreductase |
| **III** | complex III, ubiquinol:ferricytochrome *c* oxidoreductase, *cytochrome $bc_1$ complex* |
| **IV** | complex IV, ferricytochrome:oxygen oxidoreductase, *cytochrome c oxidase*, COX |
| **V** | complex V, $F_1F_0$-ATP synthase |
| **μ** | micro: $10^{-6}$ |
| **n** | nano: $10^{-9}$ |
| **p** | pico: $10^{-12}$ |
| **$e^-$** | electron |
| **%** | percent |
| **$E^o$** | standard redox potential |
| **°C** | degrees Celsius |
| **-** | negative |
| **+** | positive |

## LIST OF ABBREVIATIONS

| | |
|---|---|
| **A** | |
| **A** | absorbance |
| **A** | adenine |

| | |
|---|---|
| **$A_{260}/A_{280}$** | ratio of absorbency measured at 260 nm and 280 nm |
| **Acetyl-CoA** | acetyl-coenzyme A |
| **ADP** | adenine dinucleotide phosphate |
| **AIF** | apoptosis-inducing factor |
| **ANOVA** | analysis of variance |
| **ANT** | adenine nucleotide translocator |
| **apo-MT** | metal-free thionein |
| **ARE** | antioxidant response element |
| **ATP** | adenosine triphosphate |
| **Au** | gold |
| **Ag** | silver |
| | |
| **B** | |
| **BLAST** | Basic Local Alignment Search Tool |
| **bp** | base pair |
| **Br** | bromine |
| **BR** | brain |
| **β2MG** | β-2-microglobulin |
| | |
| **C** | |
| **C** | cysteine |
| **C** | cytosine |
| **CA** | California |
| **$Ca^{2+}$** | calcium ion |
| **Cd** | cadmium |
| **cDNA** | complementary DNA |
| **CI** | complex I |
| **CNS** | central nervous system |
| **Co** | cobalt |
| **$CO_2$** | carbon dioxide |
| **CoA** | coenzyme A |
| **CoQ** | coenzyme Q |

| | |
|---|---|
| **COX** | cytochrome *c* oxidase |
| **CS** | citrate synthase |
| **Ct** | cycle threshold |
| **Cu** | copper |
| **cys** | cysteine |
| **Cyt *c*** | cytochrome c |
| | |
| **D** | |
| ***d*** | practical significance |
| **Da** | dalton |
| **ddNTP** | 2',3'-dideoxynucleotide triphosphates |
| **DEPC** | diethyl pyrocarbonate |
| **dF** | derivative of the fluorescence |
| **D-Loop** | displacement loop |
| **DNA** | deoxyribonucleic acid |
| **dNTP** | deoxynucleotide triphosphate |
| **dsDNA** | double strand DNA |
| | |
| **E** | |
| ***Eco*RI** | *Escherichia coli* RY 13 restriction enzyme |
| **E** | PCR efficiency |
| **ELISA** | enzyme-linked immunosorbent assay |
| **e.g.** | *Exempli gratia* |
| ***et al.*** | *et alii*: and others |
| **ETC** | electron transport chain |
| **EtOH** | ethanol |
| **EtBr** | ethidium bromide: $C_{10}H_{20}BrN_3$ |
| | |
| **F** | |
| **F** | forward |
| **$F_0$** | $F_0$ subunit of ATPase complex |
| **$FAD^+$** | flavin adenine dinucleotide (oxidized) |

| | |
|---|---|
| **$F_1$** | $F_1$ subunit of ATPase complex |
| **$FADH_2$** | flavin adenine dinucleotide (reduced) |
| **$Fe^{2+}$** | iron divalent ion |
| **Fe-S** | iron-sulphur clusters |
| **FMN** | flavin mononucleotide |
| **FP** | flavoprotein fraction |
| | |
| **G** | |
| **g** | gram |
| **GPX** | glutathione peroxidase |
| **GR** | glutathione reductase |
| **GSH** | reduced glutathione |
| **G** | guanine |
| **g** | gravitational force of the earth (~10 $m.s^{-1}$) |
| **GAPDH** | glyceraldehyde-3-phosphate dehydrogenase |
| **GC content** | composition of primers, specifically G and C bases |
| **gDNA** | genomic DNA |
| **GenBank** | United States repository of DNA sequence information (GenBank® is a registred trademark of the National Institute of Health and Human Services for the Genetic Sequence Data Bank, Bethesda, MD, USA) |
| **GRE** | glucocorticoid response elements |
| **GSSG** | oxidised glutathione |
| | |
| **H** | |
| **H** | enthalpy |
| **$H^+$** | hydrogen ion/proton/s |
| **$H_2O$** | water |
| **$H_2O_2$** | hydrogen peroxide |
| **HCl** | hydrochloric acid |
| **HeLa** | Named after Helen Lane (Helen Larson) |
| **Hg** | mercury |
| **HM** | heart muscle |

| | |
|---|---|
| **hMT** | human metallothionein |
| **hMT-1 A to X** | human metallothionein subform 1, isoforms A, B, C, D, E, F ,G, H, I, J, K, L, and X |
| **hMT-3** | human metallothionein subform 3 |
| **hMT-4** | human metallothionein subform 4 |
| **HP** | hydrophobic-protein fractions |
| **HSD** | studentised range |
| | |
| **I** | |
| **i.e.** | That is |
| **IL** | interleukin |
| **IMM** | inner mitochondrial membrane |
| **IMS** | Intermembrane space |
| **IP** | iron-protein fraction |
| | |
| **K** | |
| **kg** | kilogram |
| **kb** | kilo base pairs (thousand base pairs) |
| | |
| **L** | |
| **LDH** | lactate dehydrogenase |
| **LHON** | Leber's hereditary optic neuropathy |
| **Li** | liver |
| **Ln** | natural logarithm |
| **mg** | milligram |
| | |
| **M** | |
| **M** | molar |
| **MELAS** | mitochondrial encephalomyopathy with lactic acidosis and stroke-like episodes |
| **MERRF** | myoclonic epilepsy and ragged-red muscle fibres |
| **mg** | milligram |
| **$MgCl_2$** | magnesium chloride |

| | |
|---|---|
| **MIM** | mitochondrial inner membrane |
| **min** | minutes |
| **ml** | millilitre |
| **MLV** | murine leukemia virus |
| **MLV-RT** | (moloney) murine leukemia virus reverse transcriptase |
| **mM** | millimolar |
| **MM** | molecular marker |
| **MnSOD** | manganese superoxide dismutase |
| **MOM** | mitochondrial outer membrane |
| **MPTP** | 1-methyl-4-phenyl-1,2,3,6,-tetrahydropyridine |
| **$M_r$** | molecular mass |
| **MRE** | metal responsive element |
| **MRL** | Mitochondrial Research Laboratory |
| **mRNA** | messenger ribonucleic acid |
| **MSE** | mean square error |
| **MT** | metallothionein |
| **MT-1** | metallothionein isoform 1 |
| **MT-2** | metallothionein isoform 2 |
| **MT-3** | metallothionein isoform 3 |
| **MT-4** | metallothionein isoform 4 |
| **mtDNA** | mitochondrial DNA |
| **MTF-1** | metal responsive element-binding transcription factor 1 |
| **MTP** | mitochondrial transition pore |
| | |
| **N** | |
| **n** | number |
| **N/A** | not applicable |
| **N/D** | not detected |
| **$NAD^+$** | nicotinamide adenine dinucleotide (oxidised) |
| **NADH** | nicotinamide adenine dinucleotide (reduced) |
| **NCBI** | National Centre for Biotechnology Information |
| **ND1-6** | NADH:ubiquinone oxidoreductase subunits 1, 2, 3, 4, 4L, 5, 6 |

| | |
|---|---|
| **nDNA** | nuclear DNA |
| **NDUFA5** | NADH-Ubiquinone oxidoreductase 1 alpha subcomplex 5 |
| **NDUFS1-S6** | NADH-Ubiquinone oxidoreductase Fe-S protein 1-6 |
| **NDUFV1-V3** | NADH-Ubiquinone oxidoreductase Flavoprotein 1-3 |
| **NE** | normalised expression of target genes |
| **NIH** | National Institute of Health |
| **NF** | normalisation factor |
| **ng** | nano gram |
| **Ni** | nickel |
| **nm** | nanometer |
| **NO·** | nitric oxide |
| | |
| **O** | |
| **OAA** | Oxalate acetic acid |
| **$O_2$** | oxygen |
| **$O_2^{\cdot-}$** | superoxide radical |
| **OH·** | hydroxyl free radical |
| **ONOO·** | peroxynitrite |
| **OXPHOS** | oxidative phosphorylation |
| **OD** | optical density |
| | |
| **P** | |
| **Pb** | lead |
| **PCR** | polymerase chain reaction |
| **PDH** | pyruvate dehydrogenase |
| **PEO** | progressive external opthalmoplegia |
| **pH** | indicates acidity |
| **$P_i$** | phosphate ion |
| **pMT-1** | plasmid of metallothionein isoform 1 |
| **pMT-2** | plasmid of metallothionein isoform 2 |
| **pMT-3** | plasmid of metallothionein isoform 3 |
| **pmol** | pico mol |

| | |
|---|---|
| **Q** | |
| **Q** | relative expression quantities |
| **Q** | ubiquinone |
| **$QH_2$** | ubiquinol |
| | |
| **R** | |
| **REST** | Relative Expression Software Tool |
| **R** | rotenone |
| **r** | rat |
| **R** | reverse |
| **RNA** | ribonucleic acid |
| **rRNA** | ribosomal RNA |
| **ROS** | reactive oxygen species |
| **18S rRNA** | 18 Svedberg units of ribosomal RNA |
| **28S rRNA** | 28 Svedberg units of ribosomal RNA |
| **5S rRNA** | 5 Svedberg units of ribosomal RNA |
| **RT-PCR** | reverse transcriptase PCR |
| | |
| **S** | |
| **S** | entropy |
| **SD** | standard deviation |
| **SM** | skeletal muscle |
| **SS** | statistical significance |
| **STAT** | signal transducers and activators of transcription |
| | |
| **T** | |
| **T** | thymine |
| **$T_a$** | annealing temperature |
| **TAE** | Tris-acetate buffer (Tris® is a registered trademark of the United States Biochemical Corporation, Cleaveland, OH, U.S.A) |
| ***Taq* polymerase** | DNA deoxynucleotidyltransferase, EC2.7.7.7, from *Thermus aquaticus* BM, expressed in recombinant *E.coli* |

| | |
|---|---|
| **TCA** | tricarboxyclic acid cycle |
| **$T_m$** | melting temperature |
| **$T_{red}$** | reduced apo-protein |
| **$T_{ox}$** | oxidised apo-protein |
| **tRNA** | transfer RNA |
| **Tris** | Tris(hydroxymethyl)aminomethane |
| | |
| **U** | |
| **U** | units (enzyme activity) |
| **UCS** | units per citrate synthase |
| **USA** | United States of America |
| **UTR** | untranslated region |
| **UV** | ultraviolet |
| **µg** | micrograms |
| **µm** | micrometer |
| **µl** | microlitre |
| | |
| **V** | |
| **V** | volts |
| **V/cm** | volts per centimetre |
| **VDAC** | voltage dependant anion channel |
| | |
| **W** | |
| **w/v** | weight/volume |
| | |
| **X** | |
| **x g** | gravitational acceleration |
| | |
| **Z** | |
| **Zn** | zinc |

# Acknowledgements

Completion of this dissertation resembles taking a very long journey of self-discipline, dedication and patience while researching, drafting and repeatedly revising the work. Completing such a journey requires any author to seek help and assistance from many people who provide advice and direction along the way. The study presented here was clearly influenced by the inputs of remarkable people. I thank those who supported and encouraged me during my journey. I would like to express my sincere appreciation to the following people and institutions.

- My supervisor, Prof. Francois van der Westhuizen, for his guidance, patience and compassion towards me. For being a mentor and role model in all aspects. His valuable advice and encouragement as a supervisor was outstanding!
- My co-supervisor, Prof. Antonel Olckers, for her valuable insight and inputs in the subject, and for broadening my knowledge in the field of molecular biology.
- Financial support from the National Research Foundation.
- Marco Alessandrini, who provided the rotenone-treated rat tissues for this study.
- Fimmie Reinecke, for her help and guidance in the experimental analyses.
- Mrs. Breytenbach, Prof. Steyn and Dr. Ellis at the NWU Statistical Department, for their expertise, help and valuable advice with the statistical analysis.
- Dr. Wayne Towers from the Centre of Genome Research for his valuable advice, inputs and his assistance in refining my work.
- The staff of the Mitochondrial Research Laboratory, for all their assistance and valuable advice.
- The molecular biology laboratory at the Department of Pharmacy, for the use of the iCycler real-time PCR apparatus.
- Anél Pretorius, for her encouragement and assistance throughout this study.
- Last but not least, my Mother (and memory of my Father) for all her guidance, motivation, support, encouragement and love. Both my Mother and sister (Geraldine) have left remarkable footprints throughout my journey of life!

# Chapter One

# Introduction

## 1.1 Introduction

Mitochondrial NADH:ubiquinone oxidoreductase (complex I) carries out a well defined and critical function required for cell physiology. This enzyme catalyses the first of a series of five reactions that occur in the inner mitochondrial membrane and results in the production of cellular ATP. Deficiencies of complex I, an enzyme consisting of 46 subunits, can lead to multi-system disorders that include several well known phenotypes such as type 2 diabetes mellitus, Alzheimer's disease as well as less known phenotypes such as mitochondrial encephalomyopathy with lactic acid strokes (MELAS), Leigh syndrome and myoclonus epilepsy with ragged red fibres (MERRF). A causing factor in these inherited mitochondrial diseases is the formation of reactive oxygen species (ROS) by the mitochondrial respiratory chain and the initiation of programmed cell death (apoptosis) (Cadenas & Davies, 2000; Smeitink *et al.*, 2004).

It was recently identified that the ROS-induced and ROS-scavenging proteins, metallothioneins (MTs), which exists in different isoforms, are over expressed *in vitro* in complex I deficient cell lines (van der Westhuizen *et al.*, 2003; Olivier, 2004). It has also recently been shown that these proteins have a protective effect against ROS-related pathology in a rotenone-induced complex I deficient cell line (Reinecke *et al.*, 2006). In these *in vitro* studies MT-2A was observed to be the predominantly expressed isoform of MTs in these human complex I deficient cell lines. This may, however, not be the case in other tissues affected by the disease caused by complex I deficiency. It is still not clear if MT overexpression occurs in this disease *in vivo* and, if it is indeed over expressed, and which isoforms are expressed in the various affected tissues. Furthermore, the significance of putative

over expression of MTs in the pathophysiology of the complex I or other deficiencies of the oxidative phosphorylation has not been investigated.

Mitochondrial disorders and its resulting pathology are differently expressed in tissues as a result of the specific energy demands of different tissues and also as a result of the unique characteristics of mitochondrial genetics, which are discussed in Chapter Two. The expression and possible protective role of MTs during oxidative stress can thus also be related to the tissue-specific expression of the disease and MT isoform/s that may be expressed in these affected tissues.

The main objective of this study was to investigate the expression of different MT isoforms in tissues of rotenone-treated Sprague Dawley rats, an *in vivo* model that has been used to study cell biological responses in a treatment strategy of mitochondrial complex I deficiency (Alessandrini, 2006). MT mRNA expression levels of MT-1, MT-2 and MT-3 were analysed in various tissue types using real-time PCR and quantified relative to a so-called "housekeeping gene", β-2-microglobulin. The differential expression of these MT isoforms in complex I deficient brain, liver, heart- and skeletal muscle was investigated in this study and correlated with the main biochemical parameter, complex I activity.

The potential outcome of this research was mainly to contribute to a better understanding of the expression and role of MT in complex I deficiency. Secondly, that it may complement the outcome of the before-mentioned study by Alessandrini (2006), who also provided the material for this study.

In Chapter Two several related topics will be discussed, namely the initial motivation for this study as well as a literature review where general aspects of mitochondria, complex I, mitochondrial disorders and metallothioneins are discussed. A hypothesis and experimental strategy are also outlined in this chapter. In Chapter Three a description of the materials and methodology used to perform the investigation of metallothionein expression in tissues of rotenone-treated rats is given. The results and data analyses are presented and discussed in Chapter Four. Finally, the concluding remarks and future considerations are presented in Chapter Five.

# Chapter Two

# Literature review

## 2.1 Background

Many diseases have been classified and categorised to be caused by a deficiency of complex I of the mitochondrial respiratory chain, located in the inner mitochondrial membrane (IMM) (Smeitink & van den Heuvel, 1999; Triepels *et al.*, 2001). A major consequence of complex I deficiency is the formation of ROS, which have a deleterious effect on the mitochondrion and consequently causes induction of apoptosis (Wallace, 1999). Metallothioneins (MTs), metal binding proteins, have been identified as one of the scavengers of ROS, most likely due to their high cysteine content (Thomas *et al.*, 1986; Ghoshal & Samson, 2001). In a recent study performed by van der Westhuizen *et al.*, (2003), it has been proposed that metallothioneins may have a ROS related protective effect in complex I deficient cell lines. In subsequent *in vitro* studies performed by Olivier (2004) and Reinecke *et al.*, 2006, this hypothesis was tested when the expression and role of metallothioneins with rotenone-induced complex I deficiency in HeLa cells was investigated. These studies provided evidence that MT has a protective effect against ROS-related pathology in complex I deficiency. The outcome of these studies indicated that MT-2A is the predominately expressed isoform in fibroblasts and HeLa cells. The outcome of these studies has prompted an investigation of metallothionein expression in an *in vivo* model.

Insufficient complex I activity may cause a cascade of events to occur, such as disrupting mitochondrial membrane potential, influencing oxidative phosphorylation, adjusting ion homeostasis, and increasing the formation and production of ROS and induction of apoptosis (Smeitink *et al.*, 2001; Wallace, 1999; van der Westhuizen *et al.*, 2003).

The cell biological consequences and tissue-specific response of rotenone-treated rats with complex I deficiency have been investigated by Alessandrini (2006). The

common rationale of the study presented here was to correlate MT expression with complex I deficiencies. To this end the expression of the main isoforms of metallothioneins (MT-1, MT-2 and MT-3) in brain, liver, heart muscle and skeletal muscle tissues of Sprague Dawley rats treated with different doses of rotenone was investigated. In this chapter an overview of the mitochondrion and oxidative phosphorylation, the role and the structure of complex I, and deficiencies of complex I is discussed. General properties of metallothioneins, their structure, function, and induction during oxidative stress are reviewed. Finally, a problem statement, hypothesis, aim and approach are outlined.

### 2.1.1 The mitochondrion

Outstanding discoveries of scientists such as Nobel prize winner Mitchel (1979) with their scenario's, speculations and research descriptions in the last couple of centuries made it possible to globally accept the evolution, progression and development of the mitochondrion. Continuous research that was performed during the last few decades, ultimately lead to the consensus that the mitochondrion symbolised the remainder of a prokaryotic organism that became associated in a symbiotic relationship with another cell early in the evolution on earth. According to Scheffler (2001), the serial endosymbiont theory states that: "a proto-eukaryotic cell without mitochondria evolved first, and this organism then captured a proteobacterium by endocytosis." During this symbiotic relationship some excessive genes died out, and some genes relocated from the cell to the nucleus which eventually revealed the allocation of these genes between the two genomes as it is known today (Gray, 1993; Scheffler, 2001). In addition to this theory, it also contained the likelihood that the mitochondrion was derived at the same time as the nuclear component of the eukaryotic cell, rather than a separate event. As time progressed the mitochondrion became entirely reliant on its "host" (Gray, 1993; Scheffler 2001).

### 2.1.2 Structure of the mitochondrion

Mitochondria are semi-autonomous organelles found in every cell in the human body, except for red blood cells. The vital purpose of the mitochondria's existence is to produce energy to the cell through a process called oxidative phosphorylation. Cells

can not even exist without mitochondria. Without energy, a cell can simply not function; essential metabolic pathways needed for optimal livelihood cannot be catalysed. A single cell can contain from 5 to 2000 mitochondria. The number of mitochondria in specific cell types varies considerably, although within a given cell type the number is closely regulated, for example the amount of mitochondria in the heart will differ from the amount found in the liver depending on the energy demand and function of that particular organ (Perkins and Frey, 2000). The rate and process of respiration and ATP synthesis are directly related to the number of mitochondria present in each cell and to the abundance of cristae present in each mitochondrion (Perkins & Frey, 2000; Scheffler, 2001).

The mitochondrion is an organelle that may often appear as swollen and spherical during pathological conditions, and of which the form can vary from ellipsoidal to rod-like that range from 0.5 micrometer (μm) – 5 μm in diameter at a length of 20 μm long (Perkins & Frey, 2000). Each mitochondrion consists of an inner and outer membrane, separated by a narrow intermembranous space of approximately 5-10 nanometer (nm) (Mannella, 2000; Frey & Mannella, 2000). The membranes are composed of phospholipids and proteins, which form part of the respiratory house of a large number of enzymes and exert a selective influence over the transport of ions, peptides and metabolites into mitochondria. The inner membrane of the mitochondrion is characterised by many folds, described as cristae, which are elongated and extend into the internal compartment of the mitochondrion, called the matrix. The molecules involved with electron transport and oxidative phosphorylation during aerobic respiration are built into the inner membrane (Perkins & Frey, 2000; Scheffler, 2001; Mathews & van Holde, 2000). Enzymes, such as dehydrogenases involved in metabolic pathways oxidising pyruvate, substrates of the Krebs cycle and the β-oxidation pathway are located in the matrix, and are in close proximity to the inner membrane, or within the membrane itself (Voet & Voet, 1995; Mathews & van Holde, 2000).

Mitochondria have two distinct membrane systems: the mitochondrial outer membrane (MOM), and the mitochondrial inner membrane (MIM). The voltage-dependant anion channel (VDAC) is located on the smooth and to some extent, elastic outer membrane (Perkins & Frey, 2000; Kerner & Hoppel, 2000; Passarella *et al.*,

2003). Throughout the last few decades some clarifications were made on the structure of the mitochondrion. It all started in the 1960s when two competing models arose between Palade and Sjonstrand. An outer membrane and a folded inner membrane were included in both these models. Palade's model was formulated in 1952 and stated that the cristae located in the inner membrane are "baffle-like". In 1953 Sjonstrand's model (Figure 2.1), which is still accepted today, illustrated that cristae are a stack of independent membranous lamellae, referred to as "septa". Thus, in contrast to Palade's model, there is no link between the cristae and peripherial membranes (Perkins & Frey, 2000; Scheffler, 2001).

Between the MOM and MIM, an intermembrane space (IMS) is situated and within this inner compartment the location of the gel-like matrix can be found. The matrix contains mitochondrial DNA (mtDNA) molecules, ribosomes, transfer ribonucleic acids (tRNA) and various enzymes needed in protein synthesis, the oxidation of pyruvate and fatty acids, and the citric acid cycle (Krebs cycle). The proteins in the mitochondrion, which occupy approximately 50% of the matrix, appear to be organised in a network attached to the inner surface of the inner membrane (Voet & Voet, 1995; Morin, 2000; Passarella *et al.*, 2003).

The majority of the mitochondrial proteins are synthesised in the nucleus and shuttled to the mitochondrion. Mitochondria are referred to as self-sufficient and semi-autonomous because, unlike any other organelle, they have their own mtDNA that encodes the production of subunits for four of the five enzyme complexes critical for oxidative phosphorylation. The human mitochondrial genome is comparatively small, consisting of 16,569 base pairs (bp). The mitochondrial genome encodes 13 proteins involved with oxidative phosphorylation as well as 22 tRNAs and 2 rRNAs involved in synthesis of these mitochondrial complexes (Anderson *et al.*, 1981; Scheffler, 2001; Wallace, 1999; Smeitink *et al.*, 2004).

Each mitochondrion contains 2-10 copies of the circular, supercoiled, double stranded DNA (dsDNA) found unprotected within the inner mitochondrial membrane. This circular DNA appears to be attached, at least transiently, to the inner mitochondrial membrane (Bogenhagen & Clayton, 1974; Pulkes & Hanna, 2001).

The close proximity of mtDNA to the harmful ROS by-products of oxidative phosphorylation makes mtDNA more vulnerable to ROS related damage. During oxidative phosphorylation, oxygen used in respiration is converted to superoxide anions or other ROS. It is estimated that mtDNA has a mutation rate much higher than nuclear DNA (Pulkes and Hanna, 2001). Two factors contribute to the vulnerability of mtDNA to mutate, as compared to nuclear DNA (nDNA). Firstly, coupled with close proximity to ROS, mtDNA also lacks the protective strategies associated with nDNA, such as protective histones, chromatin structure, and introns, and secondly the repair apparatus for mtDNA is much less efficient than that of nDNA. Mitochondrial DNA has two noncoding areas: a control region characterised by three variable areas as well as a displacement region (D-loop). The D-loop region contains elements that participate in the control of the mtDNA (Taanman, 1999; Chinnery, 2002).

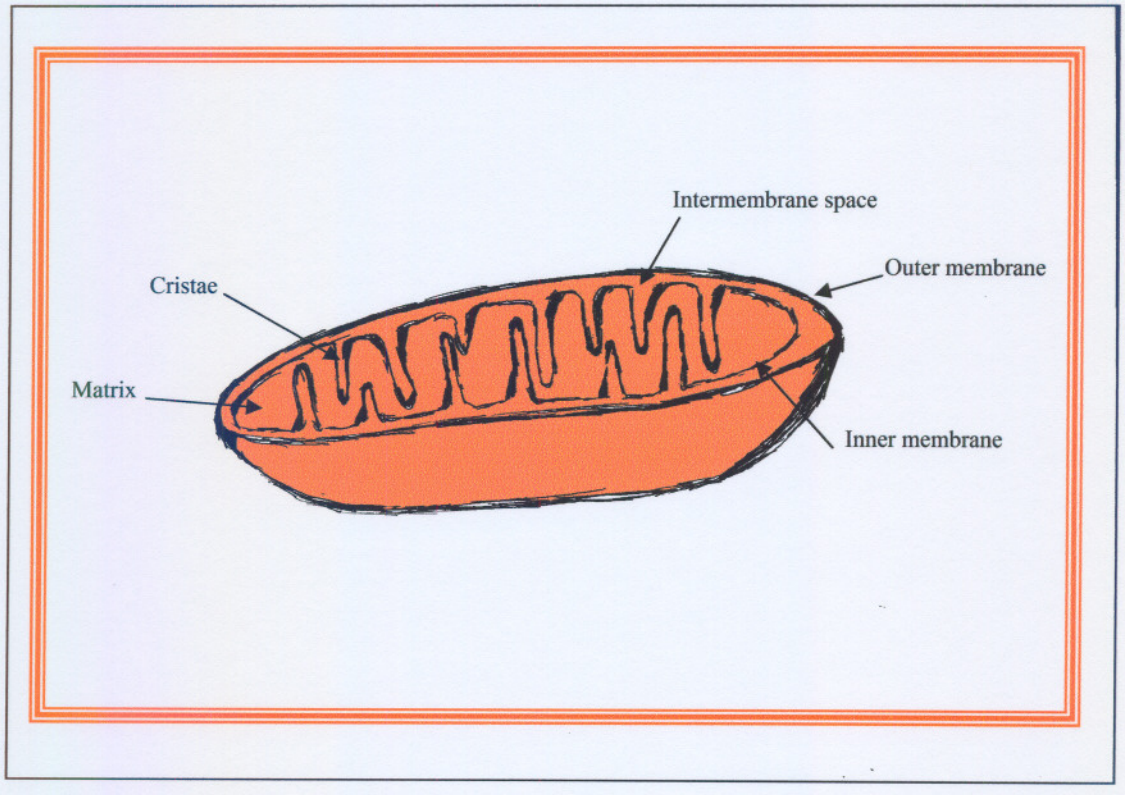


***Figure 2.1. The structural model of the mitochondrion.*** *The baffle model as it is still commonly known today. This model of Palade originated in 1952. A mitochondrion that indicates the inner membrane which is characterised by many folds, called cristae. These cristae are elongated and extended into the internal compartment of the mitochondria, namely the matrix (adapted from Grigorieff, 1998).*

### 2.1.3 Mitochondrial Biochemistry

The mitochondrion plays an integral part in cellular metabolism. Its essential role is immediately apparent, since it acts as the focus and crossroads of carbohydrate, lipid, and amino acid metabolism. In particular, the mitochondrion houses the enzymes involved in the Krebs cycle, the respiratory chain and ATP synthase, β-oxidation of fatty acids, ketone body production, urea cycle, fatty acid oxidation, biosynthesis of heme, as well as other processes (Mayes *et al.*, 2000; Mathews & van Holde., 2000; Scheffler, 2001; Carelli *et al.,* 2004). In Figure 2.2 it is illustrated that the main metabolic pathways of the mitochondrion form part of cellular bioenergetics. Glycolysis, the pentose phosphate pathway, and fatty acid synthesis all occur in the cytosol. The mitochondrion plays different roles in cellular physiology, not only to supply energy for the cell, but also to maintain the redox potential, to modulate calcium signals, and to produce heat and free radicals. Mitochondria also play an important part in initiating apoptosis (Wallace, 1999; Scheffler, 2001).

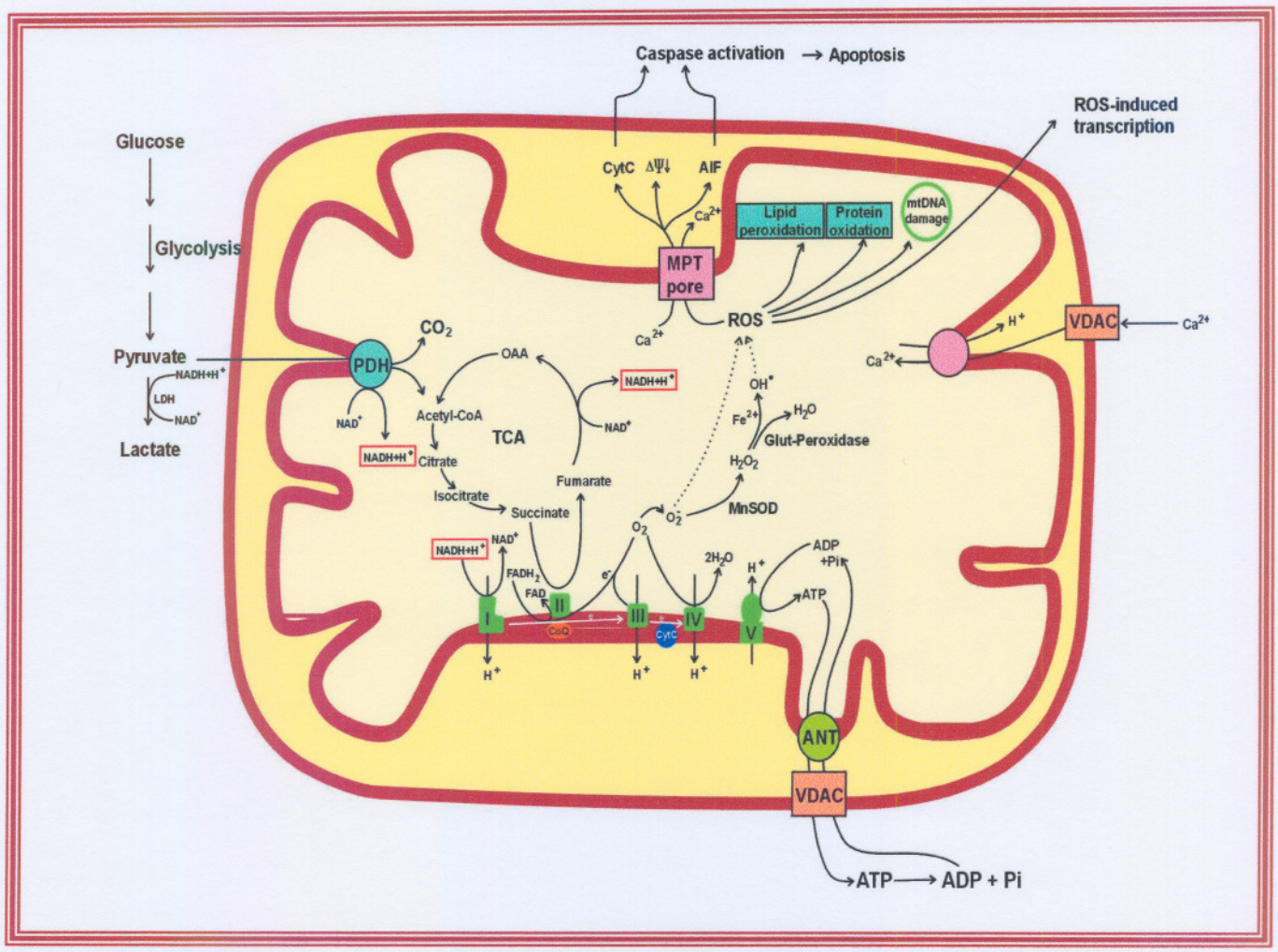


***Figure 2.2. Representation of the important metabolic activities of the mitochondria.*** *The TCA cycle (Krebs cycle) provides NADH and $FADH_2$ to complex I and complex II respectively, which are part of the oxidative phosphorylation system. The movement of electrons from one complex to another causes the translocation of protons to the inner membrane, to form an electrochemical gradient. This, in turn, provides energy for the synthesis of ATP. Electrons, transferred to the final electron acceptor $O_2$, may result in the formation of free radicals. The action of enzymes such as superoxide dismutase (SOD) and glutathione peroxidase prevents damage to mitochondria from these free radicals by transforming it to $H_2O$. In some cases, however, reactive oxygen species (ROS) may cause damage to lipids, proteins, mitochondrial DNA (mtDNA) as well as introducing the cell into apoptosis. (Reprinted with permission from F.H. van der Westhuizen).*

### 2.1.4 Electron transport system and oxidative phosphorylation

As mentioned before, the primary role of the mitochondrion is to produce energy to the cell in the form of ATP through oxidative phosphorylation (OXPHOS). This is

also the reason why the mitochondrion is often referred to as the "power house" of the cell, because it is responsible for at least 90 % of the energy generated in the cell. Substrates involved in the OXPHOS system are oxidised from glucose and fatty acids, through metabolic pathways such as glycolysis and β-oxidation. The metabolites then enter the Krebs cycle in order to produce electrons in the form of reduced equivalents, i.e. NADH (nicotinamide adenine dinucleotide) from $NAD^+$ and $FADH_2$ (flavin adenine dinucleotide) from $FAD^+$ (Mathews & van Holde, 2000; Perkins & Frey, 2000).

Redox reactions are catalysed by a series of multi-subunit enzymes or complexes that lead to the production of ATP along with ROS. Electrons are passed through these respiratory enzyme complexes (I, II, III and IV), which catalyse, and organise redox reactions with standard redox potentials ($E^0$) ranging from ± 0.320 to + 0.380 V, consecutively. These complexes are located in the inner mitochondrial membrane (MIM) as indicated in Figure 2.3 (Mitchell, 1961; Mitchell, 1979; Liu *et al.*, 2002).

Complex I (NADH:ubiquinone oxidoreductase, (EC 1.6.5.3) is one of four transmembrane multienzyme complexes within the inner mitochondrial membrane (complexes I, III, IV, V). Complex I is responsible for the oxidation of NADH, pumping four protons into the intermembrane space while reducing ubiquinone (CoQ). Complex II (succinate-ubiquinone oxidoreductase) oxidises the metabolites succinate into malate, and transfers electrons from $FADH_2$ to the hydrophobic CoQ. Complex II is unique in that it is not a transmembrane protein and contains no subunits encoded by mtDNA. Complex III (ubiquinol-cytochrome-c reductase) receives electrons shuttled by ubiquinone, liberating two protons in the process. Complex IV (cytochrome-c oxidase) is a transmembrane complex that receives electrons, reducing oxygen from water. As protons are pumped out of the matrix, each complex moves electrons along the chain. The ultimate phosphorylation of ADP to ATP occurs because of a proton gradient created by the oxidation of various compounds by the first four complexes. The electrochemical gradient ($\Delta\psi$) creates a transmembrane potential used by complex V (ATP synthase, $[F_1]$ $[F_0]$ ATPase) to drive the synthesis of ATP (Munnich & Rustin, 1996; Liu *et al.*, 2002; Carelli *et al.*, 2004).

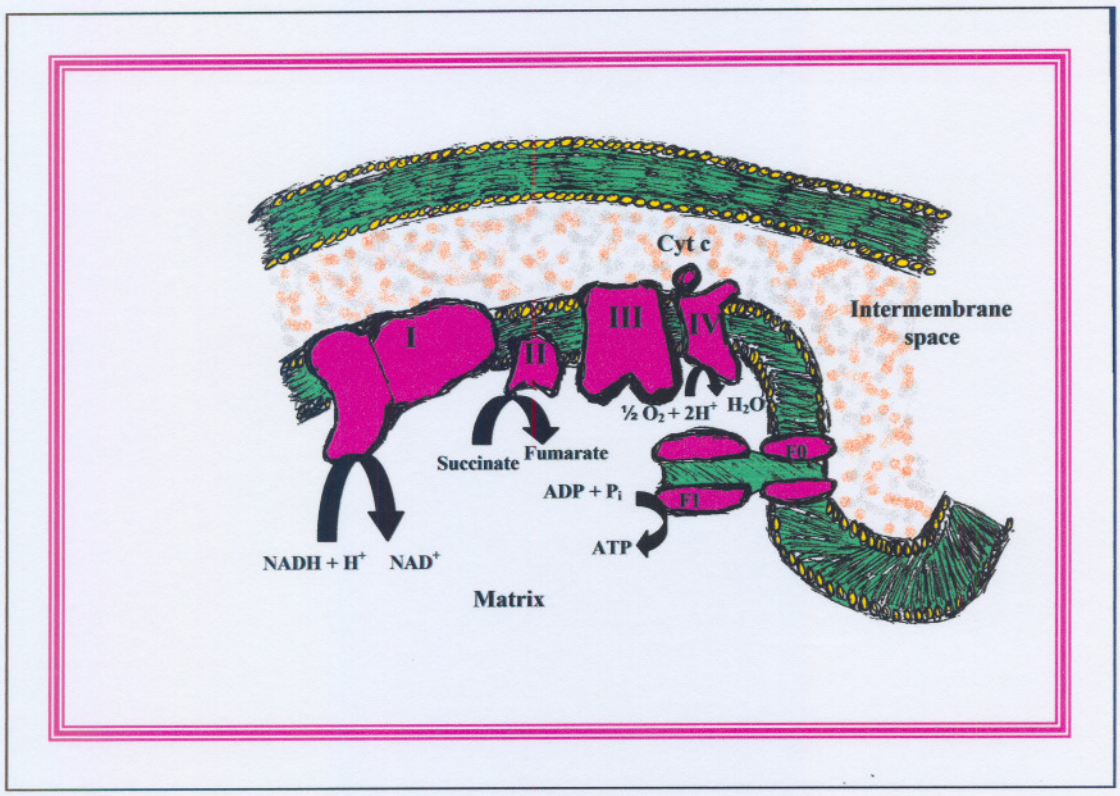


***Figure 2.3. Representation of mitochondrial oxidative phosphorylation.*** *All of the functional energy liberated during the oxidation of fatty acids and amino acids, and nearly all of that released from the oxidation of carbohydrates, is made available in mitochondria as reducing equivalents (electrons or $H^+$) or in the form of NADH and $FADH_2$ (Adapted from Mathews & van Holde, 2000).*

### 2.1.5 Complex I (NADH:ubiquinone oxidoreductase)

Among the enzyme complexes involved in the mitochondrial electron transport/oxidative phosphorylation system, complex I has the most complex structure. Complex I has at least 46 subunits and the mechanism of electron transfer and proton translocation of this complex is the least understood of all the complexes. (Fearnly & Walker, 1992; Walker *et al.*, 1992; Grigorieff, 1999; Triepels *et al.*, 2001). In addition to this, complex I also hosts the slowest electron-transfer step among its several redox components (FMN, binuclear and tetranuclear iron sulphur clusters and ubiquinone) which is the initial step of hydride ion transfer from NADH to the enzyme. From a biomedical point of view, complex I might be considered the most important of the respiratory chain enzyme complexes, because many human mitochondrial diseases result from complex I deficiencies.

Complex I (Figure 2.4) has an L-shape configuration that consists of a water-soluble peripheral arm projecting into the matrix and a water insoluble hydrophobic arm embedded in the MIM (Grigorieff, 1998; Triepels *et al.*, 2001). Complex I can be divided into three fractions: a flavoprotein fraction (FP), iron protein fraction (IP) and a hydrophobic protein fraction (HP). The peripheral arm consists of the FP and the IP and the water-insoluble arm consists of the HP (Triepels *et al.*, 2001). The FP fraction contains three subunits (NDUFV1-V3) containing flavin mononucleotide (FMN) and several Fe-S cluster binding sites. The IP fraction consists of seven subunits (NDUFA5, NDUFS1-S6) and contains a number of Fe-S cluster binding sites (Loeffen *et al.*, 2000). The HP fraction contains 30 subunits, which include ND1-ND6 (Triepels *et al.*, 2001; Hirst *et al.*, 2003). The movement of electrons through complex I is still unclear, but it is hypothesised that electron transfer starts at the FP fraction (the NDUFV1 subunit). Iron-sulphur clusters (Fe-S), distributed throughout the complex, create opportunities for additional electron transfer. The passage that the electrons follow starts at the FMN centre and continues through a series of Fe-S centers. Ubiquinone is the final electron acceptor that transfers electrons further into the respiratory chain (Scheffler, 2001; Triepels *et al.*, 2001; Hirst *et al.*, 2003; Smeitink *et al.*, 2004).

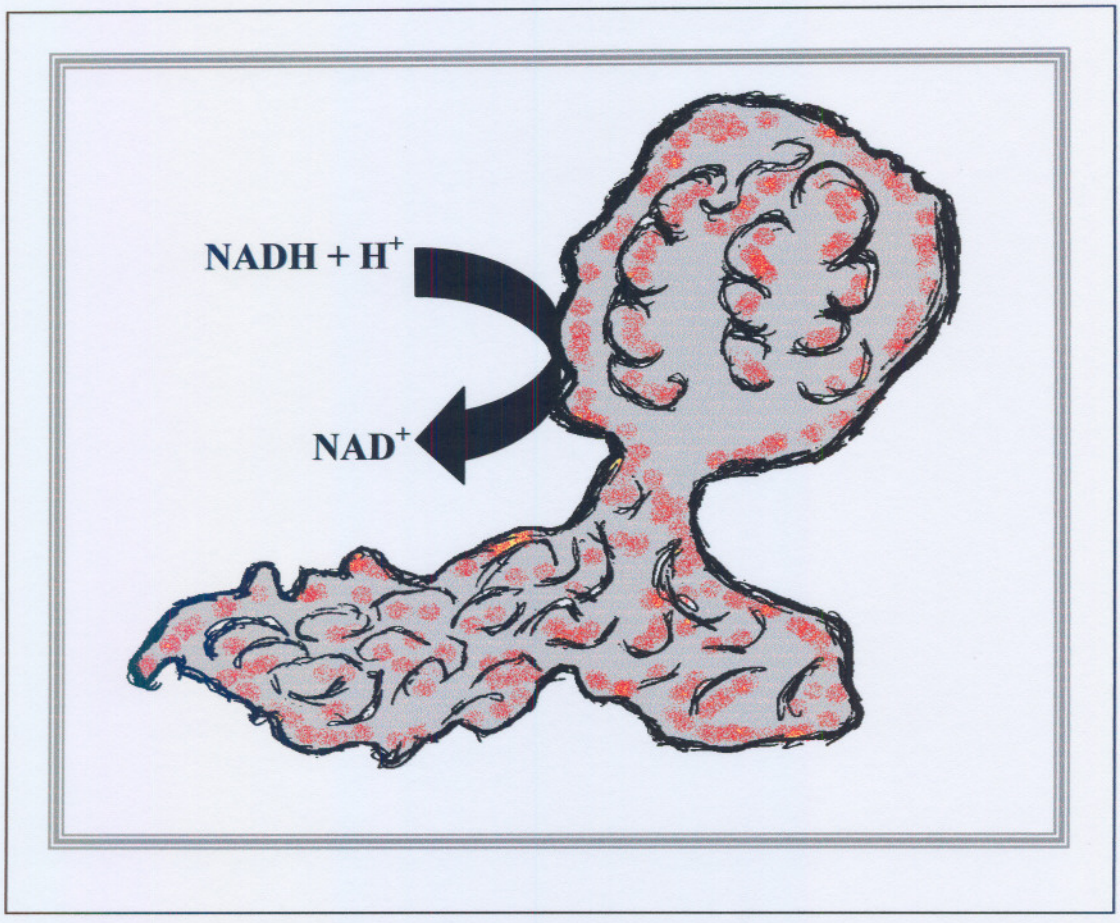


***Figure 2.4. Structural model of complex I*** *(NADH:ubiquinone oxidoreductase). The L-shape configuration of the complex can be observed in this figure. It consists of a hydrophobic arm and a water soluble peripheral arm which is partly embedded in the mitochondrial matrix and which consists of seven highly hydrophobic subunits. Electrons are passed from NADH to FMN and then through a series of Fe-S centres. Protons are also passed through the complex to the innermembrane space by FMN and CoQ. There are three fractions FP (flavoprotein), IP (iron protein), and HP (hydrophobic protein) (Adapted from Grigorieff, 1998).*

### 2.1.6 Complex I deficiency: Clinical presentation and disease cause

The majority of ATP produced from the complete oxidation of glucose to $CO_2$ and $H_2O$ come from the reoxidation of the NADH and FADH that were produced in the citric acid cycle. ATP is formed via coupling of electron transport from molecules such as NADH and FADH, with proton pumping across the inner mitochondrial membrane. Defects in any of the complexes (complexes I-IV) may reduce cellular oxidative phosphorylation. Since cells and especially neurons are highly oxidatively

dependent, the impairment of oxidative phosphorylation may cause a variety of diseases and illnesses.

Mitochondrial disorders are mostly associated with disorders that occur in the OXPHOS system. Complex I deficiency, which is the most frequently encountered defect of the OXPHOS system, was first reported in 1979 (Morgan-Hughes *et al.*, 1979). Complex I deficiency is a great contributor to metabolic inborn errors in the paediatric age group (von Kleist-Retzow *et al.*, 1999; Loeffen *et al.*, 2000). Defects of the respiratory chain can originate from any form of inheritance and may result in any symptom in any tissue and at any age (Triepels *et al.*, 2001; Chinnery, 2002). Respiratory chain dysfunction can also originate from either genetic or non-genetic causes, as a result of many toxins or environmental factors that inhibit any of the enzyme complexes. From these characteristics of respiratory chain disorders it should be clear that the cause and clinical presentation is relatively complex within inherited metabolic disorders.

### 2.1.7 Clinical symptoms of complex I deficiencies

Some of the clinical manifestations of complex I deficiency as well as brief descriptions of the symptoms that are at hand with these deficiencies are given in Table 2.1.

**Table 2.1 Clinical manifestations of complex I deficiencies**

| Complex I deficiency | Symptoms |
|---|---|
| Alpers-Huttenlocher disease | • Seizures<br>• Dementia<br>• Blindness<br>• Liver dysfunction |
| Alzheimer's disease | • Degenerative disease of the cerebral cortex |
| Parkinsonism | • Degeneration of the basal ganglia of the brain |
| Cardiomyopathy | • Defective myocardium |
| Barth syndrome | • Skeletal myopathy<br>• Cardiomyopathy<br>• Short stature<br>• Neutropenia |
| Encephalopathy | • Abnormal structure and function of tissues in the brain |
| Infantile CNS<br>(Infantile central nervous system) | • Immature neurodegeneration |
| LHON*<br>(Leber's hereditary optic neuropathy) | • Unilateral visual loss<br>• Dyschromatopsia<br>• Bilateral optic atrophy |
| Leigh Syndrome* | • Encephalopathy in infancy or childhood<br>• Necrosis involving midbrain, basal ganglia, thalamus, pons and optic nerves |
| Longevity | • Ageing |
| MELAS*<br>(Mitochondrial encephalomyopathy lactic acidosis and stroke-like episodes) | • Mutations in mtDNA<br>• Cortical blindness<br>• Hemiparesis<br>• Hemianopia |
| MERRF*<br>(Myoclonic epilepsy and ragged red muscle fibres) | • Mutations in mtDNA<br>• Seizures<br>• Mitochondrial myopathy and cerebellar ataxia<br>• Dementia |
| PEO<br>(Progressive external opthalmoplegia) | • Paralysis of the motor nerve muscles serving the eye |

* *Major syndromes of complex I deficiency (Adapted from Pulkes and Hanna, 2001; Triepels et al., 2001; DiMauro, 2004; Carelli et al., 2004).*

Current treatment for complex I deficiencies remains mostly symptomatic and does not change the course of the disease significantly. Treatment includes;

- Avoiding known mitochondrial toxins, although the risk is mostly potential rather than actual. Antibiotics such as tetracycline, which disrupts intermitochondrial protein synthesis, cyprofloxacin which depletes mtDNA, and aminoglycoside antibiotics should be avoided (Bindoff, 1999).
- Avoidance of exposure to hazardous chemicals and drugs that have a detrimental effect, such as sodium valproate (may influence fatty acid oxidation and inhibit the respiratory chain), barbiturates, and chloramphenicol.
- Prevention of oxygen radical damage (ascorbate administration)
- Dietary recommendations (high lipid-low carbohydrate diet). Avoiding obesity.
- Succinate and riboflavin supplementation can also be considered, as succinate enters the respiratory chain via complex II and riboflavin is the precursor of the flavin moiety in complex I (Munnich & Rustin, 1996; Ruitenbeek *et al.*, 1996).
- In cases of acute exacerbation of lactic acidosis, bicarbonate could relieve the symptoms (Munnich & Rustin, 1996; Ruitenbeek, *et al.*, 1996).
- Exercise is an important type of therapy, and fasting should be avoided (Bindoff, 1999).

The success of all of these supplementations cannot be assured, and in the most cases current therapeutic interventions have failed (Triepels *et al.*, 2001). Therefore, further investigation should be considered for revising current therapeutic interventions for complex I deficiencies.

### 2.1.8 Oxidative stress

Oxidative stress can broadly be defined as a condition in which there is an elevated concentration of reactive oxygen species (Bauman *et al;* 1991). According to Klaassen, there are two fundamental ways to produce oxidative stress:

(1) Increase the production of reactive oxygen species

(2) Induce oxidative stress by decreasing the defence systems involved in protection against reactive oxygen species.

Causes of oxidative stress have been associated with several clinical conditions. Reactive oxygen species are continually produced in tissues by the action of the mitochondrial electron transport system and of reduced nicotinamide adenine dinucleotide phosphate (NADH) oxidase (Wakeyama *et al.,* 1982; Cadenas & Davies, 2000).

Oxidative stress refers to cytological consequences of a variance between the production of free radicals or ROS (generated by mitochondria and produced as by-products of normal oxidative metabolism) and the ability and capacity of the cell to defend against these hazardous chemical species (Robinson, 1998). The oxygen molecule accepts an additional electron to generate superoxide, a more reactive form of oxygen, probably produced by a non-enzymatic mechanism in the mitochondria (Raha & Robinson, 2001). Oxidative stress transpires as the production of ROS increases, when scavenging of free radicals or repair of oxidatively modified macromolecules decreases, or both, (Zhou *et al.,* 2003). ROS could damage proteins, lipids, nucleic acids, and other biological macromolecules that result in the impairment of the function of various organs (Zhou *et al.,* 2003). Molecular oxygen is a vital element of life, yet limited reduction of oxygen to water during normal aerobic metabolism generates ROS which pose a serious threat to all aerobic organisms (Dalton *et al.,* 1999).

A genetic defect may lead to altered oxidative metabolism which is induced by defective synthesis of the nuclear or mtDNA encoded subunits of the enzymatic complexes of the respiratory chain (Chance *et al* 1979; Wallace, 1999). Ubisemiquinone generated in the course of the electron transport reaction in the respiratory chain donates electrons to oxygen and provides a constant source of superoxide. It has been estimated that the fate of 1-2% of all electrons passing down the electron transport chain is to be diverted into the formation of superoxide radicals. Superoxide can attack iron sulphur centres in enzymes such as aconitase, succinate dehydrogenase, and mitochondrial NADH:ubiquinone oxidoreductase, releasing iron and destroying catalytic function. Superoxide is therefore rapidly removed by

conversion to hydrogen peroxide ($H_2O_2$) in a reaction catalysed by superoxide dismutase. Three superoxide dismutases exist in mammalian systems: cytosolic CuZn superoxide dismutase (CuZnSOD), intramitochondrial superoxide dismutase (MnSOD) and extracellular CuZn superoxide dismutase (Robinson, 1998; Raha & Robinson, 2001; Wallace, 1999).

Hydrogen peroxide can, in the presence of cupric or ferric ions ($Cu^+$ or $Fe^{2+}$), produce a highly reactive hydroxyl radical, which can cause damage to proteins, lipids and DNA as illustrated in Figures 2.2 and 2.5. The formation of $H_2O_2$ by either MnSOD or CuZnSOD can be processed by glutathione peroxidase (GPX) to water. Complex I and complex III are the respiratory chain complexes responsible for the generation of superoxide in the mitochondria (Raha and Robinson, 2001; Wallace, 1999).

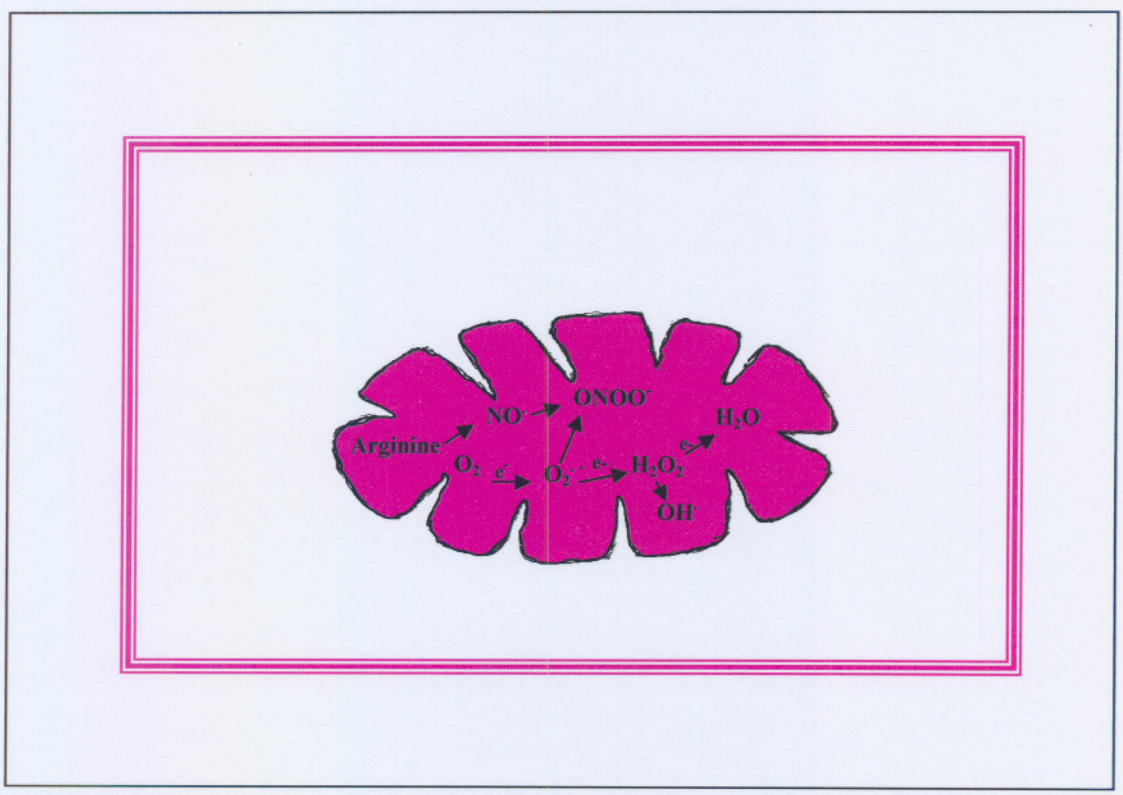


***Figure 2.5. Representation of the production of ROS from molecular oxygen.*** *Superoxide anion is converted to hydrogen peroxide by SOD. Hydrogen peroxide, if not broken down to water, can be converted to hydroxy radicals that cause damage to lipids, membranes and ultimately to DNA. (With permission of the Mitochondrial Research Laboratory).*

### 2.1.9 Inhibition of complex I by rotenone

Insufficient complex I activity will affect NADH oxidation, leading to an excess NADH and a lack of $NAD^+$ in the cells. This will ultimately lead to purposeful disruption of the regulation of metabolic pathways, such as the Krebs cycle or the β-oxidation, with the consequence of elevation of blood lactate and an increase of ketone bodies and lactate/pyruvate molar concentrations (Triepels *et al.*, 2001). Specific inhibitors of complex I have demonstrated that they are useful tools for studies investigating the mechanism of electron transfer and proton translocation in the respiratory chain. Natural inhibitors of complex I have a structural resemblance to ubiquinone, where a cyclic head corresponds to the ubiquinone ring and hydrophobic tail (Esposti, 1998). Nevertheless, there are numerous compounds, both natural and synthetic, such as rotonoids, piericidins and certain plant products, just to name a few that are effective inhibitors of complex I (Esposti, 1998). Rotenone is the most powerful member of the rotenoids, a family of isoflavonoids extracted from *Leguminosae* plants. Rotenone, which is widely used as an insecticide and fish poison, has become an established inhibitor of complex I.

Rotenone is highly lipophilic and can gain access to all organs. The structure of rotenone is indicated in Figure 2.6. This compound inhibits mitochondrial respiration by means of blocking the oxidation step of NADH, thus upholding a high $NADH/NAD^+$ ratio (Cunningham *et al.*, 1995). It binds to subunit ND1 of complex I and has features not found in two of the other commonly used complex I inhibitors, 1-methyl-4-phenyl-1,2,3,6 tetrahydropyridine (MPTP) and amytal. Unlike MPTP, which is selective for dopaminergic neurons and depends on the dopamine transporters to gain access to the neurons, rotenone is extremely lipophilic, and can cross biological membranes easily and independent of transporters. Rotenone may be a more appropriate model candidate than amytal, as rotenone binds to complex I irreversibly and specifically. As such, it is well suited for inducing a systemic inhibition of complex I in experimental animals (Greenamyre *et al.*, 2003).

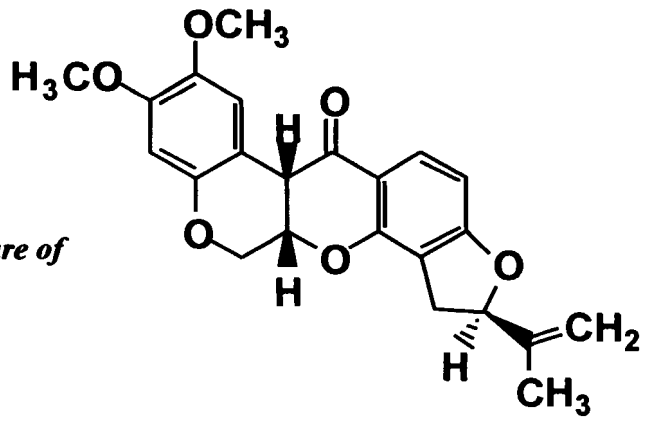


***Figure 2.6. Molecular structure of rotenone.***

## 2.2 Metallothioneins

### 2.2.1 Common properties of metallothioneins

Metallothioneins are a group of ubiquitously expressed non-enzymatic proteins which are differentiated by their resistance to thermocoagulation and acid precipitation. MTs consist of approximately 60 non-aromatic amino acids and a large number of cysteinyl residues (Kägi *et al.*, 1974; Hamer, 1986; Coyle *et al.*, 2002). MTs isolated from liver, kidney, and brain samples, seem to play an important role in homeostatic control, metabolism, and detoxification of a number of trace metals such as zinc (Zn), copper (Cu), cadmium (Cd), and mercury (Hg). Certain MTs were shown to exist as isoforms that are the products of genetic polymorphisms, characteristic of MT genes in animals and humans; consequently, they draw attention to studies of metal-mediated gene expression mechanisms (Chassaigne & Lobinski., 1998).

MTs were first discovered as cadmium and zinc proteins in horse kidney by Margoshes and Vallee in 1957 (Kägi and Vallee, 1960). MTs bind to heavy metals through clusters of thiolate bonds and the strength of the binding can vary by abundant orders of magnitude depending on the ion at stake. The synthesis of MT is regulated in cells and organisms exposed to heavy metals.

MTs are classified according to their structural features. The following are characteristic properties of metallothioneins (Kägi & Nordberg, 1979; Hamer, 1986; Coyle *et al.*, 2002).

- High content of heavy metals (4-12 atoms/molecule) bound exclusively by clusters of thiolate bonds
- High cysteine content (23-33 mol%) and general lack of aromatic and hydrophobic amino acid residues. The number and position of the cysteine residues are highly conserved and form cys-x-cys, cys-x-y-cys and cys-cys sequences, where x and y are non-cysteine amino acids
- Low molecular weight (less than 10,000 Da)
- Structural and functional homology
- MTs are classified into groups according to their electrophoretic behaviour

MTs can be used as biomarkers to metal exposure. MT is a single polypeptide chain of 61 amino acid residues with N-acetylmethionine and alanine as the N- and C-terminal residues, respectively (Sato & Bremmer, 1993). MTs high content of cysteine explains their high capacity for binding metal ions through their sulphydryl groups, forming metal thiolate complexes (Kojima *et al.*, 1988). It consists of a unique amino acid sequence (fixed distribution of cysteinyl residues) in two metallic subunits, named the α- and β-domains. In mammals, these domains are asymmetrical and consist of a four-metal cluster in the α-domain and a three-metal cluster in the β-domain.

Mammalian MTs have the ability to accommodate metal ions of different sizes and chemical reactivity without compromising the overall architecture (Vašák *et al.*, 1987). MTs constitute a family of proteins that bind to both essential and toxic metals. Due to their binding capacity (up to 7 Zn or 12 Cu ions per molecule), ubiquitous nature, and the capacity of some isoforms to be induced by metals, MTs may participate in essential metal trafficking to and from many metal-dependent proteins (Hunziker *et al.*, 1995; Koropatnick & Leibrandt, 1995; Vallee, 1995). Metallothionein is related to metabolism and detoxification of heavy metals, because it has a low affinity for the essential metal zinc and a high affinity for toxic metals such as Cd and Hg (Hunziker *et al.*, 1995).

### 2.2.2 Structure and heavy metal binding of mammalian metallothionein

Heavy metals such as Zn, Cu, Cd, Ag, Hg, Au, Ni, and Co are minor, yet ubiquitous components of the biosphere and transpire as functional elements for everyday living. Zn and Cu, which participate in a diversity of enzymatic reactions, are essential trace nutrients for all life forms but are toxic when present at inappropriately high concentrations. The other ions that serve no known essential function, are present in lower and more variable concentrations in the environment, and are generally more potent toxins. The principal targets for heavy metal poisoning are unknown. Metallothionein is the only molecule to which a clear role in the intracellular metabolism can be ascribed to (Hamer, 1986).

The structure of MT (Figure 2.7) has been studied by a variety of biophysical and biochemical techniques including ultra violet (UV) spectroscopy, amino acid sequencing and partial proteolysis and, X-ray crystallography, just to name a few. Mammalian MT is a 61- or 62-amino-acid peptide containing 20 cysteines, 6-8 lysines, 7-10 serines, a single acetylated methionine at the amino terminus, and no aromatics or histidines. The structure of a MT protein in an organism depends on the individual's status of tissue as well as the amount of exposure to heavy metals. The amount of cadmium bound to MT in the kidney will differ from the amount of cadmium bound to MT in the liver. Metals are associated with MT exclusively through thiolate bonds to all 20 cysteine residues. The metals can be removed by exposure to low pH and the resulting apothionein can subsequently then be reconstituted with 7 atoms of cadmium or zinc or 12 atoms of copper. Mammalian MT can also bind to 7 atoms of Hg, Co, Pb, and Ni or to 10-12 atoms of Ag and Au (Kägi *et al.*, 1984; Nielson *et al.*, 1985; Sato & Bremmer, 1993). Mammalian zinc-MT can reactivate various zinc-dependant enzymes including carbonic anhydrase, aldolase, thermolysin, and alkaline phosphatase with approximately the same rates as inorganic salts (Li *et al.*, 1980, Udom & Brady, 1980).

***Figure 2.7. Representation of rat MT-2.*** *In purple, two separate tetra-coordinated metal-sulphur clusters are surrounded by the polypeptide chain. The yellow indicates the cysteine residues involved in the binding metal ions, which is shown in blue (Adapted from Binz, 1999).*

### 2.2.3 Nomenclature, occurrence and detection of MTs

In 1978 the first nomenclature system for metallothionein was implemented, and in 1985 a subdivision for all the MT's was introduced into three classes (Binz & Kägi, 1999). MTs are currently classified as a family consisting of 16 genes in a cluster of about 82 kb (Karin *et al.,* 1984; Vallee, 1995; Coyle *et al*., 2002). MTs in humans has (hMT), no less than 10 of the MT genes, which cluster within the q13 region on chromosome 16, are of use, and these encode multiple isoforms of hMT-1 by the selected letters A, B, C, D, E, F, G, H and X and an isoform of hMT-2A (Karin *et al.,* 1984; Stennard *et al.,* 1994). Single genes also code for hMT-3 and -4. The non-functional MTs include MT-1I, -J, -K and -L. MT isoforms that encode for different genes are arranged in tandem head-to-tail fashion in the chromosome with a cluster of 13 closely-linked MT-1 genes (Quiafe *et al.*, 1994; Ghoshal & Samson, 2001).

A MT subfamily contains MTs which, beside to the family characters, share thorough phylogenetic features. These additional features usually involve precise monophyletic interaction between the protein sequences and/or nucleotide segments in the genes [5' or 3' untranscribed portion of the genes, 5' or 3' untranslated regions (UTR's) of the nucleotide sequences, exons, introns]. Presence, conservation or repetition of sequence patterns are different criteria which could also be incorporated where applicable. A subfamily is abbreviated with a letter character and an Arabic number (Binz & Kägi, 1999).

Isoforms or allelic forms are specifiable as components of subgroups, subfamilies and families (Binz & Kägi, 1999). Even though the general physico-chemical properties of MT isoforms are similar, the significance of the four major isoforms in the biological purpose and differential expression in specific tissue/organ systems is essential. The most extensively expressed isoforms in the body are MT-1 and MT-2, which are induced swiftly, particularly in the liver, by a wide range of metals, drugs and inflammatory mediators (Coyle *et al.*, 2002) MT-2A has indicated to be expressed more in human tissues than MT-1A. MT-3 is expressed largely in the brain, first and foremost in glutaminergic neurons, although low expression has been discovered in the tongue, stomach, pancreas, intestines, heart, kidney and reproductive tissues. MT-4 is expressed solely in the squamous epithelial cells in skin, tongue and intestinal lining, which indicates to play an important role in the differentiation of the former tissues (Stennard *et al.*, 1994; Jacob *et al.*, 1999; Ghoshal & Samson, 2001; Coyle *et al.*, 2002; Zhou *et al.*, 2003; Sato & Kondoh, 2002).

### 2.2.4 Isoforms of metallothionein

MT isoforms differ in amino acid composition other than cysteine residues and, consequently, have different isoelectric points and different hydrophobicities. Isoforms with minor differences, such as one amino acid residue, were perceived as subgroups of the two major isoforms and are termed subisoforms. Characteristic methods for the separation of MT isoforms are based on the differences in the electrical charge of the molecule induced by the variation of the primary structure,

and include anion-exchange chromatography and electrophoresis. The difference in the electrical charge induced by the substitution of one or several amino acids in the polypeptic chain is often not sufficient to affect the binding capacity on an anion-exchange column (Chassaigne & Lobinski, 1998). The possibility of MT isoforms performing different functions has been mentioned (Klaassen & Choudhuri, 2000).

In the 21$^{st}$ century, also referred to as the century of the brain (Koh *et al.*, 1996), studies of the functional analysis of MT in the brain are likely to increase. Zn is present in presynaptic terminals and is well-known to act not only as a neurotransmitter, but also to be released from the cell in brain ischemia and to injure the central nervous system (Koh *et al.*, 1996). MT, which is a Zn-binding protein, plays a significant role in the brain. These isoforms are distributed over the entire brain, and their expression in the olfactory bulb, cortex, caudate nucleus, thalamus, hippocampus, brain stem, and spinal cord has been established (Choudhuri *et al.*, 1995).

MT-3 is induced specifically in the brain, and the quantity of its expression is reduced in patients with Alzheimer's disease. Modifications in the expression of MT-3 are related to the occurrence of degenerative nerve diseases. Since reactive oxygen acts as a messenger molecule of intracellular signals, the reactive oxygen scavenging activity of MT may be strictly related to the regulation of intracellular signal transmission (Uchida *et al.*, 1991; Ye *et al.*, 2001).

MT-3 prevents aberrant neuronal sprouting and neurofibrillary tangles (Palmiter *et al.*, 1992) and give rise to intracellular defence against ROS and nitrogen species (Andrews, 2000), consequently the possibility that MT-3 restricts neuronal cell death has been mentioned (Aschner *et al.*, 1997). Research has indicated that the zinc content in some areas of the brain does not vary in young stressed mice, and the increments of MT-3 are independent of zinc (Ono *et al.*, 1997; Penkowa *et al.*, 2000). Interleukin (IL)-6 induces MT-3 mRNA expression following stress and inflammation (Andrews, 2000; De *et al.*, 1990). Stressed IL-6 null mice displayed a reduction of MT-3 mRNA expression and enhanced inflammation (Carrasco *et al.*, 1998; Penkowa *et al.*, 2000). MT-3 homeostasis is crucial for zinc turnover within the brain against inflammation (Mocchegiani *et al.*, 2004). MTs sequester more zinc ions than copper

during ageing (Mocchegiani *et al.*, 2002). Elevated concentrations of zinc-bound MT-3 have been established in the hippocampus of old mice and dogs (Giacconi *et al.*, 2003; Kojima *et al.*, 1999).

### 2.2.5 Function of metallothioneins

MTs take part in multiple biological processes and are regarded as cellular mediators for cellular detoxification of metals such as Cd, Hg, Cu and Ag because of their capability to bind to heavy metals. As MTs bind biological essential metals such as Zn and Cu, they also act as a reservoir for these metals and facilitate reversible transfer of these ions to cellular macromolecules. Many cellular proteins require zinc for their biological activity. MTs therefore control their function by acting both as a zinc donor (Zn-MT) or/and a zinc acceptor (apothionein/apo-MT) (Moffat & Denizeau, 1997; Kägi, 1991).

In cadmium toxicity, MTs stage a protecting role not just against hepatotoxicity, but also nephrotoxicity, hemetotoxicity, immunotoxicity and bone damage (Klaassen & Choudhuri, 2000; Nordberg & Nordberg, 2000). MTs also play a protecting role against oxidative damage caused by free radicals, pharmacological agents and mutagens, neuroprotection from ionising radiation, modulation of cell apoptosis and the function as a regulator of neuronal outgrowth. The protective role of MT is related to a stress situation or the presence of a toxic agent. The exposure of an organism to toxic factors induces MT expression in different tissues.

A physiological perspective on the function of MT requires consideration of the following (Davies and Cousins, 2000; Coyle *et al.*, 2002):

- MTs exhibit sequence homology and indistinguishable metal binding geometry throughout the spectrum of evolution from single-cell eukaryotic organisms to humans
- Affinity of metal binding to MT is high, particularly zinc is kinetically labile and may uphold MT thiols in a reduced redox state
- The extent of expression of MT isoforms varies among tissues

- MT synthesis and degradation are both features in determining steady-state cellular MT concentrations
- Zinc transporter activities may influence MT turnover rates through regulation of intracellular zinc pools
- MT knock out mice are in general good health, indicating that MT is not critical for standard development or reproduction
- Basal MT expression is low in wild-type and MT transgenic mice when provided adequate dietary zinc
- MT expression is responsive to a plethora of agents, and frequently accompanies/produces changes in intracellular and extracellular zinc trafficking.

### 2.2.6 Epigenetics of MT

Epigenetics indicates a change in phenotype but not DNA sequence and can occur on several levels such as gene expression. An example for epigenetics is, for instance, a mechanism that either activates or inactivates selective genes involved in specific gene functioning. Gene expression is a well controlled process, where genes are expressed as needed at selected sites, and at required quantities (Sato & Kondoh, 2002). The range of MT gene structure, organisation and evolution of metallothionein, varies in each animal species. MT genes are expressed in most tissues and organisms, and the transcription of these genes is regulated by metals, growth factors, glucocorticoids, cytokines, and stress conditions (Karin *et al.*, 1984). MTs are the most abundant intracellular, metal binding proteins and are expressed in all eukaryotes, including plants, yeast, worms, flies and vertebrates (Andrews, 2000; Ghoshal & Samson, 2001). There are significant quantitative variations in levels of MT expression upon various stimuli. MT expression is induced by a wide range of stressors including not only chemical stressors, such as heavy metals and activated oxygen generators, but also physical stressors and is considered to have a protective effect against the disruption of homeostasis due to environmental stress (Sato & Kondoh, 2002). At more complex levels, MT expression can be altered by changes in gene structure, such as amplification and methylation, and by cellular differentiation

and development. Research has indicated that MTs play a role in intracellular redox potential, activated oxygen detoxification, and sulphur metabolism (Hamer, 1986).

The promoter region of the MT gene consists of glucocorticoid response elements (GREs), which consist of six common *cis*-acting metal response elements (MREs) located in the proximal promoter, the antioxidant response elements, and the elements activated by signal transducers and activators of transcription (STAT) (Ghoshal & Samson, 2001). These elements are present in the upstream region of the chromosome that encodes for the MT gene, and are induced by glucocorticoids, Zn, activated oxygen, and cytokines as shown in Figure 2.8 (Davies & Cousins, 2000). The MRE promoter is considered to be involved in the MT induction by metals, *trans*-activated by transcription factors such as the six zinc-finger MTF-1. MTF-1 regulates Zn-dependent MT-induction as a sensor of Zn concentration of the cytoplasm (Dalton *et al.*, 1997; Bittel *et al.*, 1998; Andrews, 2000). The various non-identical MRE replicas, (MREa-MREg) consist of multiple copies of 13-15 multiple repeats in either orientation and contain the consensus sequence CTC**TGCRCBC**XGCCC, where R is purine, B is any base other than A, X represents G/C, and bold-face residues are absolutely required for heavy metal response (Goshal & Samson, 2001).

Removal of the 3'-UTR causes loss of mRNA and subsequent protein localisation (Chabonon *et al.*, 2004). It has been shown that the 3'-UTR mediated association of MT-1 mRNA with the cytoskeleton around the nucleus is necessary for the nuclear localisation of the MT-1 protein during the G1/S phase transition of the cell cycle (Levadoux-Martin *et al.*, 1999).

Although MTF-1 activity is induced by a variety of heavy metals, only zinc can mediate binding to DNA in a cell-free system. MTF-1 is therefore directly responsive only to zinc, suggesting that zinc activates the protein directly by allosteric interaction. Free zinc will be available to bind MTF-1 and increase its DNA binding and transactivation capabilities. Zinc induction results in increased MTF-1 DNA-binding activity that correlates with increased MT transcription (Haq *et al.*, 2003).

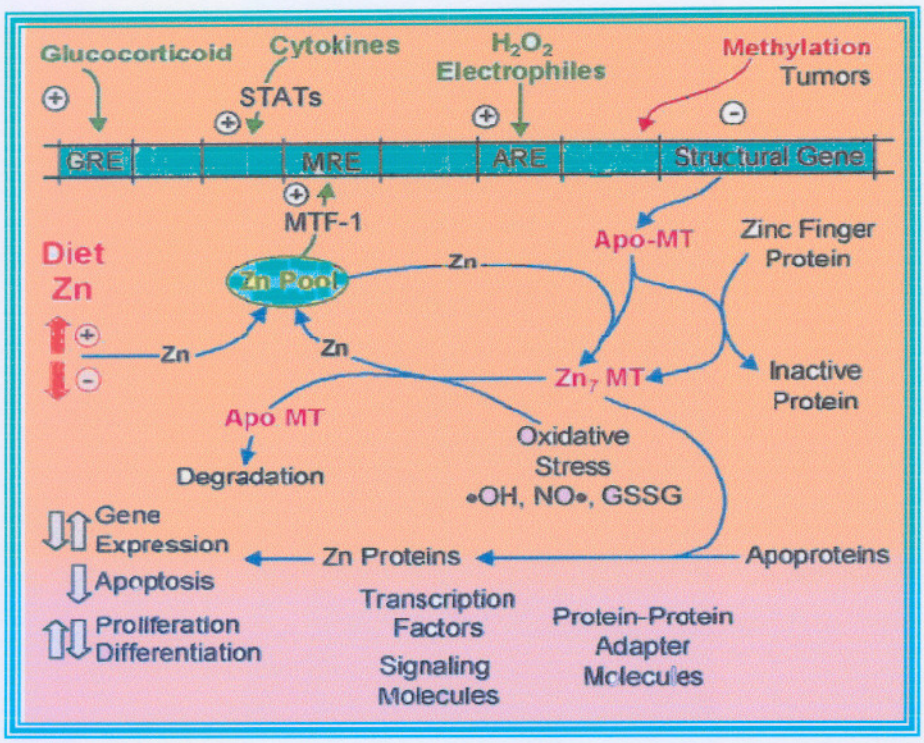


***Figure 2.8. Representation of metallothionein (MT) gene regulation and function.*** *The MT promoter (that regulates transcription) has many response elements, that include; 1. MRE activated by MTF-1 after zinc occupancy, which is dietary zinc supply function. 2. GRE. 3. STAT proteins activated elements through cytokine signalling. 4. ARE activated in response to redox status. Expression may be down regulated through methylation in several tumour cells. Dietary zinc intake and zinc transporter activity influence the cellular zinc pools, which provide a source of zinc bound to MT. MT bound zinc exhibits high thermodynamic stability and kinetic liability. The function of Apo MT (thionein, more rapidly degraded) and Zn7MT is to subtract and donate zinc from or to zinc metalloproteins. Key processes like gene regulation, cell proliferation and differentiation, signal transduction and apoptosis, oxidative damage caused by oxidative stress and electrophiles are all influenced by the cellular MT level through various zinc coordination sites of proteins. (Adapted from Davies and Cousins, 2000).*

### 2.2.7 Radical scavenging properties of metallothioneins

A chemical alteration assay confirmed that MT definitely exists as a mixture of holo- and apoprotein in most tissues (Yang *et al.,* 2001). Both thionein and MT are redox proteins in the cellular environment. Oxidation of sulphur ligands in the zinc/thiolate clusters of MT releases zinc. Biological oxidants such as nitric oxide, disulfides, and peroxide release zinc within the cell (Quesada *et al.,* 1996, Richards, 1989). MT

participates in many redox reactions (Maret &Vallee, 1998). MT exists in many states (Figure 2.9) and is a dynamically regulated protein (Andrews, 2000). Thus, in different cell lines the overall amount of MT varies at least 400-fold (Woo *et al.*, 1997). The ability of MT to capture hydroxyl radicals, which are primarily accountable for the toxicity, is more than 300 times greater than that of glutathione (Sato & Kondoh, 2002; Zhou *et al.*, 2003).

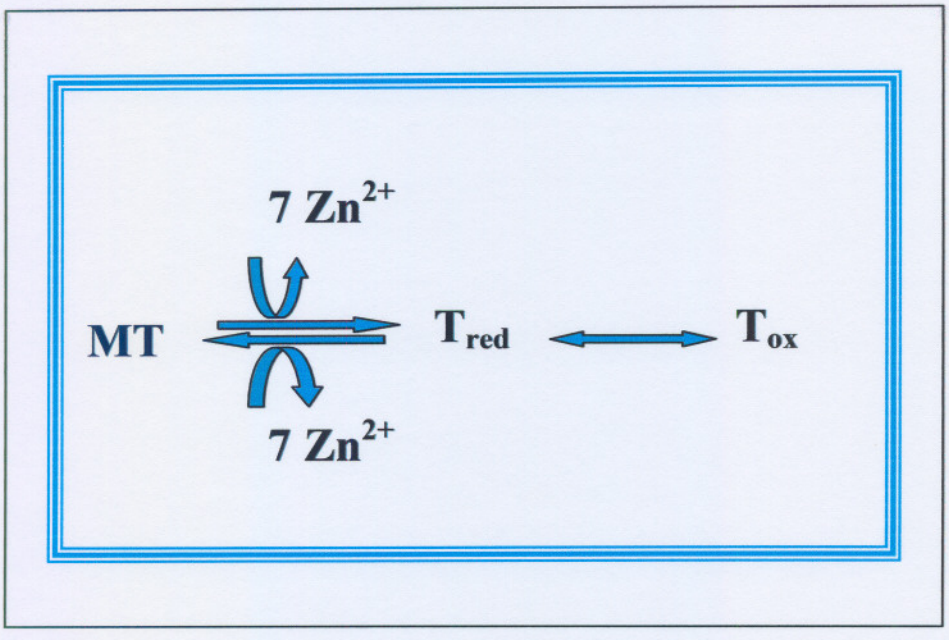


***Figure. 2.9. Different species of MT.*** *There are three evident species of metallothionein: 1: Metal-loaded form (MT), 2: the reduced apo-protein ($T_{red}$), 3: The oxidised apo-protein ($T_{ox}$). The isolation and characterization of partially metallated and/or oxidised forms of metallothionein from normal or pathological tissue remains a challenging analytical difficulty (Haase & Maret, 2004). $MT_{ox}$ is not able to bind to metals, so it does perform a scavenger function (Santon et al., 2004).*

Cu gathers in the liver mostly in the chemical form of Cu-metallothionein, which in this case metallothionein is performing the role as the reducing agent that forms disulfide bonds in $MT_{ox,}$ to reduce cupric to cuprous ions in the Fenton reaction (Suzuki *et al.*, 1999). Once the Cu accumulation in the liver exceeds its ability to induce adequate MT for Cu detoxification, the cupric ions ($Cu^{+}$) induces hepatic dysfunction, and a large amount of Cu-MT accumulated in the liver is then released into the bloodstream. Cu bound to MT is present as long as cells maintain the capacity to synthesise sufficient MT to accommodate Cu and Zn within cells. Cu, Zn-MT functions as an anti-oxidant as long as excess Cu is reduced and sequestered by MT

by replacing Zn (Santon *et al.*, 2004). Zn-metallothionein is an efficient antagonist of cell-damaging lipid peroxidation (Thomas *et al.*, 1986).

## 2.3 Problem statement, hypothesis, strategy, aim and approach

The increased production of ROS due to the complex I deficiencies is a widely accepted event, and has been shown to lead to various other severe consequences, such as DNA, lipid and protein damage. It has been shown in previous studies that metallothioneins have a protective effect in the cytoplasm and nucleus against ROS, either by scavenging ROS or by increasing free zinc levels, which stimulates other cell responses with protective effects. It was recently identified that ROS-sensitive proteins such as metallothioneins (MTs), are expressed in complex I deficient cell lines (*in vitro*) and have a protective effect against ROS-related pathology. It is still not clear if isoform-specific MT expression occurs in this disease and if it plays a significant role *in vivo*.

**The hypothesis that was tested in this study is that an induced complex I deficiency will lead to an increase of MT mRNA expression *in vivo*.** As MTs are expressed in different isoforms in different tissues, MT expression of different isoforms were investigated in four tissue types.

The aim of this study was therefore to investigate the expression of different MT isoforms in rotenone-treated Sprague Dawley rats, an *in vivo* model that has been used to study cell biological responses of mitochondrial complex I deficiency, and to report the tissue differential expression of MT-1 to MT-3 isoforms in complex I deficient brain, liver, heart and skeletal muscle. It is important to note that this study was performed in collaboration with a PhD study that investigated the cell biological consequences of rotenone-treated rats and treatment strategies (Alessandrini, 2006). Tissue samples prepared, as well as key biochemical data generated during that study were used to do the MT expression investigation described in this dissertation.

The strategy design of this study is summarised in Figure 2.10. The experimental outline of this strategy and choice of groups, dose treatment and collection of tissues was fist examined by Rautenbach (2004) in a pilot study where differentiated tissue response to rotenone-induced complex I deficiency in rats was investigated.

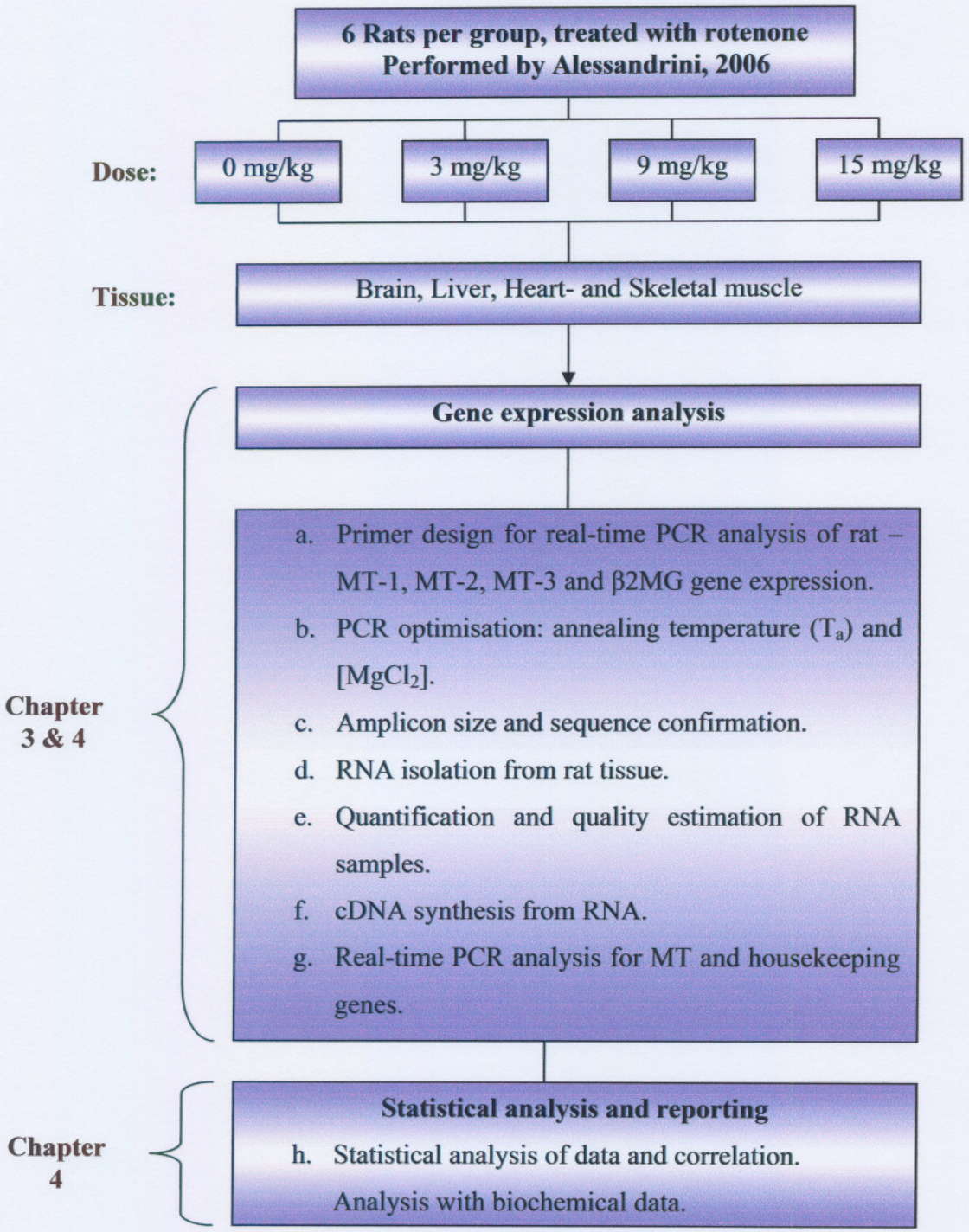


***Figure 2.10:*** *The above strategy was followed to accomplish the objective of this investigation.*

# Chapter Three

## Experimental design and procedure

### 3.1 Introduction

An overview of the experimental strategy was given in Chapter 2. In short, it described the use of tissue obtained from rotenone-treated rats to investigate isoform-specific MT expression. For this RNA expression study it was fortunate that a previous study successfully developed and standardised several techniques that could be used (Olivier, 2004). This included RNA isolation, cDNA synthesis and real-time PCR strategies. The choice of strategy, techniques and certain conditions were therefore to a certain extent an informed choice based on previous results. These did not, however, include choice of primers, PCR optimisation and data analysis, which required new design or optimisation. For the quantification of the RNA transcripts, as described previously, real-time PCR was used. The reasons for this choice are, firstly, because of the homology that exists between MT isoforms which may result in unspecific identification and quantification of transcripts when using hybridization techniques such as northern blot. Secondly, real-time PCR enables the relative quantification of specific transcripts in a fast and effective manner. The apparatus and expertise for this technique was also readily available on our campus.

The exact protocols followed in this study were performed according to the specifications included with the respective kits/reagents utilised, or according to published protocols. Modifications of these protocols are indicated throughout the text. As mentioned in Chapter 2, rotenone-treated rats were used as the *in vivo* model for complex I deficiency. The tissue material for this study was kindly provided by Alessandrini (2006). The precise treatment strategy as well as selected clinical and biochemical characterisations of rotenone-treated Sprague Dawley rats are described in his thesis (Alessandrini, 2006). Table 3.1 summarises the rotenone treatment and rat designation as provided by Mr. Alessandrini and which was subsequently used in this study.

**Table 3.1 Sample designation and rotenone treatment of Sprague Dawley rats**

| Rotenone dose* 0, 3, 9, 15 mg/kg/day | | | |
|---|---|---|---|
| R0-Ar | R3-Ar | R9-Ar | R15-Ar |
| R0-Br | R3-Br | R9-Br | R15-Br |
| R0-Cr | R3-Cr | R9-Cr | R15-Cr |
| R0-Dr | R3-Dr (N/A) | R9-Dr | R15-Dr |
| R0-Er | R3-Er | R9-Er | R15-Er |
| R0-Fr | R3-Fr | R9-Fr | R15-F |

*RX-Yr: R = rotenone dose; X = dose (0,3,9,15 mg/kg/day); Y = rat number (A-F); r = rat. *Four groups of Sprague Dawley rats dosed with various concentrations of rotenone over a period of 14 days. Tissue was collected from whole brain (BR), liver (Li), heart muscle (HM), and skeletal muscle (SM). All tissue samples for R3-Dr were not available (N/A) for use in this study.*

## 3.2 PCR

### 3.2.1 Primer design for PCR

For the design of rat MT isoform specific primers some critical parameters were considered. The first was the length of the primer, which had to be approximately 18-30 bp in length. The base composition had to be 45-60% GC rich (Chen *et al.*, 2003). Primer sequences were also verified for primer dimer formation and self complementarities. The oligonucleotide primer pairs were designed to have equivalent melting temperatures (Chen *et al.*, 2003). The calculated temperature, at which a primer set for a specific reaction is utilised, is known as the calculated mean melting temperature ($T_m$). These parameters for the MT-1, MT-2, MT-3 and β2MG primers used for real-time PCR were evaluated and designed using DNAMAN software (version 4.13, Lynnon BioSoft, Quebec, Canada). The primers were chosen to be in different exons of the gene. This allows the identification when genomic DNA (gDNA) contamination is present as the amplicon will then be larger due to the presence of introns. The amplicon had to be approximately 200 bp in length which makes it suitable for real-time PCR. Finally, the specificity of primers were evaluated using the nucleotide-nucleotide Basic Local Alignment Search Tool (BLAST) from the National Centre for Biotechnology Information (NCBI) from the National Institutes of Health (NIH) at http://www.ncbi.nlm.nih.gov/BLAST/. The primers were only considered if perfect homology with the target gene was obtained and when there

was no significant homology, as defined by the BLAST result, with any other sequence.

PCR, which offers a fast and convenient method of amplifying a specific DNA segment was first described by Mullis (1986). PCR is the basis of various important methods in molecular biology. It can be used to detect very small amounts of DNA and to create customised fragments of DNA. It has been applied to clinical diagnosis and therapy, to forensics and vast numbers of research applications. This technique involves denaturation of the DNA template, primer annealing to a target sequence and strand synthesis. This three step procedure is performed for a number of cycles where the target sequence is exponentially amplified. Table 3.3 shows the basic PCR procedure used in this study. PCR reactions were performed in a total volume of 50 µl in thin walled PCR tubes (Bio-Rad, CA, USA) and consisted of the following components:

- 1 x PCR buffer containing 10 mM Tris-HCl®, pH 9.0 (Fermentas)
- 2.0 to 3.5 mM $MgCl_2$ (Fermentas)
- 1 µl of a (10 mM) dNTP solution (Fermentas)
- 20 pmol of both forward and reverse primer
- 1 U *Taq* DNA polymerase (Promega®)
- 3 µg of reverse transcribed RNA template (cDNA)

The primers listed in Table 3.2, were purchased from Inqaba Biotechnical Industries (Pty) Ltd, Pretoria, which included a calculated melting temperature ($T_m$) value. DNAMAN software program also provided the $T_m$ of each primer set which took complex thermodynamic parameters into consideration as stated in Equation 3.1. The nearest neighbour method utilise the actual sequence to calculate $T_m$.

**Equation 3.1 Calculation of the primer melting temperature with thermodynamic parameters**

$$T_m = H\,[S + R \ln (C/4)] - 273.15\ ^{\circ}C + 16.6 \log_{10} [K^+]$$

*Most software that is designed to calculate $T_m$ values such as DNAMAN provide the melting temperatures of oligonucleotides that are most accurately calculated using nearest neighbour thermodynamic calculations. H is the enthalpy, S is the entropy for helix formation, R is the molar gas constant, and C is the concentration of primer.*

An equation used most often to determine the $T_m$ value, is that of Thein and Wallace (1986) as presented in Equation 3.2, where the adenine/thymine (A+T) and guanine/cytosine (G+C) content is calculated to determine the $T_m$ value and does not include complex thermodynamic parameters.

**Equation 3.2 Calculation of the primer melting temperature without thermodynamic parameters**

$$T_m = [(A+T) \times 2^{\circ}C] + [(G+C) \times 4^{\circ}C]$$

*Most frequently used equation for calculating $T_m$ values. The nucleotides, adenine (A), thymine (T), guanine (G), cytosine (C) form part of the primer sequence. (Thein and Wallace, 1986).*

However, in general, PCR conditions used for amplification are optimised from a temperature approximately 2 °C or more below that of the $T_m$ value. This estimated annealing temperature ($T_a$) of the primer set can serve as a starting point from where the experimental annealing temperature can be increased or decreased to achieve optimal amplification. Table 3.2 also indicates the annealing temperatures used for primer pairs in this study. The equation for the calculation of $T_a$ is presented in Equation 3.3. The position of the primers designed in this study is illustrated in Figure 3.1, for rat MT-1 to MT-3 and β2MG.

**Equation 3.3 Calculation of estimated annealing temperature of primer sets**

$$T_a = \text{Mean } T_m - 2^{\circ}C$$

*$T_a$ = experimental annealing temperature of primer set in °C; Mean $T_m$ = the mean melting temperature of the primer set in °C.*

Table 3.2 summarises the primer sequences, annealing temperatures for primer pairs, as well as amplicon size. The equation for the calculation of $T_a$ is presented in Equation 3.3.

**Table 3.2 Sequences of primers used for Real-time PCR**

| Primer | Primer sequence 5'-3' | $T_m$ (°C) | $T_a$ (°C) | Size (bp) | Amplicon size (bp) |
|---|---|---|---|---|---|
| **F:** MT1-F | ccccaactgctcctgctccac | 60 | 59 | 21 | 186 |
| **R:** MT1-R | tcacttcaggcacagcacg | 62 | 59 | 19 | |
| **F:** MT2-F | tgatctccaactgccgcct | 62 | 61 | 19 | 205 |
| **R:** MT2-R | cagctgcacttgtccgaagc | 64 | 61 | 20 | |
| **F:** MT3-F | gcctggatatggaccctgaga | 64 | 62 | 21 | 251 |
| **R:** MT3-R | cagggacacgcagcactattc | 64 | 62 | 21 | |
| **F:** β-2MG-F | tcgtgcttgccattcagaaa | 58 | 57 | 20 | 212 |
| **R:** β-2MG-R | gtgagccaggatgtagaaa | 60 | 57 | 19 | |

*For each set of forward (F) and reverse (R) primers the average calculated melting temperature, $T_m$, as well as the experimental annealing temperature, $T_a$ is indicated. The expected amplicon sizes for each primer set using cDNA templates are listed.*

The sequences and positions of the annealing sites of the primers, as well as the reading frame are indicated in Figure 3.1. The sequences amplified for MT-1 to MT-3 cDNA is 186 bp, 205 bp and 251 bp respectively, and 212 bp for housekeeping gene β2MG.

| A<br>Nucleotide number | **Sequence of *Rattus norvegicus* (Norway rat) for MT-1** |
|---|---|
| 1<br>61<br>121<br>181<br>241<br>301<br>361 | tcccgacttc agcagcccga ctgccttctt gtcgcttaca ccgttgctcc agattcacca<br>gatctcggaa tggaccccaa ctgctcctgc tccaccggcg gctcctgcac ctgctccagc<br>tcctgcggct gcaagaactg caaatgcacc tcctgcaaga agagctgctg ctcctgctgc<br>cccgtgggct gctccaaatg tgcccagggc tgtgtctgca aaggtgcctc ggacaagtgc<br>acgtgctgtg cctgaagtga cgaacagtgc tgctgccctc aggtgtaaat aatttccgga<br>ccaactcaga gtcttgccgt acacctccac ccagtttact aaaccccgtt ttctaccgag<br>catgtgaata ataaaagcct gtttattct |
| **B**<br>**Nucleotide number** | **Sequence of *Rattus norvegicus* (Norway rat) for MT-2** |
| 1<br>61<br>121<br>181<br>241 | gaactctaca gcgatctctc gttgatctcc aactgccgcc tccattcgcc atggacccca<br>actgctcctg tgccacagat ggatcctgct cctgcgctgg ctcctgacaa atgcaaacaa<br>tgcaaatgca cctcctgcaa gaaaagctgc tgttcctgct gccccgtggg ctgtgcgaag<br>tgctcccagg gctgcatctg caaagaggct tcggacaagt gcagctgctg cgcctgaagt<br>gggggcgtcc tcacaatggt gtaaataaaa caacgtaagg aacctagcc |
| **C**<br>**Nucleotide number** | **Sequence of *Rattus norvegicus* (Norway rat) for MT-3** |
| 1<br>61<br>121<br>181<br>241<br>301<br>361 | gggacgcagc gcatccgctt gcctggagga actaagctac agtctctcgc ggctgctggc<br>ctggatatgg accctgagac ctgcccctgt cctactggtg gttcctgcac ctgctcggac<br>aaatgcaaat gcaagggctg caaatgcacg aactgcaaga agagctgctg ctcctgttgc<br>cctgcaggat gtgagaagtg tgccaaggac tgtgtttgca aaggcgaaga gggggccaag<br>gccgagaaat gcagctgctg ccagtgagga ctcccacaca gcctatgtga atagtgctgc<br>gtgtccctgg tggggcgtgg ctgttgcccc cctccctggc ttcctgctcc gggggtgtga<br>ataaatccca tgcacagcaa aaaaaaaaaa aaaaaaaaaa aaaaaaaa |
| **D**<br>**Nucleotide number** | **Sequence of *Rattus norvegicus* (Norway rat) for β2MG** |
| 1<br>61<br>121<br>181<br>241<br>301<br>361<br>421<br>481<br>541<br>601 | cggcacgatg gctcgctcgg tgaccgtgat ctttctggtg cttgtctctc tggccgtcgt<br>gcttgccatt cagaaaactc cccaaattca agtgtactct cgccatccac cggagaatgg<br>gaagcccaac ttcctcaact gctacgtgtc tcagttccac ccacctcaga tagaaattga<br>gctactgaag aatggaaaga agataccaaa tatcgagatg tcagatctgt ccttcagcaa<br>ggactggtct ttctacatcc tggctcacac tgaattcaca cccaccgaga ccgatgtata<br>tgcttgcaga gttaaacacg tcactctgaa ggagcccaaa accgtcacct gggaccgaga<br>catgtaatca agctctatgg agctctgaat catctggacc agtttaactc cagatccggt<br>ttctaatatg ctatacaatt tatccacaaa gtaaagaata gcaatgagca caccatcttc<br>ttcatatctt accttaaata ttttatgcat gttttaaaaa aaattggaga ctaatatcct<br>agatttccgg aataataaag cttcaatgag tgttttgatc agaataataa atatggttaa<br>gaac |

***Figure 3.1. cDNA sequence of rat MT-1 (A)*** *GenBank accession number NM_138826.* ***MT-2 (B)*** *GenBank accession number M11794.* ***MT-3(C)*** *GenBank accession number NM_053968 and* ***β2MG (D)*** *GenBank accession number NM_012512. The sequence of the forward primer is highlighted in yellow, and the position for the reverse primer is highlighted in blue. The underlined text indicates both the initiation codon (solid straight line) and stop codon (dashed straight line) respectively, which indicates the sequence of the gene's reading frame.*

Detection of PCR amplicons was carried out by performing agarose gel electrophoresis and EtBr staining using 1% (w/v) mini and midi agarose gel. Various types of DNA molecular weight markers were used to estimate the size of DNA fragments. A 100 or 50 bp molecular weight marker consisting of bacteriophage λ DNA which was cleaved with a restriction enzyme *Eco*RI has been synthetically prepared in the Mitochondrial Research laboratory (MRL) and was used for the estimation of the sizes of the smaller fragments. The mini 1% agarose gel was made up to a final volume of 30 ml. Agarose gel prepared for the amplification products contained 0.3 g analytical grade agarose, 30 ml of 1 x TAE buffer (Tris-acetate) composition and 3 µl of 10 $g.mol^{-1}$ EtBr. The PCR product was added to loading buffer composed of bromophenol blue, and electrophoresis was carried out for approximately 30 to 50 minutes at 10 volts per centimetre (V/cm) in 1 x TAE buffer. The fragments were visualised by illumination with ultraviolet (UV) light and the images were documented by means of a gel documentation system, ChemiGenius using the Genecaptive software programme.

**Table 3.3 Standard PCR procedure and reaction conditions**

| PCR step | Number of cycles | Action | Temperature (°C) | Duration (min) |
|---|---|---|---|---|
| 1 | 1 | Denaturation | 94 | 5:00 |
| 2 | 30 | Primer annealing | X | 1:00 |
| | | Extension | 72 | 0:40 |
| | | Denaturation | 94 | 1:00 |
| 3 | 1 | Final extension | 72 | 10:00 |
| 4 | 1 | Cooling | 4 | Hold |

*X indicates the specific $T_a$ for each primer set indicated in Table 3.2.*

Plasmids containing cloned rat MT-1, MT-2 and MT-3 cDNA were kindly provided by Dr. Juan Hidalgo (University of Barcelona, Spain) for use as positive controls for PCR of the respective MT isoforms in this study. The identity of the base vector of the

plasmids was not provided in accordance with the agreement on the use of these plasmids. These plasmids were also used for the optimisation of PCR conditions. β2MG amplification conditions were standardised on cDNA prepared from RNA samples. Two critical parameters were optimised for the amplification of target cDNA (MT and β2MG) in this study. These were the primer $T_a$ and $MgCl_2$ concentration. The $T_a$ for each primer set (Table 3.2) was firstly optimised using a range of temperatures spanning the melting temperature of the primer pairs. After establishing an ideal $T_a$, $MgCl_2$ concentration was optimised over a range of 2.0 mM to 3.5 mM, depending on the MT isoform in question. The criteria for choosing a optimal annealing temperature was that only one DNA fragment of correct size was observed and that the visual amount of the fragment was the highest in the particular set of optimisation reactions. The optimal annealing temperatures are discussed in Chapter Four.

### 3.2.2 Verification of MT amplicon sequences

The most commonly used method for DNA sequencing, the dideoxy method which was first described by Sanger *et al.* (1977) was used to determine the sequence of MT-1 to MT-3 and β2MG cDNA. This method utilises analogues of 2',3'-dideoxynucleotide triphosphates (ddNTP) that lack a 3'-OH group which is necessary for the formation of phosphodiester bonds. Consequently, the DNA chain is specifically terminated at the position where a ddNTP is incorporated. This process is also known as the chain termination method (Alphey, 1997). The amplicons that were sequenced in this study were prepared as described in Section 3.2.1. The sequencing reaction as well as analysis was performed by Inqaba Biotechnical Industries (Pty) Ltd., Pretoria.

The sequencing done for this investigation is essentially the same as that described by Sanger *et al.* (1977) with the exception that the dideoxy nucleotides are fluorescently labelled. Four colours; red, green, blue and black were each assigned to represent one of the four nucleotides that were detected under the UV light. With the use of capillary electrophoresis, the different fluorophores are detected because of their different emission spectra. Fragments can be identified by size as smaller fragments migrate faster through the column compared to larger fragments. The cycle

sequencing consists of the same basic four steps as described for PCR in Table 3.3 in Section 3.2.1. The various amplicons were sequenced using both forward and reverse primers in separate sequencing reactions. This was done to get sequence data at close proximity to the primer annealing sites and to verify sequences obtained.

## 3.3 RNA extraction

For the isolation of RNA, the phenol/chloroform/guanidine isothionate extraction method, using the QIAzol™ reagent (QIAGEN, Hilden, Germany) was utilised. In this method total RNA is prepared, including the relatively small MT RNA transcripts, and was successfully used in the preliminary studies by Olivier (2004) and Reinecke (2006). For the RNA preparation procedures all plastic consumables were nuclease-free as marked by the supplier Eppendorf ® (Eppendorf AG, Hamburg, Germany). Further precautions for the handling of RNA were taken as suggested by QIAGEN. The extraction method was performed as described by the manufacturer of the reagent. Although some modifications to the procedure were made such as additional tube transfer and washing steps. The modifications such as transferring samples to new sterile centrifuge tubes and adding an additional washing step to the extraction methods are also indicated and discussed in full detail in the following section.

Different rat tissue (brain, liver, heart muscle and skeletal muscle) as provided by Alessandrini (2006) were stored at -70°C. Frozen animal tissues were not allowed to thaw during handling by keeping it in a flask containing liquid nitrogen. Before RNA isolation, a small piece of approximately 100 mg was cut off each frozen tissue sample and placed into a microcentrifuge tube. Tissue samples were lysed by adding 1 ml of QIAzol™ Lysis Reagent. Samples were homogenised manually in the microcentrifuge tubes by using a small Potter-Elvehjem-type teflon pestle after which samples were further disrupted by pipetting. For dissociation of nucleoprotein complexes the samples were incubated for 5 min at room temperature. After incubation, 0.2 ml chloroform (HOLPRO Analytic Division, Midrand, South Africa) was added followed by shaking samples vigorously for 15 seconds. The homogenates were incubated at room temperature for 3 min before centrifugation at 12 000 x g for

15 min at 4°C. After centrifugation, each sample was separated into three phases, an upper colourless aqueous phase containing the RNA, a white interphase, and a lower, red, organic phase. The upper aqueous phases were transferred into sterile microcentrifuge tubes before 0.5 ml of isopropanol (HOLPRO Analytic Division, Midrand, South Africa) was added. The tubes were mixed thoroughly by vortexing, followed by incubating samples for 10 min at room temperature. After the 10 min incubation period, to ensure the sterility of the environment the RNA was isolated in, the samples were yet again transferred to sterile microcentrifuge tubes before they were centrifugated at 12 000 x g for 10 min at 4°C. Supernatants were carefully removed from the RNA pellets which were visible as a white pellet at the bottom of each tube. To the pellets, 1 ml of 75 % ethanol (EtOH) (LABCHEM) was added to remove any remaining salts from the pellets and a final centrifugation step at 7500 x g for 5 min at 4°C was performed. This washing step was repeated once more. The supernatants were carefully discarded by inversion of the tubes before the pellets were allowed to air dry for approximately 30 min. The pellets were redissolved in 100 µl of RNAase free diethyl pyrocarbonate (DEPC) treated water, which was prepared as described by Maniatis *et al.*, 1982.

### 3.3.1 Evaluation of RNA yield and purity

The RNA concentration of the total isolated RNA samples were estimated by measuring the absorbance at 260 nm by ultraviolet (UV) spectrophotometry using a BIO-TEK Instruments Uvikon XS double beam spectrophotometer and were calculated using the equation presented in Equation 3.4 (Maniatis *et al.*, 1982). To determine whether the samples were contaminated with protein, the purity of the samples were estimated with the ratio of readings at 260 nm and 280 nm ($OD_{260}/OD_{280}$). Values of approximately 1.7 to 1.9 were considered sufficiently pure RNA preparations with little contamination of protein. The RNA integrity was estimated by electrophoresis and ethidium bromide staining with an agarose gel containing formaldehyde to denature the secondary structure of RNA. The relative intensities of the 28S and 18S rRNA fragments, slightly visible tRNA fragments as well as 5S RNA lower on the gel and the lack of high molecular weight DNA was

used as an indication of relatively good quality RNA samples suitable for cDNA synthesis that is discussed in Section 3.3.2

**Equation 3.4 Calculation of the total RNA concentration**

$$[RNA] \text{ in } \mu g.\mu l^{-1} = (A_{260}-A_{320}) \times 40 \text{ ng}.\mu l^{-1} \times \text{dilution factor} / 1000$$

*RNA concentration and $A_{260}$, absorbance values of samples at 260 nm. $A_{320}$, absorbance values of samples at 320 nm. (Maniatis et al., 1982).*

### 3.3.2 cDNA Preparation

For the synthesis of cDNA from RNA templates a two-step RT-PCR (reverse transcriptase polymerase chain reaction) strategy was used. This entailed the priming of RNA templates using random hexamers and reverse polymerase to synthesise a first strand cDNA. This was done in the following way: a reaction mixture containing 1 µl of 0.5 µg of random hexamer primers (Promega®) were added to 3 µg of isolated RNA in a PCR tube and incubated at 70°C for 5 min. The PCR tube was placed directly on ice for a few minutes to allow primer annealing. To this tube a reaction mixture, composing of 1.25 µl dNTPs (Fermentas), 1 µl MMLV RT (Moloney Murine Leukemia Virus Reverse Transcriptase 200 units, Promega®), 5 µl MLV buffer (Promega®) and diethyl pyrocarbonate (DEPC) treated $H_2O$ to a final volume of 50 µl was added to the sample. The first strand cDNA synthesis was performed in a Thermo Hybaid Cycler® (Bio-Rad, CA, USA), using an extension cycle at 37 °C for 60 minutes followed by an enzyme activation step at 80 °C for 10 minutes. To determine whether the cDNA synthesis was successful, the subsequent PCR that was performed and formation of amplicons was evaluated by means of agarose gel electrophoresis. The cDNA preparations were stored at -20 °C until used for real-time PCR.

### 3.3.3 Expression analysis of metallothionein RNA using semi-quantitave real-time PCR

This method involves detection of the binding of a fluorescent dye (SYBR® Green) to double stranded DNA (dsDNA) during PCR. SYBR® Green is a fluorogenic minor

groove-binding dye that exhibits little fluorescence when in solution. It binds to the nascent double stranded DNA and emits a strong fluorescent signal with an excitation and emission maxima at 494 nm and 521 nm, respectively. During denaturation, the dye dissociates and fluorescence measurements are only performed during the extension step on every dsDNA. Signal intensities increase with cycle number due to the accumulation of the PCR product. Relative quantification of gene expression levels can be calculated by determining the ratio between the amount of a target gene and one or more endogenous reference genes, such as β-2-microglobulin (Bustin, 2000). For this study β-2-microglobulin was chosen as reference gene as this gene was shown to be one of five genes wherein stable expression was observed during a similar intervention *in vitro* study (Olivier, 2004). To assess the relative expression levels of rat MT-1, MT-2, and MT-3, quantitative real-time PCR was performed with specific primer sets as listed in Table 3.2.

The 75 ng cDNA samples that were stored at -20 °C for real-time PCR were used in a reaction, containing 10 µl iQ™ SYBR® Green Supermix, 20 pmol of forward and reverse primers (Table 3.2), 1µl ( ± 75 ng) of prepared cDNA, and 8 µl RNase-free water in thin wall PCR tubes (Bio-Rad, CA, USA) to a final volume of 20 µl. The reactions were subjected to the PCR conditions listed in Table 3.4. Real-time PCR was carried out with the iCycler iQ™ (Bio-Rad, CA, USA) and iCycler iQ Real-time Detection System Software, version 3.0 (Bio-Rad, CA, USA) was used to visualize and analyse the results.

**Table 3.4 Real-time PCR conditions**

| PCR step | Number of cycles | Action | Temperature (°C) | Duration (min) |
|---|---|---|---|---|
| 1 | 1 | Denaturation | 95 | 3:00 |
| 2 | 30 | Denaturation | 95 | 0:20 |
| | | Primer Annealing † | X† | 0:10 |
| | | Extension | 72 | 0:20 |
| | | Fluorescence measurement | 82 | 0:05 |
| 3 | 1 | Extension | 72 | 5:00 |
| | | Denaturation | 95 | 1:00 |
| 4 | 1 | Extension | 55 | 1:00 |
| 5 | 80 | Melting curve program* | 55-95 | 0:05 |
| 6 | 1 | Cooling | 4 | Hold |

**The melting curve program (step 5) occurred at a heating rate of 0.5 °C per 5 seconds. † Primer annealing, X = variable for $T_a$ specific for each set of samples*

The melting curve analysis is a dynamic tool used to measure the melting temperature of dsDNA molecules. The use of this analysis is based on the fact that the melting temperature is specific to a particular dsDNA amplicon. Therefore, the appearance of more than one peak on the curve will be an indication of the formation of more than one amplicon which may occur when unspecific primer hybridization occurs. One of the most important determinants for accurate real-time PCR is establishing the specificity of the primers chosen for amplification as discussed in Section 3.2.1. A particular primer pair may induce primer dimer formation and/or amplify other non-specific products. In turn, these non-specific products can greatly reduce amplification efficiency as well as diminish the overall dynamic range of a standard curve. Specificity was thus ensured through the assurance of correct primer pairs by means of sequencing analysis. Therefore, identification of all products amplified by a particular primer pair would be useful for optimisation of real-time PCR assays. To

ensure effective quantitative real-time PCR results the following steps were pursued since quantitative PCR is a very sensitive technique:

a) A disinfected sterile work surface was set aside for only quantitative PCR.
b) Disinfected gloves were worn at all times and changed regularly.
c) Particular autoclaved quantitative real-time PCR tubes (Bio-Rad, CA, USA) with caps were utilised for analysis.
d) Sterilised filter tips and a calibrated micropipette dedicated for quantitative PCR was utilised.
e) Only autoclaved MilliQ water was used.
f) A no-template control for each reaction set was used for verification of the absence of contaminating templates.
g) All reactions were performed in triplicate from a sufficient volume of master mix which contained all the reaction components. All the samples were aliquoted one tube at a time.

The real-time software determined a cycle threshold (Ct) value, which was defined as the number of PCR cycles where the fluorescence signal exceeds a specifically assigned detection threshold value for that sample. The threshold should be set (either manually or automatically) when the product is in exponential phase. The threshold is set after the background noise of the particular gene has been discarded. This threshold was set to the logarithmic linear range of the amplification curve and kept constant for data analysis throughout the study. During real-time PCR the amount of PCR product at each cycle was quantified and the threshold detection was used for relative abundance quantification. To ensure comparability between the analyses, PCR efficiency for each primer set was calculated by the comparative Ct method by measuring serial dilutions of ± 75 ng cDNA in triplicate, using REST software tool (Pfaffl *et al.*, 2002). Every assay included a no-template control, five serial dilution points (in steps of 5 folds) of a cDNA mixture, as well as each of the test cDNA's. The PCR reactions have shown efficiencies between 87 % - 99 %. After the PCR efficiencies were established and a set threshold value was determined the quantitative analysis were performed on the rat tissue samples. All samples were amplified in triplicate and the mean value was used for further calculations. As mentioned before, β-2-microglobulin was utilised for normalisation of MT-1, MT-2, and MT-3

expression performed with individual samples. A normalisation factor was calculated from the Ct values of each of the samples from the triplicate set of reactions. The equation set employed for quantitative PCR data is shown in Equation set 3.5.

**Equation set 3.5 Calculation of relative expression of MT-1, MT-2, and MT-3**

(1) - $$SD_{Ct} = \sqrt{\frac{sum(x - mn)^2}{n-1}}$$

(2) - $$E = 10^{(-1/S)} - 1$$

(3) - $$Q = E^{\Delta Ct}$$

(4) - $$Q = E^{(\text{minCt-SampleCt})}$$

(5) - $$SD_Q = E^{\Delta Ct}.\ln E.SD_{sampleCt}$$

(6) - $$NF_n = \sqrt[n]{Q_{HG1}xQ_{HG2}x....xQ_{HGn}}$$

(7) - $$SD_{NFn} = \sqrt{\left(\frac{SD_{QHG1}}{n.Q_{HG1}}\right)^2 + ... + \left(\frac{SD_{QHGn}}{n.Q_{HGn}}\right)^2}$$

(8) - $$NE = \frac{Q}{NF}$$

(9) - $$SD_{NEn} = NE_n.\ \sqrt{\left(\frac{SD_{NFn}}{NF_n}\right)^2 + \left(\frac{SD_{Qn}}{Q_n}\right)^2}$$

*Each real-time PCR sample run is done in triplicate, resulting in three Ct values. Thus the mean of the Ct values and standard deviation was calculated. SD = standard deviation. Ct = cycle threshold. Express Ct values as relative expression quantities. E = amplification efficiency (2 = 100%). S = Slope of standard curve of ΔCt against log ng total RNA utilised. ΔCt = lowest Ct value minus Ct value of sample. Q = relative quantity (sample quantity relative to sample with highest expression). Ln E = natural logarithm of the amplification efficiency. NF = normalisation factor based on number (n) of housekeeping genes. n = number of housekeeping genes utilised. NE = Normalised expression of target genes (MT-1, MT-2, and MT-3). HG = Housekeeping gene (Vandescompele et al., 2002; Pfaffl et al., 2002).*

## 3.4 Statistical analysis and presentation of data

Advanced computer programmes namely STATISTICA version 7.1, StatSoft, Inc. (2005) was used to perform statistical tests on the data. Statistical analyses were

performed on the data normalised to the housekeeping gene, although in Tables 4.3, 4.7 and 4.12 the expression ratios were calculated relative to the baseline (control) group. A one-way analysis of variance (ANOVA) was performed on the data to detect differences between the means of the expression values for brain, liver, skeletal muscle and heart muscle for the given rotenone concentrations of 0, 3, 9, 15 mg/kg/day. The assumptions of the data according to this method of analysis were met if the data complied with two stipulations i.e.

(1) Variance of the given group, 0, 3, 9, 15 mg/kg/day at a given MT isoform (MT-1 to MT-3) must be equal respectively for brain, liver, skeletal muscle, and heart muscle. This analysis is done by performing the Bartlett test.

(2) Data must be normally distributed (by performing a normality test on residuals). If data were normally distributed the probability of outliers occurring were disregarded. If normality did not hold, and/or variances were not equal, a non-parametric test was performed. Thus, if the assumptions for an ANOVA were not met, the non-parametric Kruskal-Wallis test was done, followed by non-parametric multiple comparisons. In this case it is better to present the data with Boxplots, however it was not used in this study for consistency purposes.

The ANOVA was followed by a Post hoc analysis namely the Tukey studentised range (HSD) test for unequal groups. This test was performed due to unequal cohorts in dose group 3 mg/kg/day. The significant level was set at 0.05. All statistically significant data were defined at a 5% level of significance i.e. $p < 0.05$. In this study the level of confidence was selected at 95%, which is highly recommended for empirical work (Steyn *et al.*, 1998). A post hoc test has been performed to compare group means in a pairwise manner. If data was statistically significant, Cohen's effect sizes were calculated to determine if the differences were practically significant i.e. indicating the biological worth of the data. In this case practical significance was determined by calculating the difference between the two means divided by the root of the mean square error (MSE) from the ANOVA. The formula to calculate practical significance between $\bar{x}_i$ and $\bar{x}_j$ is given in Equation 3.6.

**Equation 3.6 Formula for practical significance of effect sizes for means**

$$d = \left| \frac{\bar{x}_i - \bar{x}_{\cdot}}{\sqrt{MSE}} \right|$$

*Adapted from Ellis and Steyn, 2003.*

Correlation of biochemical parameter measurement between MT expression and CI activity was determined by calculating Spearman rank correlation for monotone relationships and Pearson product moment correlation for linear relationships.

# Chapter Four

# Results and discussion

## 4.1 Introduction

Methods used in the analysis of data and experimental design were discussed in Chapter Three. The optimisation of the different protocols will be discussed briefly in this chapter. All results obtained in this study will be presented either graphically or in tabular form and followed by short discussions to explain how the results were interpreted.

## 4.2 PCR optimisation

PCR conditions were optimised by optimising annealing temperatures, and $MgCl_2$ concentration was kept at a specific range from 2.0 mM to 3.5 mM. In addition to the obvious importance of determining the optimal annealing temperature it is also very important to determine the optimal $MgCl_2$ concentration for a reaction because $MgCl_2$ facilitates the enzyme to make a PCR product. The optimisation of the amplification of the different isoforms of MT at various annealing temperatures and $MgCl_2$ concentrations is photographically illustrated in Figures 4.1 to 4.8. The most ideal/effective $T_a$ and $MgCl_2$ concentration for a specific primer set was chosen on the amplification of only one correct size DNA fragment (amplicon) and the visual intensity of the fragment. The optimal annealing temperatures for each of the primer pairs were summarised in Table 3.2.

Separation of nucleic acids was performed by agarose gel electrophoresis, separating nucleic acid macromolecules by their size and charge. This is achieved due to the resistance of their movement caused by the gel matrix. Shorter or smaller molecules migrate through the agarose matrix faster and unhindered thus travelling farther in a given time period. Larger molecules will have more difficulty passing through the gel pores. As these molecules migrate at a certain speed it forms a fragment when stained with EtBr. Through the process of electrophoresis the agarose gel separates DNA

molecules according to size. The electrophoretic mobility of a DNA fragment allows for the estimation of the molecular mass ($M_r$) of DNA by running a number of standard molecular weight markers of known $M_r$ on the same gel (Wilson & Walker, 2000). Thus, in this study the molecular weight marker served as a size standard for comparison. This was accomplished by running a sample of bacteriophage λ DNA cleaved with a restriction enzyme, *Eco*RI on the same gel.

During this study the gels were submerged in the 1 x TAE buffer solution. The buffer solution contains ions which conduct electrical charges. The nucleic acid is negatively charged and migrates toward the positive anode. The speed with which the DNA moves through the gel is determined by the size of the DNA fragment and voltage set for the experiment. Prior to loading the samples, the DNA was mixed with a loading dye containing glycerol and bromophenol blue. The loading dye increased the density of the DNA sample, allowing it to sink to the bottom of the wells. The bromophenol blue served as visual marker indicating how far the DNA (which was not visible) had migrated through the gel. Primers for the housekeeping gene, GAPDH were designed and tested in all tissue for expression. PCR for GAPDH failed to make a clear and reproducible fragment and was therefore not used in this study. Only β2MG was used as a housekeeping gene for normalisation as it proved to be expressed in all the tissues.

The optimised conditions described in this section were used to investigate the presence of cDNA, prepared from RNA samples isolated from rat tissues. Figures of gel representations of the electrophoresis experiments are given, and the proposed optimal parameters are indicated in bold type. The contrast and resolution for each figure has been adjusted to make the representation of the gel more visible. The unedited versions of these gel representations will be given in appendix A. The negative control (lacking template) was only loaded with the optimisation of $MgCl_2$. Negative controls were run with all the real-time PCR samples. Some resolution of the photographic representations was lost due to electronic formatting and importing.

The results for the optimisation of $T_a$ for MT-1 are portrayed in Figure 4.1. This image shows an ethidium bromide-stained gel of five PCR reactions run parallel in individual lanes. This image portrays a clear and single fragment in lane 6 at $T_a$ =

60°C of approximately 186 bp. Surprisingly, only one fragment was generated at 60 °C, and no amplification was observed at any of the lower temperatures. This $T_a$ value was subsequently used in this study. A small discrete less visible fragment is shown just below 186 bp. This phenomenon was commonly observed in most of the amplicons detected during this study as can be viewed in following figures. This fragment was probably not a non-specific or secondary product, in view of the melting curve analysis that clearly showed one melting temperature optimum for each real-time PCR (results not shown). The reason for this phenomenon is not clear. Very slight smearing and fragments are observed in lane 7. Smearing that can be observed in this and most of the other agarose gels can be a result of the quality of primers that was used. These primers were not additionally purified, and contain incomplete smaller primers formed during synthesis which then may result in a wide range of unspecific amplification. As these two common observations occurred often in following figures, it will not be mentioned or discussed further. This, however, should not have an effect on the real-time PCR values as the possible background effect that this might lead to should be excluded due to the threshold setting that is implemented. As a result, background signals do not contribute to the Ct value. Another aspect that will be observed in following figures is that in some of them the primers are not visible. Unfortunately when taking the pictures for these photographic representations the area that showed the primers was not included, as they should have been.

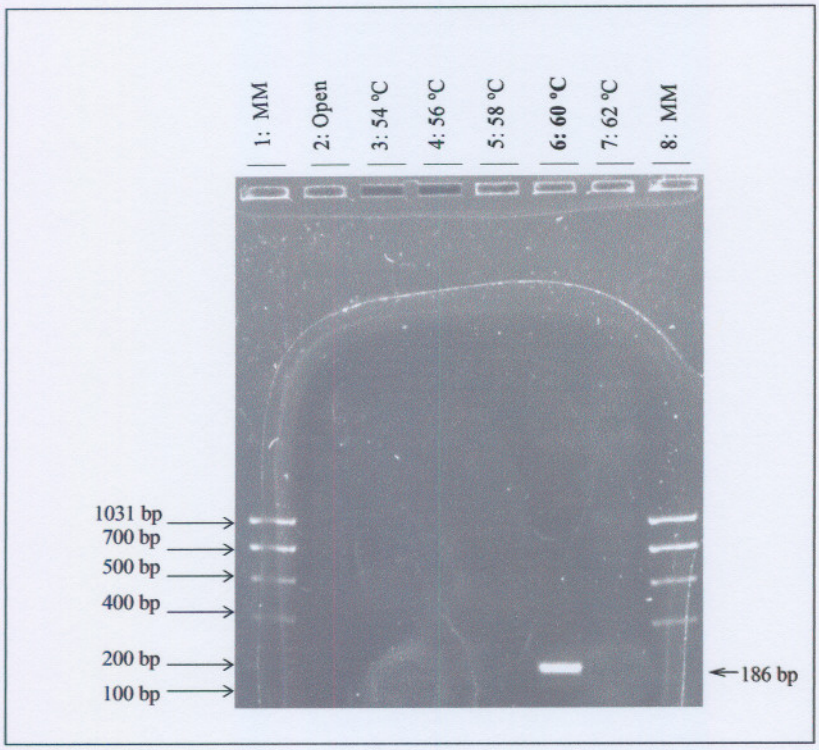


***Figure 4.1. Optimisation of $T_a$ for MT-1 PCR.*** *This figure shows a photographic representation of a 1% agarose gel with EtBr staining, where 10 µl of five PCR reactions for MT-1 at different $T_a$ were loaded. The reactions were loaded as indicated above. The fragment sizes (bp) are indicated with arrows. The lane indicated in bold type illustrates the most optimal $T_a$ as discussed in the text. MM = molecular marker. The image control of this picture was formatted and set at a brightness of 77 % and contrast of 77 %.*

The results for the optimisation of $MgCl_2$ concentration for MT-1 are portrayed in Figure 4.2. This image shows an ethidium bromide-stained gel of five PCR reactions run parallel in individual lanes. The negative control showed no amplicon formation. Only lane 5 shows one visible fragment. This image portrays a clear and single fragment of approximately 186 bp in lane 5 at 2.5 mM $MgCl_2$ concentration.

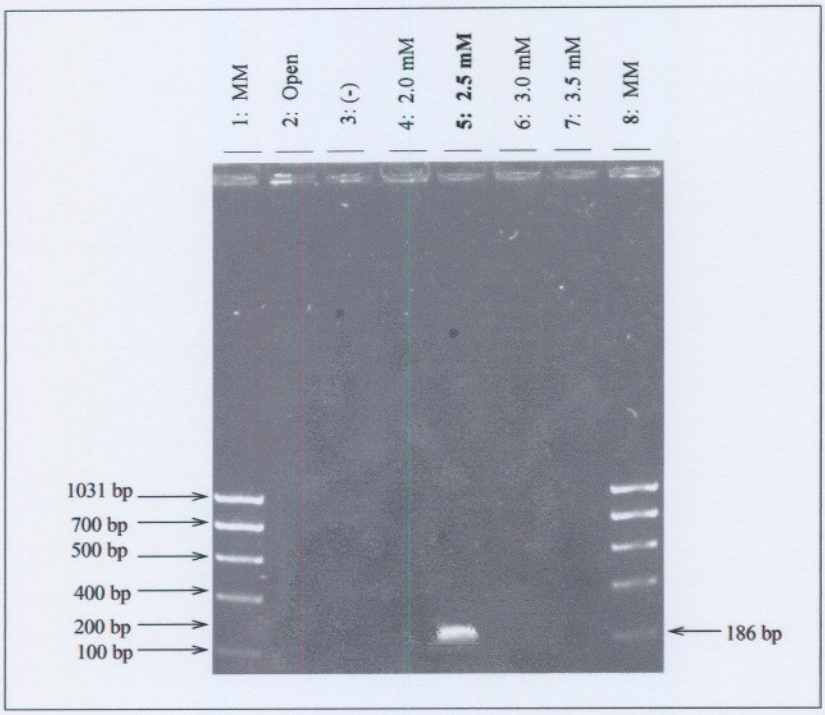


***Figure 4.2. Optimisation of $MgCl_2$ concentration for MT-1 PCR.*** *This figure shows a photographic representation of a 1% agarose gel with EtBr staining, where 10 µl of five PCR reactions for MT-1 at different $MgCl_2$ concentrations were loaded. The reactions were loaded as indicated above. The fragment sizes (bp) are indicated with arrows. The lane indicated in bold type illustrates the most optimal $MgCl_2$ concentration as discussed in the text. MM = molecular marker. The image control of this picture was formatted and set at a brightness of 77 % and contrast of 77 %. (-) = Negative control.*

The results for the optimisation of $T_a$ for MT-2 are portrayed in Figure 4.3. This image shows an ethidium bromide-stained gel of six PCR reactions run parallel in individual lanes. Lanes 2 to 5 present visible separation as one or more distinct fragments. This image portrays a clear and single fragment in the above mentioned lanes as well as very faint fragments just higher than 1000 bp, which may be due to unspecific hybridisation of primers. In lane 3 at $T_a = 58$ °C, a visibly sharper fragment of approximately 205 bp is observed. This $T_a$ was subsequently used for MT-2 amplification in this study. Whilst observing Figure 4.3 the fragments do not appear to be in a straight horizontal line, but slightly tilted. In this case, by means of making use of a straight dashed line (as indicated in Figure 4.3), the fragments are all connected to the line and the line is connected to the molecular markers in lane 1 and 8. Ultimately, it can be concluded that the fragment migrated to its expected position and that all the

fragments observed in this representation are of the same size. The reason for this phenomenon is not clear although it might be due to a difference in the salt content in different areas of the gel. It was not further investigated as it did not occur often.

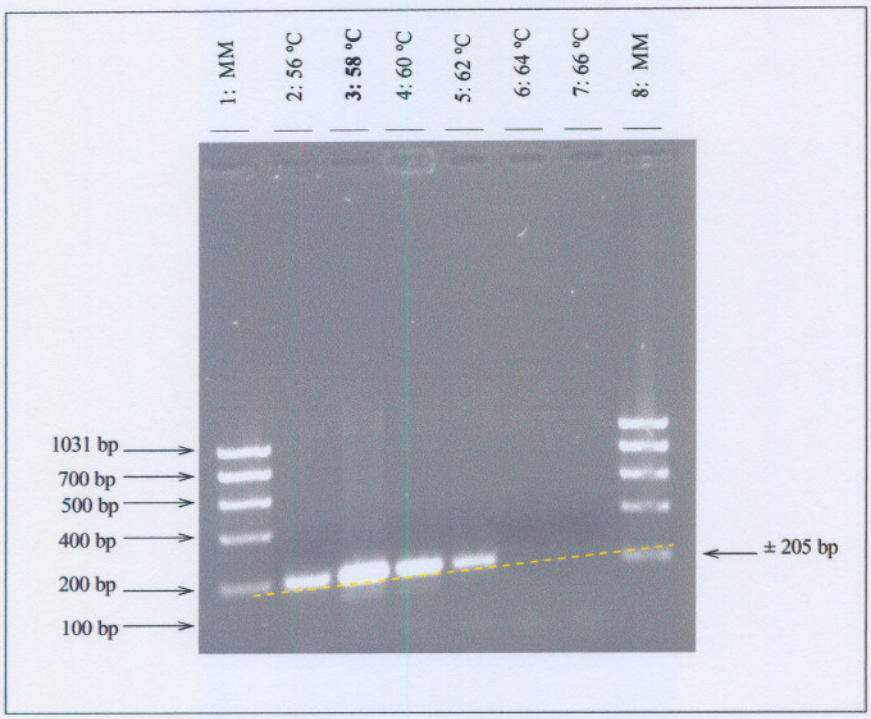


***Figure 4.3. Optimisation of $T_a$ for MT-2 PCR.*** *This figure shows a photographic representation of a 1% agarose gel with EtBr staining, where 10 µl of six PCR reactions for MT-2 at different $T_a$ were loaded. The reactions were loaded as indicated above. The fragment sizes (bp) are indicated with arrows. The lane indicated in bold type illustrates the most optimal $T_a$ as discussed in the text. MM = molecular marker. The image control of this picture was formatted and set at a brightness of 77 % and contrast of 77 %.*

The results for the optimisation of $MgCl_2$ concentration for MT-2 are portrayed in Figure 4.4. This image shows an ethidium bromide-stained gel of five PCR reactions run parallel in individual lanes. The negative control for MT-2 again did not produce any amplification. Lanes 3 to 6 shows visible separation of the components from the original mixture as one or more distinct fragments. This image portrays a clear and single fragment in the above mentioned lanes. In lane 5 at 3.0 mM $MgCl_2$ concentration a sharper and clearer fragment of approximately 205 bp can be observed. Smearing can be observed in lane 6, in other lanes smearing may also be present, but resolution of the detection method is not sensitive enough to show it. The

very intense fragment in lane 6 illustrates that there is sufficient product visible with this detection method. This $MgCl_2$ concentration was subsequently used in this study.

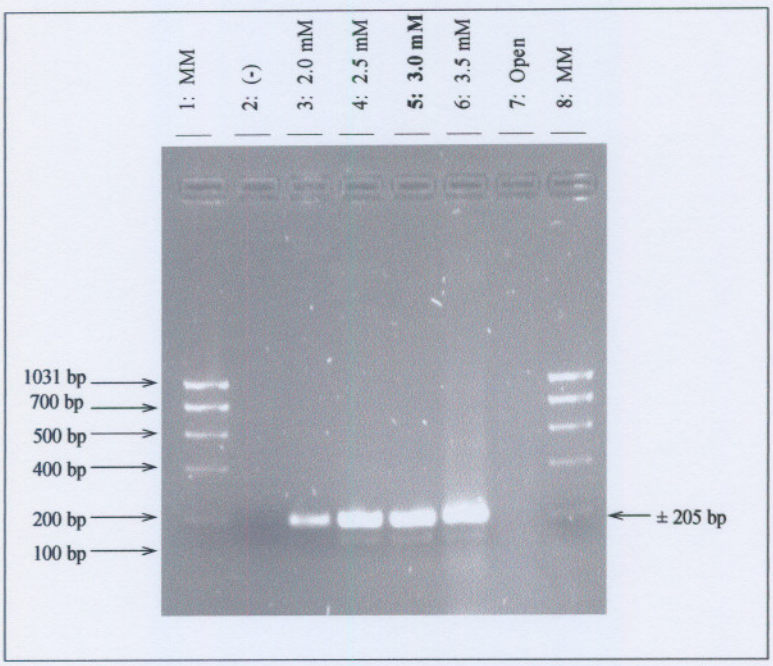


***Figure 4.4. Optimisation of $MgCl_2$ concentration for MT-2 PCR.*** *This figure shows a photographic representation of a 1% agarose gel with EtBr staining, where 10 µl of five PCR reactions for MT-2 at different $MgCl_2$ concentrations were loaded. The reactions were loaded as indicated above. The fragment sizes (bp) are indicated with arrows. The lane shown in bold type indicates the most optimal $MgCl_2$ concentration as discussed in the text. MM = molecular marker. The image control of this picture was formatted and set at a brightness of 77 % and contrast of 77 %. (-) = Negative control.*

The results for the optimisation of $T_a$ for MT-3 are portrayed in Figure 4.5. This image shows an ethidium bromide-stained gel of six PCR reactions run parallel in individual lanes. Lanes 2 and 3 shows visible separation of the components from the original reaction mixture as one or more distinct fragments. This image portrays a clear and single fragment in the above mentioned lanes. In lane 2 at $T_a = 58$ °C a much clearer fragment of approximately 251 bp is observed compared to lane 3. This $T_a$ value was subsequently used for amplification of MT-3 in this study.

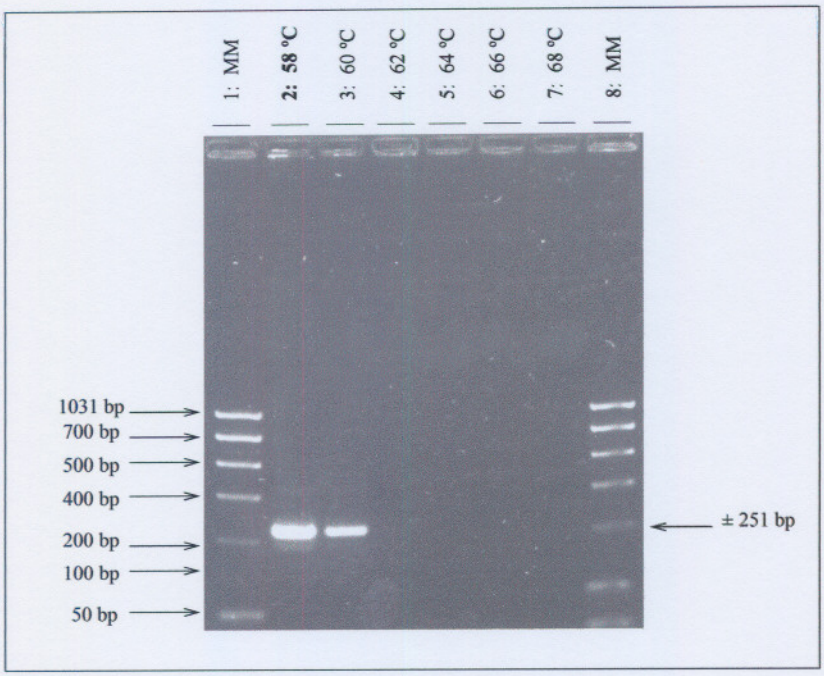


***Figure 4.5. Optimisation of $T_a$ for MT-3 PCR.*** *This figure shows a photographic representation of a 1% agarose gel with EtBr staining, where 10 µl of six PCR reactions for MT-3 at different $T_a$ were loaded. The reactions were loaded as indicated above. The fragment sizes (bp) are indicated with arrows. The lane indicated in bold type illustrates the most optimal $T_a$ as discussed in the text. MM = molecular marker. The image control of this picture was formatted and set at a brightness of 77 % and contrast of 77 %.*

The results for the optimisation for $MgCl_2$ concentration for the amplification of MT-3 are portrayed in Figure 4.6. This image shows an ethidium bromide-stained gel of five PCR reactions run parallel in individual lanes. Lanes 3 to 6 shows visible separation of the components from the original mixture as one or more distinct fragments, one clear and sharp fragment per lane. This image portrays a clear and single fragment in the above mentioned lanes. In lane 3 at 2.0 mM $MgCl_2$ concentration a sharper and clearer fragment of approximately 251 bp is observed. This $MgCl_2$ concentration was subsequently used in this study for amplification of MT-3. Some smearing and at least two clear fragments larger that 3000 bp appeared in lanes 3 to 6. This may be due to too much plasmid template that was used. If this is the reason for the appearance of these fragments, it is somewhat surprising that effective amplification, as is apparent in the figure, still occurred after the first amplification step of the PCR. Because of this observation the original plasmid mixture was diluted ten fold and subsequent

MT-3 amplification occurred without the appearance of these fragments as can be seen in Figures 4.5, 4.9 and 4.10. Ultimately, standard working solutions were used for the plasmids, pMT-1 to pMT-3.

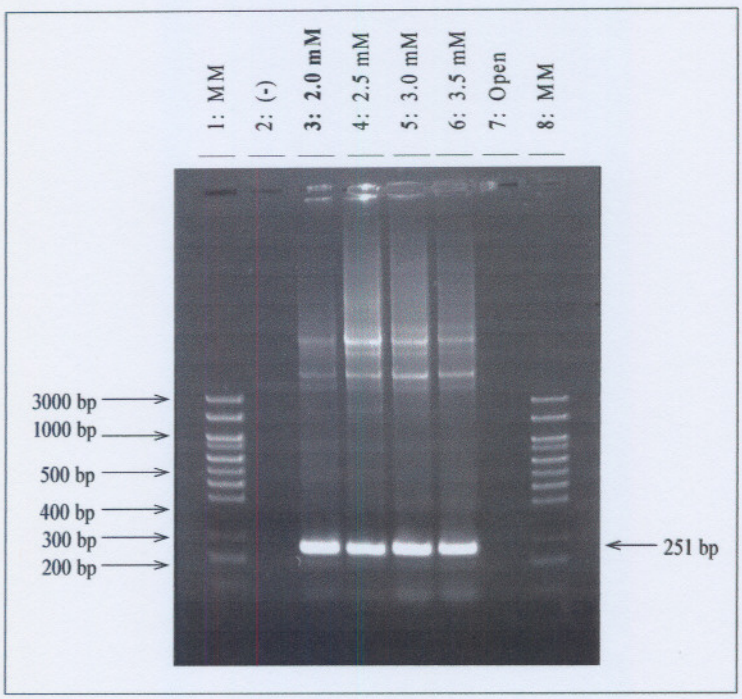


***Figure 4.6. Optimisation of $MgCl_2$ concentration of MT-3 PCR.*** *This figure shows a photographic representation of a 1% agarose gel with EtBr staining, where 10 µl of five PCR reactions for MT-3 at different $MgCl_2$ concentrations were loaded. The reactions were loaded as indicated above. The fragment sizes (bp) are indicated with arrows. The lane shown in bold type indicates the most optimal $MgCl_2$ concentration as discussed in the text. MM = molecular marker. The image control of this picture was formatted and set at a brightness of 55 % and contrast of 55 %. (-) = Negative control.*

The results for the optimisation of $T_a$ for β2MG using a cDNA sample prepared from total RNA is portrayed in Figure 4.7. This image shows an ethidium bromide-stained gel of six PCR reactions run parallel in individual lanes. Lanes 2 to 4 shows visible separation and distinct fragments. This image portrays a clear and single fragment in the above mentioned lanes. Again the fragments appeared tilted similar to Figure 4.3, but in view of the fragments in the two marker lanes, it can be seen that the size of the fragments in lanes 2 to 4 are the same. A less visible fragment of approximately 400 bp can also be observed in lane 3. This fragment may be due to unspecific

hybridisation of the primers at that $T_a$ but did not appear at lower $T_a$ as would be expected. In lane 3 at $T_a$ = 56 °C the fragment of approximately 212 bp was the sharpest of the three lanes and this $T_a$ value was subsequently used for amplification of β2MG in this study.

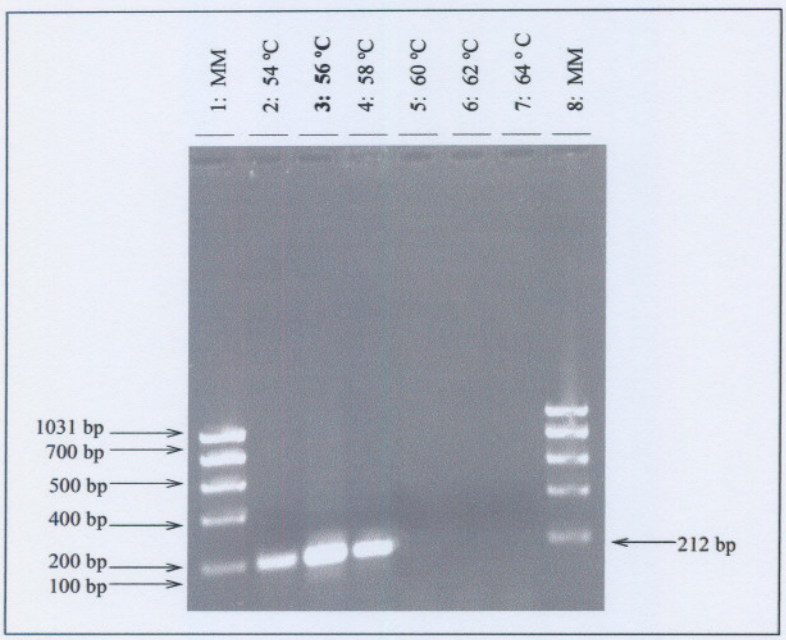


***Figure 4.7. Optimisation of $T_a$ for β2MG PCR.*** *This figure shows a photographic representation of a 1% agarose gel with EtBr staining, where 10 µl of six PCR reactions for β2MG at different $T_a$ were loaded. The reactions were loaded as indicated above. The fragment sizes (bp) are indicated with arrows. The lane indicated in bold type illustrates the most optimal $T_a$ as discussed in the text. MM = molecular marker. The image control of this picture was formatted and set at a brightness of 77 % and contrast of 77 %.*

The results for the optimisation of $MgCl_2$ concentration for the β2MG amplicon are portrayed in Figure 4.8. This image shows an ethidium bromide-stained gel of five PCR reactions run parallel in individual lanes. Lanes 3 to 6 each shows a major single fragment of approximately 212 bp. In lane 4 at 2.5 mM $MgCl_2$ concentration a sharper and clearer fragment is observed. This $MgCl_2$ concentration was subsequently used for β2MG in this study. Discrete, less visible fragments are observed between 300 to 500 bp in lane 6. These are probably due to unspecific hybridisation of the primers at that high $MgCl_2$ concentration.

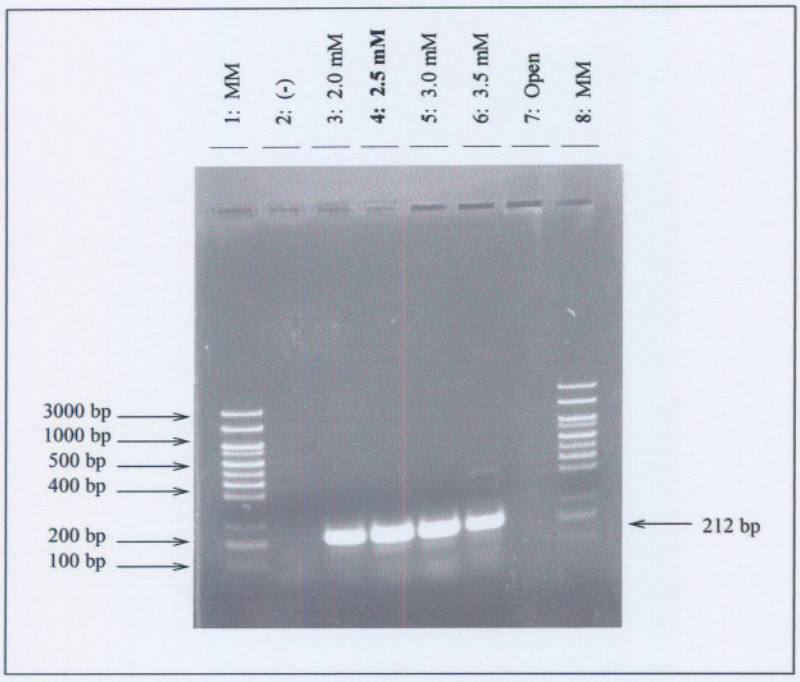


***Figure 4.8. Optimisation of $MgCl_2$ concentration for β2MG PCR.*** *This figure shows a photographic representation of a 1% agarose gel with EtBr staining, where 10 µl of five PCR reactions for β2MG at different $MgCl_2$ concentrations were loaded. The reactions were loaded as indicated above. The fragment sizes (bp) are indicated with arrows. The lane shown in bold type indicates the most optimal $MgCl_2$ concentration as discussed in the text. MM = molecular marker. The image control of this picture was formatted and set at a brightness of 77 % and contrast of 77 %. (-) = Negative control.*

To summarise, the optimal PCR conditions for $T_a$ and $MgCl_2$ that were deduced from the results, are outlined in Table 4.1. These conditions were subsequently used in further PCR and real-time PCR analysis throughout the study.

**Table 4.1 Optimal PCR conditions for $T_a$ and $MgCl_2$ concentration**

| Isoform/Houskeeping gene | $T_a$ (°C) | $MgCl_2$ (mM) |
|---|---|---|
| **MT-1** | 60 | 2.5 |
| **MT-2** | 58 | 3.0 |
| **MT-3** | 58 | 2.0 |
| **β2MG** | 56 | 2.5 |

## 4.3 MT isoform specificity

As the optimisation of $T_a$ and $MgCl_2$ for all the MT isoforms was determined using control cDNA, it was critical to make sure that the primers were specific to the correct MT isoform. Thus, MT1 to MT-3 PCR reactions were performed using all three MT cDNA templates (pMT-1 to pMT-3), respectively. This was performed to estimate whether the correct primer pair would anneal to the correct template, thus confirming the specificity of the primers. This result is shown in Figure 4.9. A negative control, containing no template was used for all three of the isoform specific reactions. Three single fragments are observed in lanes 4, 8 and 12. Each of these fragments represents a specific isoform, MT-1, MT-2 and MT-3 respectively. MT-1 is observed at a fragment size of approximately 186 bp, MT-2 approximately at 205 bp and MT-3 at approximately 251 bp. Again, less visible fragments are observed just below the fragments in lanes 2, 8 and 12. Very faint DNA fragments are observed in lanes 3 to 5, 7 to 9 and 11 to 13 which are larger than the expected product and may again be due to some unspecific hybridisation to the template due to the quality of the primers.

Upon initial viewing of Figure 4.9 it appears that the fragments are situated in a linear line to each other, which one might conclude are fragments of the same size. The single fragments observed in lanes 8 and 12 appear to be quite clear and dense, possibly due to their specific concentration, which might be a probable reason why they appear to be in a straight line, but in fact are not. Just to confirm that the fragments are not of the same size, a mini gel with six PCR reactions containing pMT-1 to pMT-3 as template was run and except for pMT-1 gave clear and distinctive visible results. These results are presented in Figure 4.10 indicating that the fragments, excluding MT-1, migrated to their expected positions. Ultimately this experiment proved that the primers hybridised specifically to the appropriate MT isoforms. Throughout the study, amplification of MT-1 cDNA was not very reproducible. This can be also be deduced from the very specific $T_a$ and $MgCl_2$ conditions (Section 4.2). The exact conditions for effective amplification of this isoform had to be constant and specific. With subsequent real-time PCR the positive control for the amplification (MT-1 cDNA) was closely checked to make sure the conditions were correct.

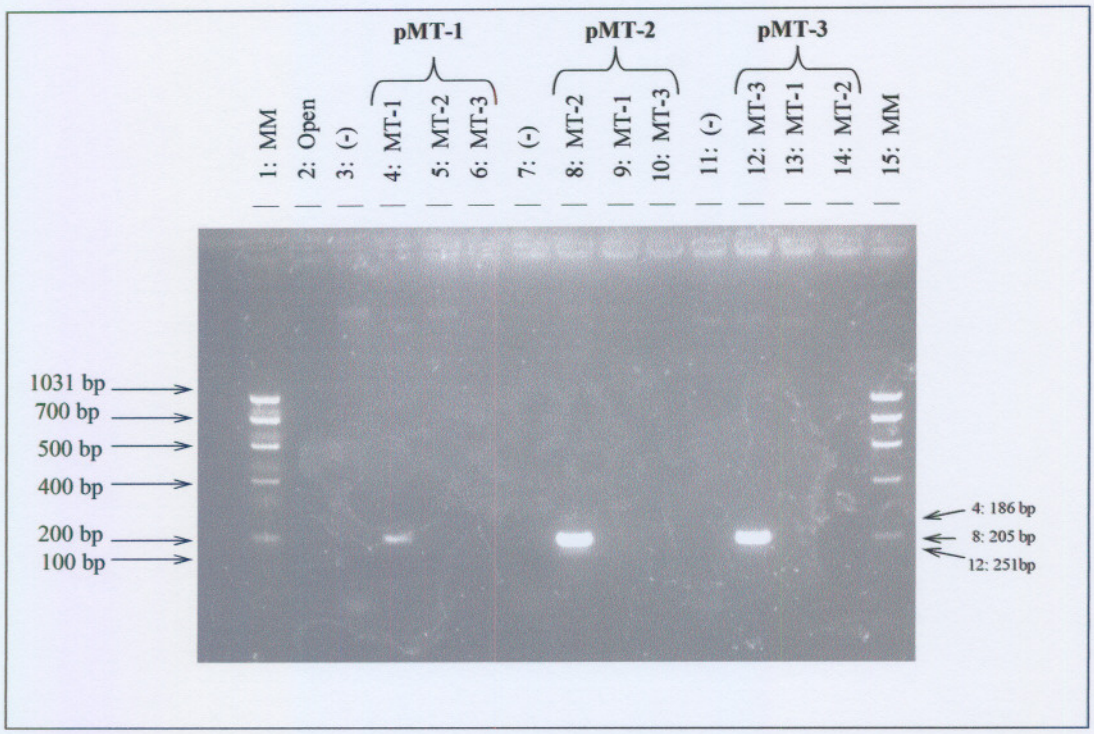


***Figure 4.9. MT isoform specificity for pMT-1, pMT-2 and pMT-3.*** *This figure shows a photographic representation of a 1% agarose midi gel with EtBr staining, where 15 µl of twelve PCR reactions for pMT-1 to pMT-3 at optimal PCR reactions were loaded. The reactions were loaded as indicated above. The fragment sizes (bp) are indicated with arrows. MM = molecular marker. The image control of this picture was formatted and set at a brightness of 77 % and contrast of 77 %. (-) = Negative control.*

The photographic representation in Figure 4.10 indicates that the PCR products of pMT-2 and pMT-3 migrated to their expected positions, respectively, but not pMT-1. This image is shown to prove that the products did not migrate to the same position as might be concluded from the observation of Figure 4.9.

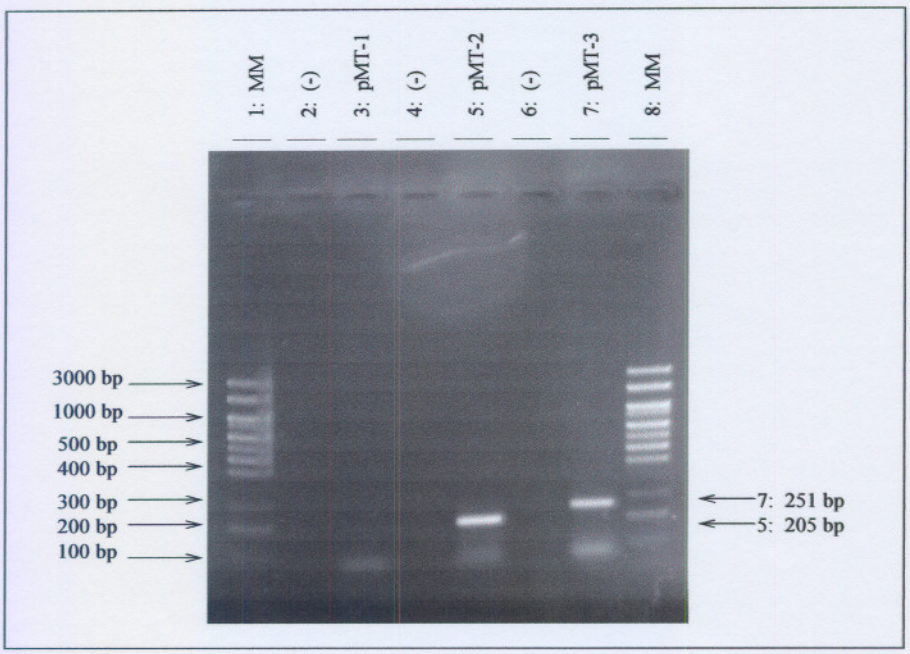


***Figure 4.10. MT isoform specificity for pMT-1, pMT-2 and pMT-3.*** *This figure shows a photographic representation of a 1% agarose mini gel with EtBr staining, where 10 µl of six PCR reactions for pMT-1 to pMT-3 at optimal PCR reaction conditions were loaded. The reactions were loaded as indicated above. The fragment sizes (bp) are indicated with arrows. MM = molecular marker. The image control of this picture was formatted and set at a brightness of 77 % and contrast of 77 %. (-) = Negative control.*

## 4.4 Sequencing

Sample preparation and sequencing of the different MT isoforms was performed by Inqaba Biotechnical Industries (Pty) Ltd. The PCR amplicons were first extracted from a gel and then purified prior to the sequencing analysis. The PCR products were approximately 150-260 bp in length, the PCR reaction was run with 75 ng of the cDNA template which was ultimately utilised for sequencing. The forward and reverse sequences were studied and aligned using the software programme CHROMAS, version 3.2. In some cases the sequence for one of the strands was not clear from the electropherogram. The best matching sequence or best quality sequence result of the two strands was used and is displayed in the following figures. Furthermore, only partial sequences of the amplicons were obtained. An example of the sequence data generated is provided in Figure 4.11.

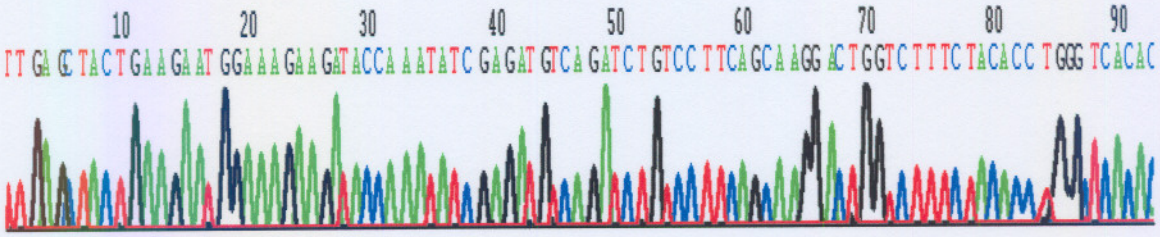


***Figure 4.11. Example of an electropherogram of β2MG.*** *Automated fluorescent sequencing detection using single-lane gel and charge-coupled device. This figure illustrates the automated base calling retrieved with the computer programme CHROMAS. A = adenine (Green), G = guanine (Black), C =cytosine (Blue), T = thymine (Red).*

The processed sequences were analysed for sequence homology using the nucleotide-nucleotide Basic Local Alignment Search Tool (BLAST) of NCBI. Sequence homology analysis for MT-1 to the MT-3 PCR amplicon as well as the housekeeping gene β2MG PCR amplicon is given in Figures 4.12 A to D. From these results it was clear that the partial sequences obtained were almost perfectly matched to the reference sequences on the NCBI database. Two exceptions occurred. An additional C (insertion) at position 847 (of reference sequence) was observed for MT-1 and a G→A transition at position 24 (of reference sequence) was observed for MT-3. Although only partial sequences for the four amplicons were obtained, the purpose of confirming that the amplicons contained the correct target sequences presented with sufficient evidence to conclude that the four PCR's were suitable for use in the subsequent MT expression analysis.

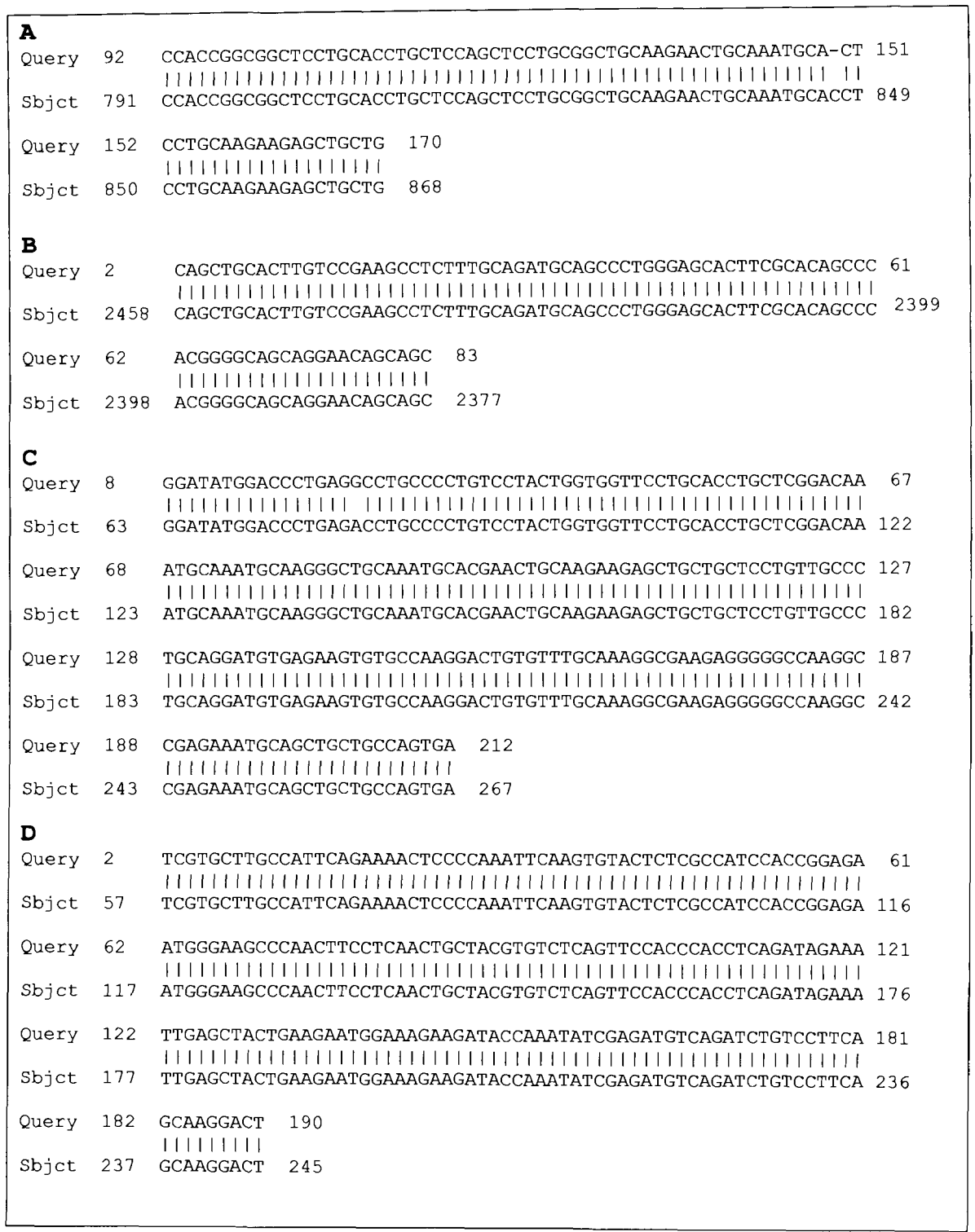


***Figure 4.12. Sequence homology analysis for rat MT-1 (A), MT-2 (B), MT-3 (C) and β2MG (D) PCR amplicons using Basic Local Alignment Search Tool (BLAST).*** *The four figures show alignment of partial sequences obtained from the sequence data generated by Inqaba Biotec from the aformentioned PCR products. Correct alignment is indicated by vertical lines between sequences of the PCR amplicon (Query) and reference sequence (Sbjct). The reference sequences for the four amplicons were as follows: For MT-1, GenBank sequence NM_138826; for MT-2, GenBank sequence M11794; for MT-3, GenBank sequence NM_053968 and for β2MG, GenBank sequence NM_012512. A = adenine, G = guanine, C = cytosine, T = thymine.*

## 4.5 RNA isolation

RNA was isolated from all the tissue samples as described in Section 3.3. RNA concentration and purity was determined via UV spectrophotometry and calculated using Equation 3.4. The $A_{260}/A_{280}$ ratios were between 1.7 and 1.9 which provided an estimate of the RNA purity of each sample with respect to contaminants, particularly proteins that absorb in the ultraviolet light range at 280 nm. It should be mentioned that analysis of RNA and DNA samples using the BIO-TEK Instruments Uvikon XS double beam spectrophotometer that was utilised in this study gave different results compared to the Nanodrop™ analysis (personal communication F. Reinecke), which only became available after completion of this study.

All samples were analysed on a denaturing (formaldehyde containing) agarose gel. For the evaluation of the intensity of the RNA samples a number of guidelines were used. Firstly, clear 28S and 18S rRNA fragments similar to those illustrated in Figure 4.13 had to be present. The 28S rRNA fragment should be approximately twice as intense as the 18S rRNA fragment (Wilson & Walker, 2000). Partially degraded RNA will have a highly smeared appearance, or either lacks the sharp rRNA fragments associated with 28S and 18S rRNA. Secondly, it had to be determined whether any genomic DNA was present on the gel. As mentioned before, all RNA isolated in this study was tested for quality on a denaturing agarose gel and only those samples that were found to be of good quality, purity and integrity were used for cDNA synthesis. The $A_{260}/A_{280}$ ratio for the rats in the group displayed in Figure 4.13 ranged from 1.6 to 1.85, which was considered to be acceptable. This illustration indicates that the 28S and 18S rRNA are intact and do not give a poor quality low molecular weight smear, thus making the samples available for use in cDNA synthesis.

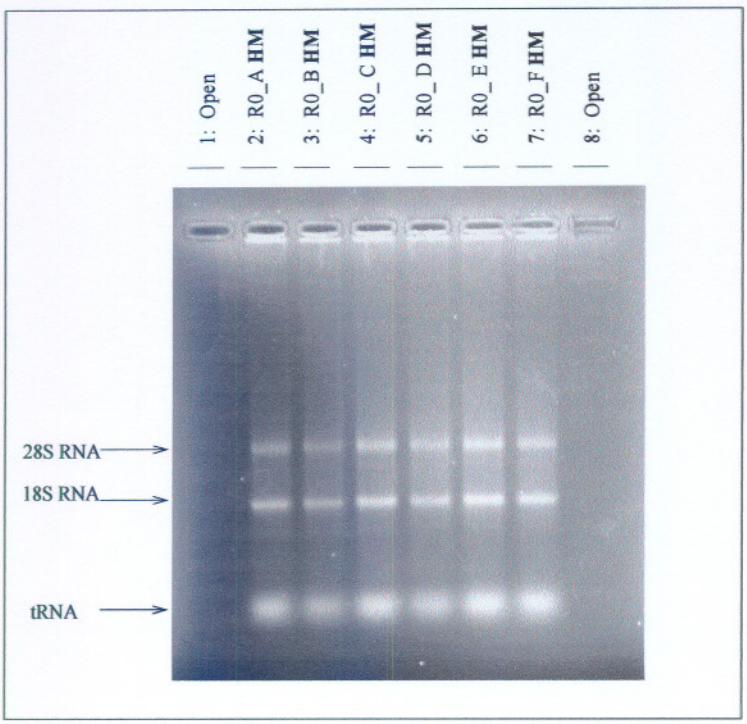


***Figure 4.13. Integrity analysis of isolated RNA samples.*** *This figure shows a photographic representation of a 1% agarose gel with EtBr staining where 10 µl of 3 µg RNA obtained from heart muscle of the six rats of the control group. The arrows indicate where the 28S, 18S and tRNA are situated.*

## 4.6 Evaluation of successful cDNA synthesis

After determining that the RNA was of acceptable quality, RNA was reverse transcribed with reverse transcriptase and random primers to synthesise cDNA from the total pool of RNA transcripts. Subsequent PCR amplification using MT primers ensured the generation of the second complementary strand followed by subsequent amplification of target sequence using PCR. This was evaluated by means of agarose gel electrophoresis with ethidium bromide staining. Figure 4.14 shows a representative illustration of PCR evaluation of cDNA synthesis in brain tissue RNA of untreated (control) rat. As can be observed in this figure the fragment sizes of MT-2 are approximately at 205 bp and β2MG is observed at approximately 212 bp, and MT-3 approximately at 251 bp. MT-1 did not express in these brain samples but did amplify from liver and heart muscle cDNA (data not shown). MT-3 is an isoform that is mainly expressed in the brain, and as this reaction was amplified cDNA of brain tissue it can be clearly observed that MT-3 is expressed in the rat brain indicated

in lane 4. The housekeeping gene, GAPDH in lane 5 failed to express as it did in most of the other tissue samples. Possible speculations for this phenomenon might either be the time between excision and snap freezing of tissues, or RNA yield from the different tissue types, where GAPDH mRNA expression might express significant differently between tissues according to tissue energy demands. Visible fragments are observed in lanes 2 to 6 and just below the bright fragments in lanes 3, 4 and 6. This may indicate some excessive primer but it is likely to be due to higher contrast and resolution settings (see Figure 4.14).

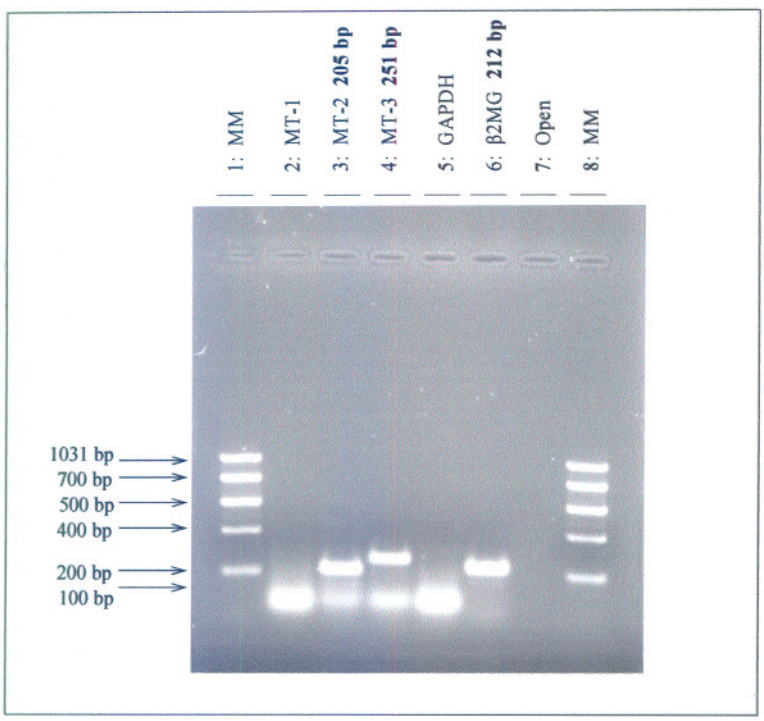


***Figure 4.14. PCR amplification of cDNA prepared from the RNA sample R0_A Br.*** *This figure shows a photographic representation of a 1% agarose gel with EtBr staining, where 10 µl of five PCR reactions for MT-1 to MT-3 and the housekeeping genes GAPDH and β2MG at optimal PCR reactions were loaded. The reactions were loaded as indicated above. MM = molecular marker. The fragment sizes (bp) of the molecular weight marker are indicated with arrows.*

### 4.7 Real-time PCR analysis for the expression of MT genes

Real-time PCR was performed on cDNA prepared from tissue of rats treated with rotenone at concentrations of 0, 3, 9, and 15 mg/kg/day which is summarised in Table 3.1. Ct values were obtained from real-time PCR results similar to that displayed in

the graph shown in Figure 4.15. The Ct values are then calculated to determine the amount of the gene expression. The formulas needed to calculate the total gene expression are shown in Equation 3.5. The expression of MT genes was normalised with the stable housekeeping gene β2MG. The expression of MT genes are expressed as fold changes relative to the housekeeping (reference) gene. The different rat tissues are indicated in the figures outlined below and will be discussed individually.

Figure 4.15 and Table 4.2 illustrate an example of data obtained from quantitative PCR analysis. The graphical representation in Figure 4.15 illustrates different coloured lines that have been assigned to different reaction samples. Real-time experiments were done in triplicate. After real-time analysis has completed its cycles, a Ct value is given for each of the coloured lines, which is illustrated in tabular form in Table 4.2. In the example in Figure 4.15 the threshold set point is indicated as an orange line (71.1). The purple and green line that can be observed just beneath the threshold line indicates the negative control for this experiment, from which no Ct value could be assigned and was denoted as "not applicable" (N/A) by the software analysis result. Several calculations are performed on the Ct values (formulas indicated in Equation 3.5) to ultimately establish the amount of gene expression. The amount of expression for the given dose groups 0, 3, 9, and 15 mg/kg/day rotenone for the given tissues of brain, liver, heart muscle and skeletal muscle is summarised in tabular form in Tables 4.3, 4.7 and 4.12.

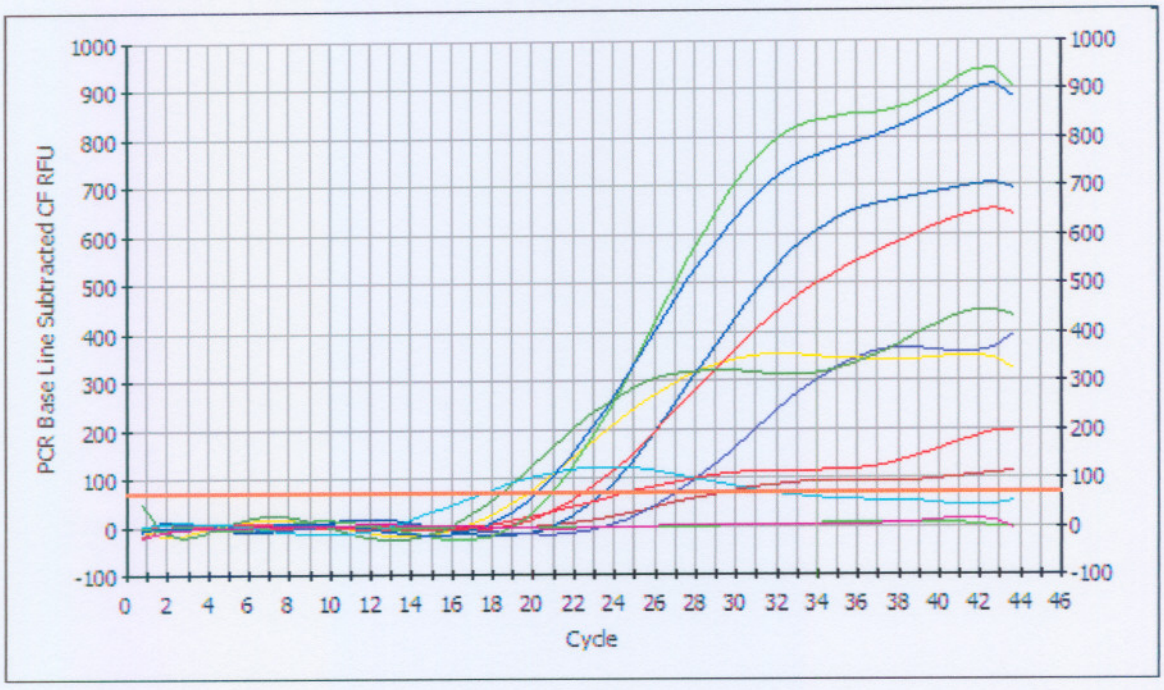


***Figure 4.15. Real-time PCR graph using SYBR® Green as DNA binding dye.*** *A representative experiment with cDNA's from twelve samples of R0_ABr, and R0_BBr. MT-1 to MT-3 and β2MG were amplified and total fluorescence was measured at the end of each cycle. The lines indicate the samples listed in Table 4.2.*

Table 4.2 shows an example of the result obtained from real-time PCR, using specific MT-primers. These Ct values were obtained from data provided from the real-time analysis as illustrated in Fig 4.15. In this particular case, which is an example to demonstrate the result, a duplicate sample for MT-3 for both rats was performed, for comparative reasons in Ct value estimation. A typical Ct value ranges from 10 to 30. A higher Ct-value indicates less DNA amplification.

**Table 4.2 Real-time PCR results for twelve samples of R0_ABr, and R0_BBr. MT-1 to MT-3 and β2MG primer expression values are indicated as Ct values.**

| Well | Identifier | Ct |
|---|---|---|
| C03 | MT-1 | 30.1 |
| C04 | MT-2 | 22.4 |
| C06 | MT-3 | 19.7 |
| C07 | MT-3 | 18.8 |
| C08 | β2MG | 20.5 |
| C09 | (-) | N/A |
| E03 | MT-1 | 28.5 |
| E04 | MT-2 | 20.9 |
| E05 | MT-3 | 18.4 |
| E06 | MT-3 | 18.9 |
| E07 | β2MG | 20.1 |
| E08 | (-) | N/A |

*(-) = Negative control. N/A = not applicable (no expression).*

Figure 4.16 displays the change in the negative of the first derivative of the fluorescence (–dF) as a function of temperature change. The software identifies peaks and assigns melting temperatures from this plot

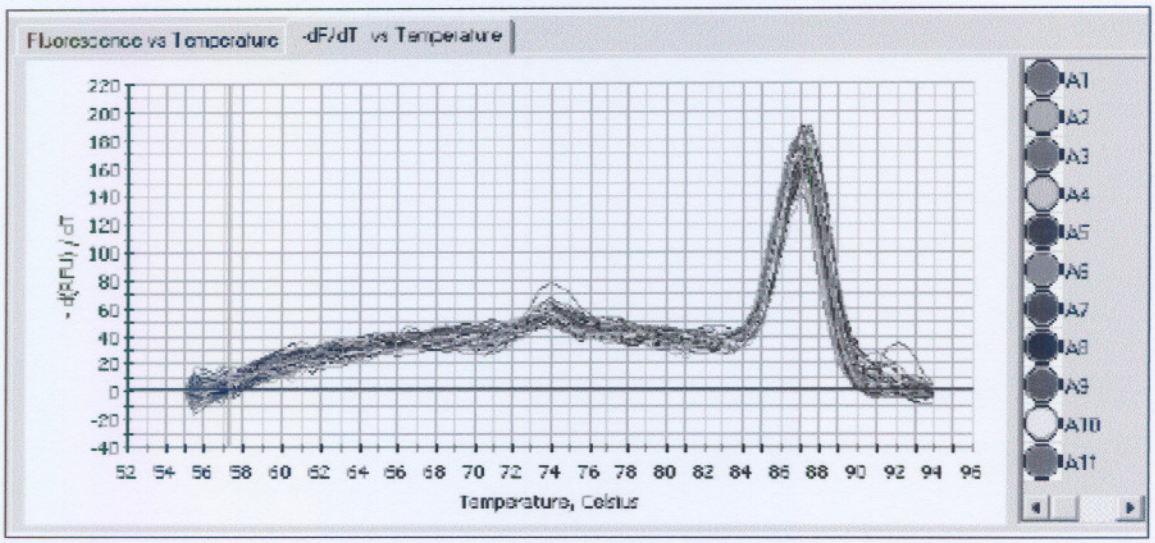


***Figure 4.16: Melting curve analysis during real-time PCR.*** *An example of a melting curve.*

## 4.8 MT-1 expression in rotenone-treated rat tissues

Table 4.3 summarises the expression ratios of MT-1 in the various rotenone-treated rat tissues. The various statistical analyses of the data are further discussed in the following sections. MT-1 expression could be detected in all tissue except skeletal muscle as can be observed in Table 4.3.

### 4.8.1 Statistical analysis of real-time expression ratios

The expression of MT is expressed as fold change relative to the baseline cDNA (0 dose group). For easier comparison of expression ratios, values of untreated rat tissues were also arbitrarily denoted as 1. The statistical analysis of the different rat tissue is displayed in the tables below and will be discussed individually. Confidence intervals were set at 95%, which is highly recommended for empirical work (Steyn *et al.*, 1998). Statistical significance ($p < 0.05$) was obtained by means of a one-way analysis of variance (ANOVA) if data was distributed normally. If the data was not normally distributed, the Kruskal-Wallis test was performed. The effect sizes of the

differences between means were determined by utilising the effect size ($d$) as indicated in Equation 3.6 to determine practical significance. If a *d value* was determined to be $d = 0.2$, the difference in means had a small effect, while for $d = 0.5$ a medium effect existed. If a *d value* was $d = 0.8$, the effect was large. Data with $d \geq 0.8$ was regarded as practically significant (Ellis and Steyn, 2003).

**Table 4.3 MT-1 RNA expression ratios in tissues of rats treated with rotenone**

| Tissue | [Rotenone] mg/kg/day | Mean | Expression ratio | SD |
|---|---|---|---|---|
| **Brain** | 0 | 0.59667 | 1.00 | 0.018619 |
| | 3 | 0.66 | 1.11 | 0.121861 |
| | 9 | 0.67 | 1.12 | 0.071274 |
| | 15 | 1.01 | 1.69 | 0.032863 |
| **Liver** | 0 | 1.0883 | 1.00 | 0.039707 |
| | 3 | 1.56 | 1.43 | 0.09798 |
| | 9 | 1.67 | 1.53 | 0.046476 |
| | 15 | 1.77 | 1.63 | 0.044721 |
| **Heart muscle** | 0 | 0.795 | 1.00 | 0.018708 |
| | 3 | 0.96 | 1.21 | 0.044721 |
| | 9 | 0.97 | 1.22 | 0.054037 |
| | 15 | 0.97 | 1.22 | 0.074564 |
| **Skeletal muscle** | 0 | N/D | N/D | N/D |
| | 3 | N/D | N/D | N/D |
| | 9 | N/D | N/D | N/D |
| | 15 | N/D | N/D | N/D |

*Expression ratio is calculated relative to the baseline (control) group. Mean = six samples done in triplicate before normalising it relative to the control group. N/D = Not detected*

### 4.8.2 MT-1 expression in brain tissue

Statistical analysis for MT-1 in the brain proved to have unequal variances ($p = 0.002$) according to the Bartlett test. A normal probability plot was done on the residuals to determine if the data was normally distributed. After the indication, as can be observed in Figure 4.17, that the assumption of normality did not hold, a non-parametric Kruskal-Wallis test was performed to determine statistical significance ($p < 0.05$). A post hoc test for unequal numbers (n) was performed due to the unequal sample sizes in the dose concentration of 3 mg/kg/day. In Table 4.4 the statistical results on MT-1 for the brain are given.

For MT-1 in the brain it was indicated that the given groups (0, 3, 9, and 15 mg/kg/day) have unequal variance on the dependent variable. After statistical significance was established between various dose groups for MT-1, practical significance was calculated by means of effect size with the means squared error. Data which prove to be practically significant ($d \geq 0.8$) is represented in Table 4.4.

As can be observed in the statistical analysis displayed below, statistically and practically significant expression changes occurred for MT-1 expression in the brain at the given rotenone concentrations.

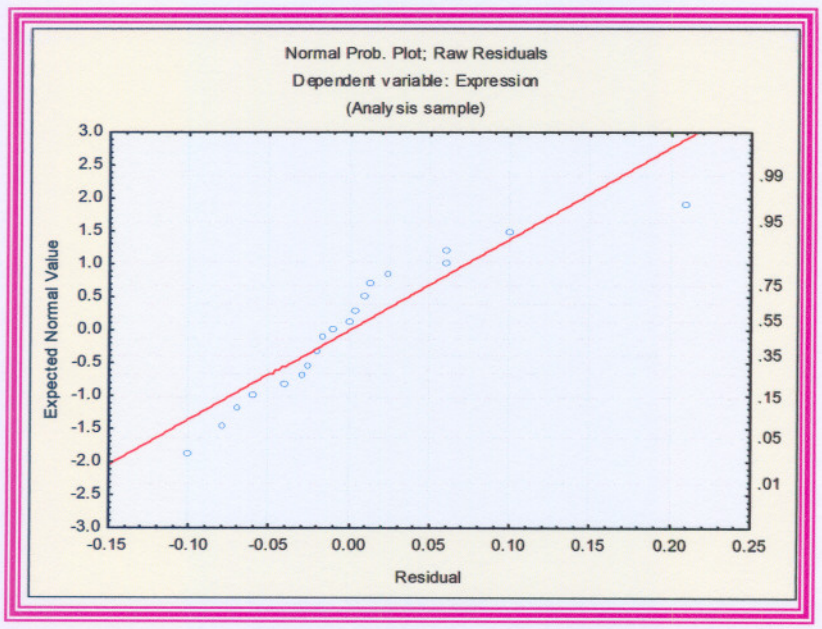


***Figure 4.17. Probability plot for MT-1 expression in the brain.*** *The appearance of the manner with which the data is spread in comparison to the red straight line indicates that the data for this particular tissue for MT-1 is not normally distributed and does thus not comply with the assumptions of ANOVA. Ultimately a Kruskal-Wallis test for multiple comparisons was performed for this particular tissue dataset.*

Table 4.4 summarises the statistical outcome of MT-1 expression in brain tissue. In this particular case the non-parametric Kruskal-Wallis test for multiple comparisons was performed on the data set. This table also indicates the presence of statistical significance between the dose groups as well as the biological worth of the significant data (practically significant).

**Table 4.4. Results of the multiple comparison of MT-1 RNA expression in the brain**

| MT-1 Brain: Statistical significance ($p < 0.05$) | | | | | SS dose groups: mg/kg/day | Practical significance ($d$ = effect size) |
|---|---|---|---|---|---|---|
| **Dose: mg/kg/day** | **0** | **3** | **9** | **15** | | |
| **0** | | 1.000000 | 1.000000 | **0.001641** | 0 and 15 | 5.9412 |
| **3** | 1.000000 | | 1.000000 | **0.044383** | 3 and 15 | 5.0309 |
| **9** | 1.000000 | 1.000000 | | 0.115407 | - | - |
| **15** | **0.001641** | **0.044383** | 0.115407 | | - | - |

*This table indicates $p < 0.05$ (in red), thus statistical significance amongst the means for MT-1 expression in brain tissue was present. SS = Statistical significance.*

The expression ratios (normalised to the reference gene) are also illustrated in Figure 4.18. As already supported by the statistical analysis it can be visually observed that when rats were treated with a rotenone concentration higher than 9 mg/kg/day, MT-1 RNA expression in the brain increased significantly compared to lower dosages. It therefore appears that a threshold is reached at approximately 9 mg/kg/day before expression of this isoform is increased.

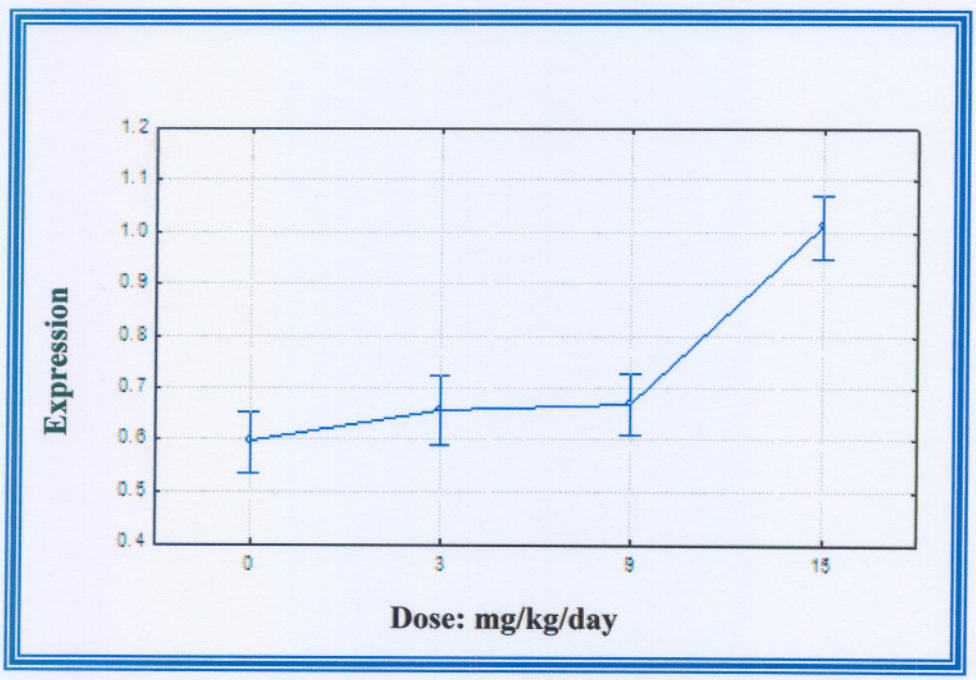


***Figure 4.18. MT-1 RNA expression in the brain at given rotenone dose concentrations.*** *Expression is indicated as the means (n=6). The vertical bars indicate the 95% confidence interval determined from the mean squared error $p < 0.05$.*

### 4.8.3 MT-1 expression in liver tissue

For MT-1 in the liver it was determined that the given groups (0, 3, 9, and 15 mg/kg/day) have approximately equal variance for the dependent variable. The Bartlett test for MT-1 in liver tissue indicated $p = 0.18$, specifying that the variances in the data set are equal. Also, data for MT-1 in the liver comply with normal distribution as can be observed in Figure 4.19. A parametric test was performed on MT-1 data, which indicated statistical significance ($p < 0.05$) and a post hoc test on unequal group sizes was performed to indicate the differences of statistical significance between means for various dose groups as it is represented in Table 4.5.

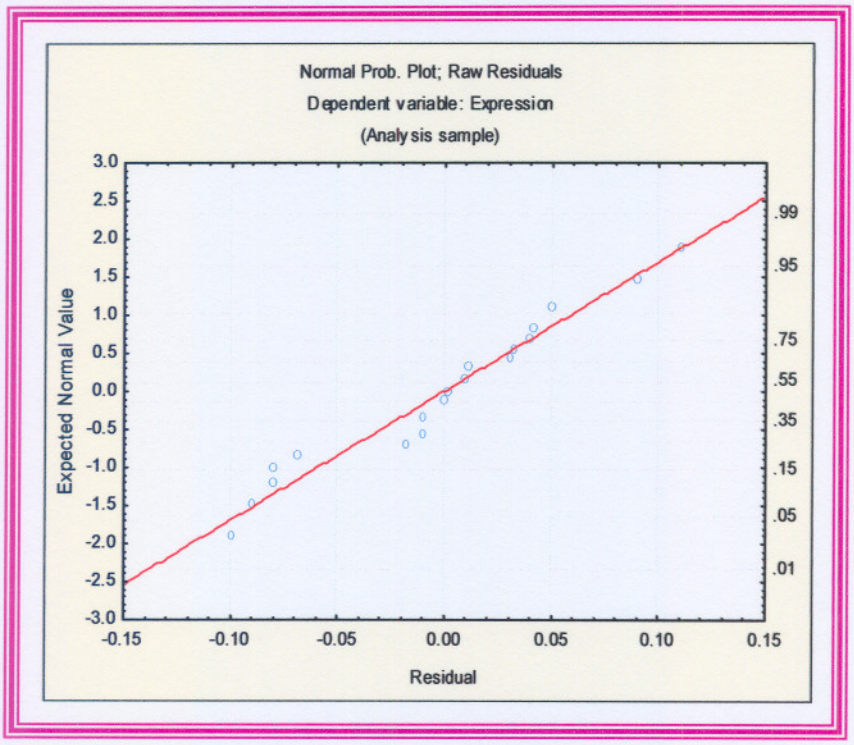


***Figure 4.19. Probability plot for MT-1 expression in the liver.*** *The appearance of the manner with which the data is spread in comparison to the red straight line indicates that the data for this particular tissue for MT-1 is normally distributed and does thus comply with the assumptions of ANOVA.*

Table 4.5 summarises the statistical outcome of MT-1 expression in liver tissue. In this particular case the ANOVA parametric test and the unequal post hoc test was performed on the data set. This table also indicates the presence of statistical

significance between the dose groups as well as the biological worth of the significant data (practically significant).

**Table 4.5. ANOVA and unequal post hoc results for MT-1 RNA expression in the liver**

| MT-1 Liver: Statistical significance ($p < 0.05$) | | | | | SS dose groups: mg/kg/day | Practical significance ($d$ = effect size) |
|---|---|---|---|---|---|---|
| **Dose: mg/kg/day** | **0** | **3** | **9** | **15** | | |
| **0** | | **0.000181** | **0.000181** | **0.000181** | 0 and 3 | 7.93923 |
| **3** | **0.000181** | | **0.039642** | **0.000285** | 0 and 9 | 9.79065 |
| **9** | **0.000181** | **0.039642** | | **0.040636** | 0 and 15 | 11.4738 |
| **15** | **0.000181** | **0.000285** | **0.040636** | | 3 and 9 | 1.96932 |
| | - | - | - | - | 3 and 15 | 3.53453 |
| | - | - | - | - | 9 and 15 | 1.68311 |

*This table indicates $p < 0.05$ (in red), thus statistical significance amongst the means for MT-1 expression in liver tissue was present. SS = Statistical significance.*

The statistically significant data obtained from the ANOVA analysis shows that MT-1 expression increased significantly with an increase of the rotenone dosage. This is also obvious from Figure 4.20 where an almost two-fold increase of the isoform from 1.1 to almost 1.8 expressions can be seen between 0 and 15 mg/kg/day. This trend is different from the pattern observed in the brain because at 3 mg/kg/day a significant ($p$ = 0.000181), although slight increase occurred. At dosages higher than 3 mg/kg/day the significant increase continues, however not so markedly.

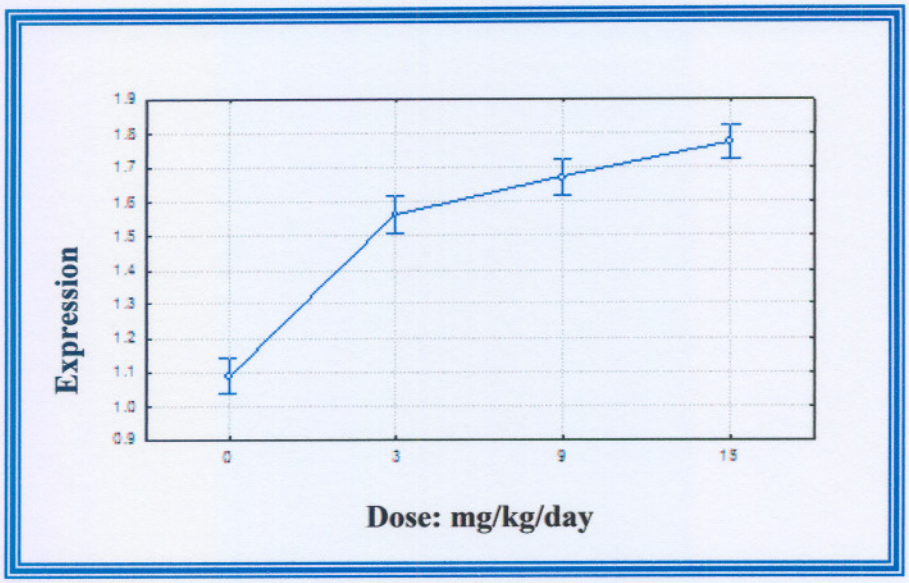


***Figure 4.20. MT-1 RNA expression in the liver at given rotenone dose concentrations.*** *Expression is indicated as the means (n=6). The vertical bars indicate the 95% confidence interval determined from the mean squared error p <0.05.*

### 4.8.4 MT-1 expression in heart muscle

For MT-1 expression in heart muscle it was indicated that the given dose groups (0, 3, 9, 15 mg/kg/day) have approximately equal variance for the dependent variable. The Bartlett test for MT-1 in heart muscle tissue was determined to be $p= 0.069$, specifying that the variances in the data set are equal. Also, the data for MT-1 in heart muscle comply with the assumption of a normal distribution as can be observed in Figure 4.21. A parametric test was performed on MT-1 data which indicated $p < 0.05$ statistical significance. If $p < 0.05$ and a post hoc test on unequal group sizes was performed to indicate the statistically significant differences between the means of the various dose groups as it is represented in Table 4.6.

After statistical significance was established between the various dose groups for MT-1 expression, practical significance was calculated by means of effect size with the means squared error. Data which proved to be practically significant ($d \geq 0.8$) are represented in Table 4.6.

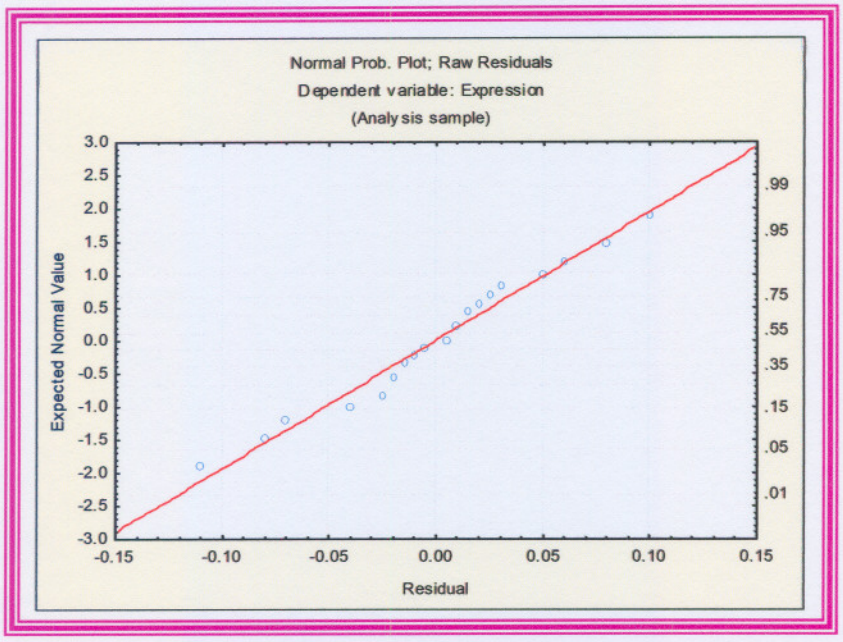


***Figure 4.21. Probability plot for MT-1 expression in heart muscle.*** *The appearance of the manner with which the data is spread in comparison to the red straight line indicates that the data for this particular tissue for MT-1 is normally distributed and does thus comply with the assumptions of ANOVA.*

Table 4.6 summarises the statistical outcome of MT-1 expression in heart muscle tissue. In this particular case the ANOVA parametric test and unequal post hoc test was performed on the data set. This table also indicates the presence of statistical significance between the dose groups as well as the biological worth of the significant data (practical significance).

**Table 4.6 ANOVA and unequal post hoc results for MT-1 RNA expression in heart muscle**

| **MT-1 Heart muscle: Statistical significance ($p < 0.05$)** | | | | | **SS dose groups: mg/kg/day** | **Practical significance ($d$ = *effect size*)** |
|---|---|---|---|---|---|---|
| **Dose: mg/kg/day** | **0** | **3** | **9** | **15** | | |
| **0** | | 0.000592 | 0.000249 | 0.000249 | 0 and 3 | 3.15216 |
| **3** | 0.000592 | | 0.990207 | 0.990207 | 0 and 9 | 3.3432 |
| **9** | 0.000249 | 0.990207 | | 1.000000 | 0 and 15 | 3.3432 |
| **15** | 0.000249 | 0.990207 | 1.000000 | | - | - |

*This table indicates $p < 0.05$ (in red), thus statistical significance amongst the means for MT-1 expression in liver tissue was present. SS = Statistical significance.*

The statistically significant results obtained from the Unequal N post hoc analysis for MT-1 expression in the heart muscle are indicated in Figure 4.22. Figure 4.22 indicates only a small but significant increase of rotenone dosage in MT-1 expression from 0 mg/kg/day to 3 mg/kg/day which then remained similar at higher dosages. Mean values and 95% confidence intervals are graphically displayed in Figure 4.22.

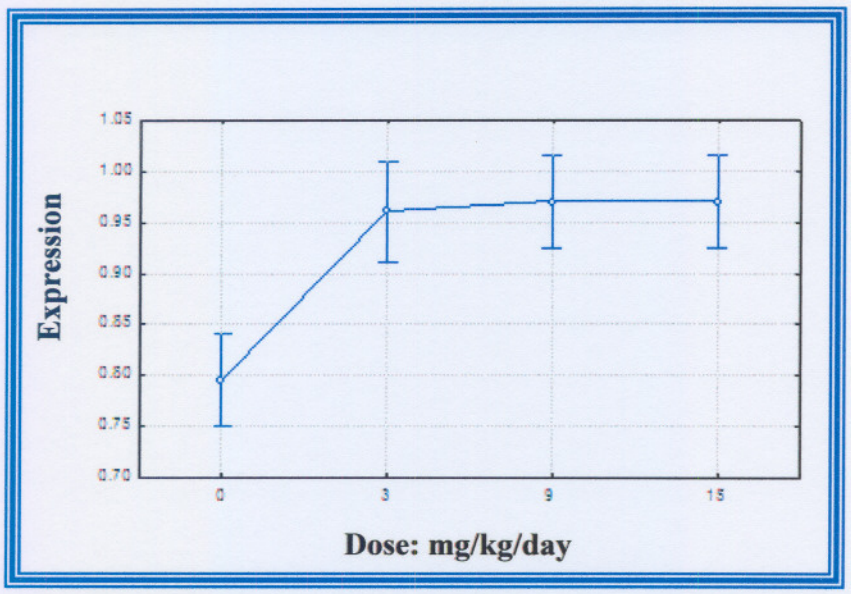


***Figure 4.22. MT-1 RNA expression in heart muscle at given rotenone dose concentrations.*** *Expression is indicated as the means (n=6). The vertical bars indicate the 95% confidence interval determined from the mean squared error $p < 0.05$.*

## 4.9 MT-2 expression in rotenone-treated rat tissues

Table 4.7 gives a summary of the expression ratios of MT-2 in the various rotenone treated rat tissues. The various statistical analyses of the data are further discussed in the following sections. As can be seen in Table 4.7, MT-2 RNA expression in general was higher than MT-1 expression due to the relatively higher normalised expression ratios. The expression of this isoform could easily be detected in all tissues.

**Table 4.7 MT-2 RNA expression ratios in tissues of rats treated with rotenone**

| Tissue | [Rotenone] mg/kg/day | Mean | Expression ratio | SD |
|---|---|---|---|---|
| **Brain** | 0 | 1.1983 | 1.00 | 0.063061 |
| | 3 | 2.25 | 1.88 | 0.282046 |
| | 9 | 2.37 | 1.98 | 0.123774 |
| | 15 | 2.44 | 2.04 | 0.04899 |
| **Liver** | 0 | 2.1633 | 1.00 | 0.113431 |
| | 3 | 3.00 | 1.39 | 0.027386 |
| | 9 | 4.14 | 1.91 | 0.023664 |
| | 15 | 4.95 | 2.29 | 0.020976 |
| **Heart muscle** | 0 | 0.855 | 1.00 | 0.036194 |
| | 3 | 0.98 | 1.15 | 0.060415 |
| | 9 | 1.34 | 1.57 | 0.029665 |
| | 15 | 1.92 | 2.25 | 0.02 |
| **Skeletal muscle** | 0 | 0.83333 | 1.00 | 0.038297 |
| | 3 | 1.34 | 1.61 | 0.022361 |
| | 9 | 0.97 | 1.16 | 0.014142 |
| | 15 | 0.98 | 1.18 | 0.014142 |

*Expression ratio calculated relative to the baseline (control) group. Mean = six samples done in triplicate before normalising it relative to the control group.*

### 4.9.1 MT-2 expression in brain tissue

Statistical analysis for MT-2 in the brain proved to have unequal variances ($p = 0.002$) according to Bartlett test. A normal probability plot was done on the residuals to determine if the data was normally distributed. After the indication, as can be observed in Figure 4.23 that the assumption of normality did not hold, a non-parametric Kruskal-Wallis test was performed to determine statistical significance ($p < 0.05$). In Table 4.8 the statistical results of MT-2 for the brain are given.

For MT-2 in the brain it was determined that the given dose groups (0, 3, 9, 15 mg/kg/day) have unequal variances for the dependent variable. After statistical significance was established between various dose groups for MT-2, practical significance was calculated by means of effect size with the means squared error. Data which proved to be practically significant ($d \geq 0.8$) are represented in Table 4.8.

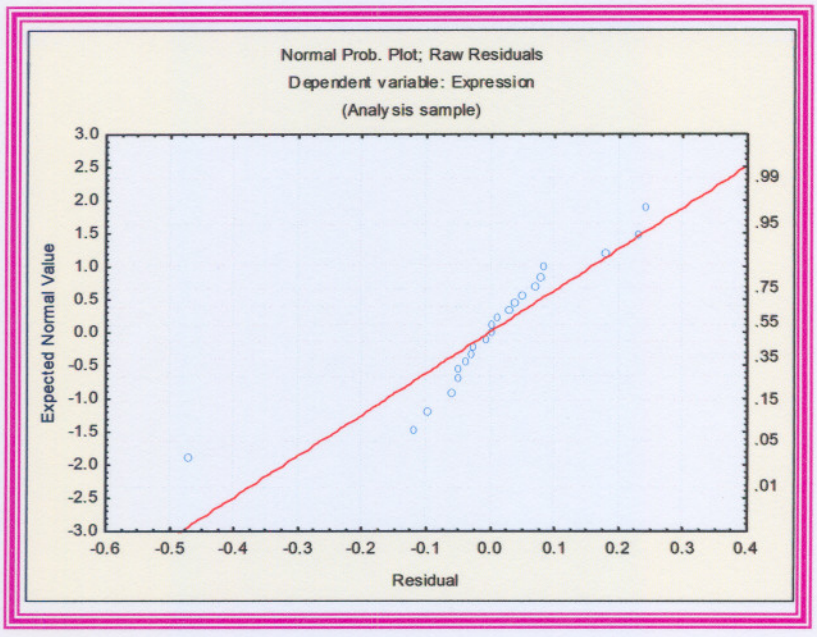


***Figure 4.23. Probability plot for MT-2 expression in the brain.*** *The appearance of the manner with which the data is spread in comparison to the red straight line indicates that the data for this particular tissue for MT-2 is not normally distributed and does thus not comply with the assumptions of ANOVA. Ultimately a Kruskal-Wallis test for multiple comparisons was performed for this particular tissue data.*

Table 4.8 summarises the statistical outcome of MT-2 expression in brain tissue. In this particular case the non-parametric Kruskal-Wallis test for multiple comparisons was performed on the data set. This table also indicates the position of statistical significance between the dose groups as well as the biological worth of the significant data (practically significant).

**Table 4.8 Results of the multiple comparisons of mean ranks of MT-2 RNA expression in the brain**

| MT-2 Brain: Statistical significance ($p < 0.05$) | | | | | SS dose groups: mg/kg/day | Practical significance ($d$ = *effect size*) |
|---|---|---|---|---|---|---|
| **Dose: mg/kg/day** | **0** | **3** | **9** | **15** | | |
| **0** | | 0.116471 | 0.060135 | **0.001279** | 0 and 15 | 7.01757 |
| **3** | 0.116471 | | 1.000000 | 1.000000 | - | - |
| **9** | 0.060135 | 1.000000 | | 1.000000 | - | - |
| **15** | **0.001279** | 1.000000 | 1.000000 | | - | - |

*This table indicates $p < 0.05$ (in red), thus statistical significance amongst the means for MT-2 expression in brain tissue was present. SS = Statistical significance.*

Mean values and 95% confidence intervals are graphically displayed in Figure 4.24. As mentioned before, MT-2 expression could be detected in brain tissue. When observing the analysis for MT-2 expression in the brain it evidently indicates a statistically and practically significant difference between dose groups 0 mg/kg/day and 15 mg/kg/day. At 3 mg/kg/day the increase was already approximately two-fold although it was not statistically significant at this dosage. The expression value was similar but slightly higher at 9 and 15 mg/kg/day.

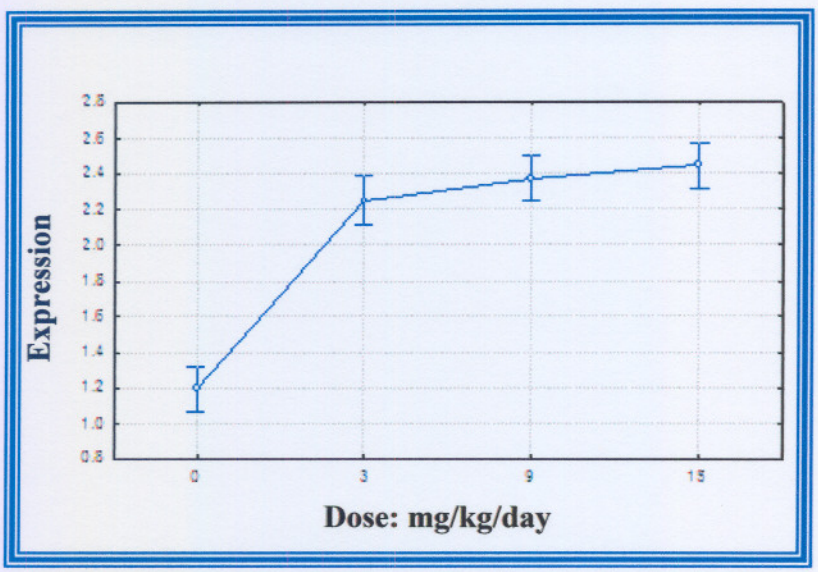


***Figure 4.24. MT-2 RNA expression in the brain at given rotenone dose concentrations.*** *Expression is indicated as the means (n=6). The vertical bars indicate the 95% confidence interval determined from the mean squared error $p < 0.05$.*

### 4.9.2 MT-2 expression in liver tissue

Statistical analysis for MT-2 in the liver proved to have unequal variances ($p = 0.0003$) by performing the Bartlett test. A normal probability plot was done on the residuals to determine if the data was normally distributed. After this calculation, as can be observed in Figure 4.25, the assumption of normality did not hold, thus a non-parametric Kruskal-Wallis test was performed to determine statistical significance ($p < 0.05$). With STATISTICA version 7.1, an Unequal post hoc test was performed due

to unequal sample sizes in dose concentration 3 mg/kg/day. In Table 4.9 the statistical results on MT-2 for the liver are given.

For MT-2 in the liver it was indicated that the given dose groups (0, 3, 9, 15 mg/kg/day) have unequal variance for the dependent variable. After statistical significance was established between various dose groups for MT-2, practical significance was calculated by means of effect size with the means squared error. Data which proved to be practically significant ($d \geq 0.8$) are represented in Table 4.9.

As can be observed in the statistical analysis for MT-2 in the liver displayed below, significant and practical expression changes occurred for MT-2 expression in the liver at the given rotenone concentrations.

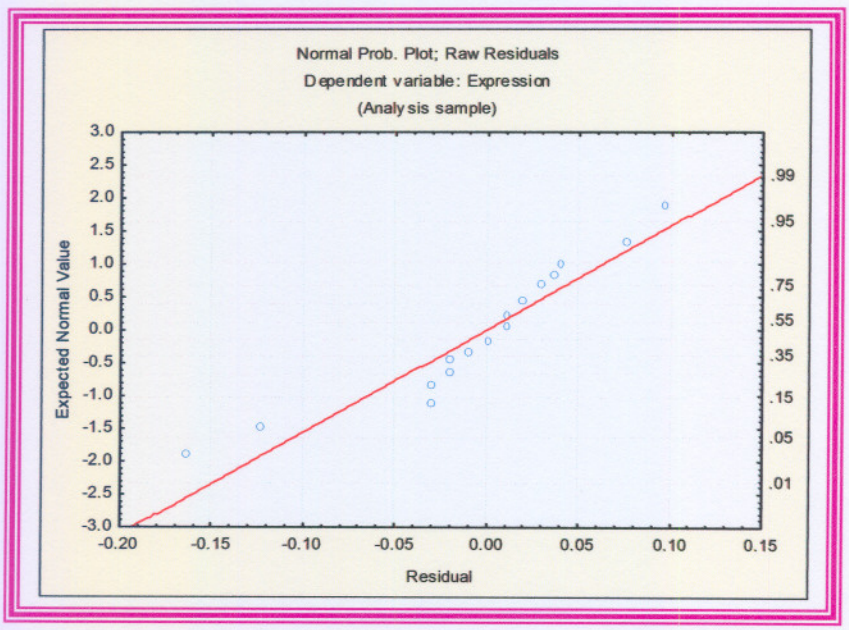


***Figure 4.25. Probability plot for MT-2 expression in the liver.*** *The appearance of the manner with which the data is spread in comparison to the red straight line indicates that the data for this particular tissue for MT-2 is not normally distributed and does thus not comply with the assumptions of ANOVA. Ultimately a Kruskal-Wallis test for multiple comparisons was performed for this particular tissue data.*

Table 4.9 summarises the statistical outcome of MT-2 expression in liver tissue. In this particular case the non-parametric Kruskal-Wallis test for multiple comparisons was performed on the data set. This table also indicates the presence of statistical

significance between the dose groups as well as the biological worth of the significant data (practically significant).

**Table 4.9 Results of the multiple comparisons of mean ranks of MT-2 RNA expression in the liver.**

| MT-2 expression in the liver: Statistical significance ($p < 0.05$) | | | | | SS dose groups: mg/kg/day | Practical significance ($d$ = *effect size*) |
|---|---|---|---|---|---|---|
| **Dose: mg/kg/day** | **0** | **3** | **9** | **15** | | |
| **0** | | 1.000000 | **0.029804** | **0.000085** | 0 and 9 | 32.0242 |
| **3** | 1.000000 | | 1.000000 | 1.000000 | 0 and 15 | 45.1469 |
| **9** | **0.029804** | 1.000000 | | 0.752747 | 3 and 15 | 31.5916 |
| **15** | **0.000085** | **0.030646** | 0.752747 | | - | - |

*This table indicates $p < 0.05$ (in red), thus statistical significance amongst the means for MT-2 expression in liver tissue was present. SS = Statistical significance.*

The mean values and 95% confidence intervals are graphically displayed in Figure 4.26. For MT-2 expression in the liver the statistically and practically significant values occurred between dose groups 0, 9 and 15 mg/kg/day and 3 and 15 mg/kg/day. In the liver, the MT-2 expression increased steadily unlike the trend observed in brain. The expression increased more than two fold over the dosage range and appears to be able to possibly increase even further at higher dosages.

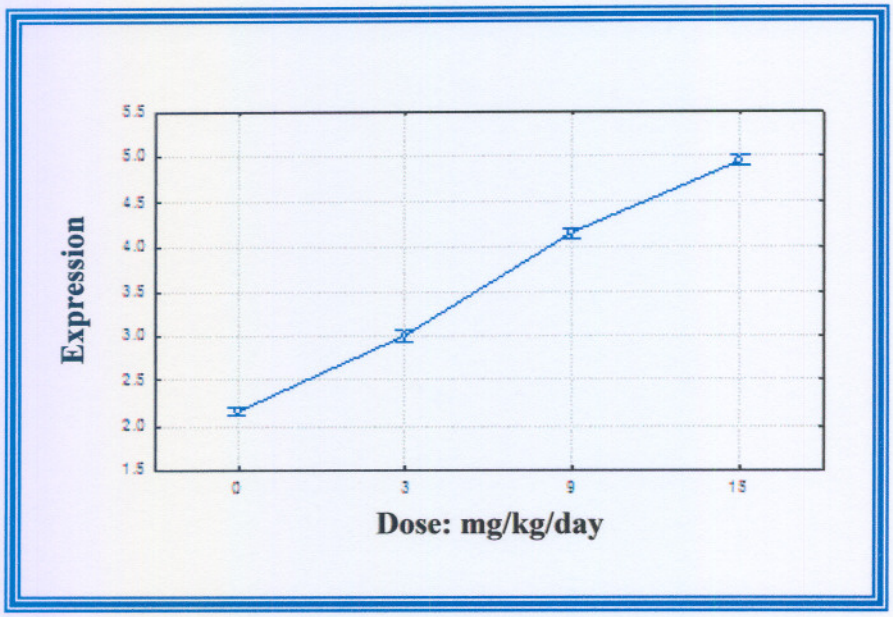


***Figure 4.26. MT-2 RNA expression in the liver at given rotenone dose concentrations.*** *Expression ratios are indicated as the means (n=6). The vertical bars indicate the 95% confidence interval determined from the mean squared error p <0.05.*

### 4.9.3 MT-2 expression in skeletal muscle

For MT-2 in skeletal muscle it was indicated that the given groups (0, 3, 9, 15 mg/kg/day) have approximately equal variance for the dependent variable. The Bartlett test for MT-2 in skeletal muscle tissue indicated *($p = 0.09$),* specifying that the variances in the data set were equal. Also, data for MT-2 in skeletal muscle comply with normal distribution as can be observed in Figure 4.27. A parametric test was performed on MT-2 data which indicated statistical significance if $p < 0.05$ and a post hoc test on unequal group sizes was performed to determine the difference of statistical significance between means for various dose groups as it is represented in Table 4.10.

After statistical significance was established between various dose groups for MT-2, practical significance was calculated by means of effect size with the means squared error. Data which proved to be practically significant *($d \geq 0.8$)* are represented in Table 4.10.

As can be observed in Figure 4.28 and Table 4.10 displayed below, significant and practical expression changes occur for MT-2 expression in skeletal muscle at the given rotenone concentrations. Statistically significant analysis occurred at all the given rotenone dose concentrations except between 9 mg/kg/day and 15 mg/kg/day.

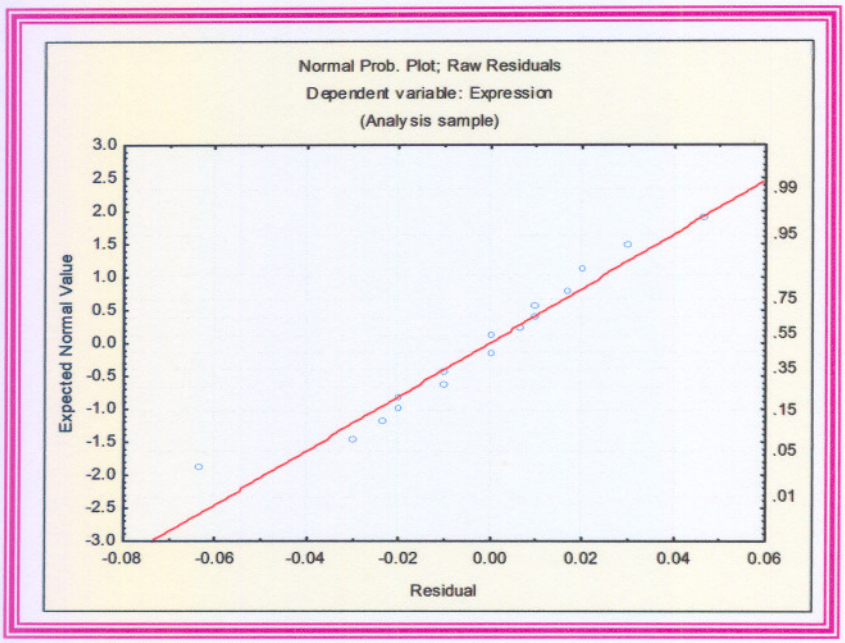


***Figure 4.27. Probability plot for MT-2 expression in skeletal muscle.*** *The appearance of the manner with which the data is spread in comparison to the red straight line indicates that the data for this particular tissue for MT-2 is normally distributed and does thus comply with the assumptions of ANOVA.*

Table 4.10 summarises the statistical outcome of MT-2 expression in skeletal muscle tissue. In this particular case the ANOVA parametric test and unequal post hoc test was performed on the data set. This table also indicates the presence of statistical significance between the dose groups as well as the biological worth of the significant data (practical significant).

**Table 4.10 ANOVA and unequal post hoc results for the MT-2 RNA expression in skeletal muscle.**

| MT-2 expression in skeletal muscle: Statistical significance ($p < 0.05$) | | | | | SS dose groups: mg/kg/day | Practical significance ($d$ = *effect size*) |
|---|---|---|---|---|---|---|
| **Dose: mg/kg/day** | **0** | **3** | **9** | **15** | | |
| **0** | | 0.000181 | 0.000181 | 0.000181 | 0 and 3 | 20.6847 |
| **3** | 0.000181 | | 0.000181 | 0.000181 | 0 and 9 | 5.57953 |
| **9** | 0.000181 | 0.000181 | | 0.892290 | 0 and 15 | 5.98778 |
| **15** | 0.000181 | 0.000181 | 0.892290 | | 3 and 9 | 15.1059 |
| | - | - | - | - | 3 and 15 | 14.69694 |

*This table indicates $p < 0.05$ (in red), thus statistical significance amongst the means for MT-2 expression in skeletal muscle tissue was present. SS = Statistical significance.*

For MT-2 expression in skeletal muscle the statistically and practically significant values occurred between dose groups 0, 3, 9 and 15 mg/kg/day and 3, 9 and 15 mg/kg/day. Mean values and the 95% confidence intervals are graphically displayed in Figure 4.28. Unlike any of the previous trends observed, the MT-2 expression increased significantly at 3 mg/kg/day, but then surprisingly decreased at higher dosages to levels similar to the control sample, albeit still significantly higher.

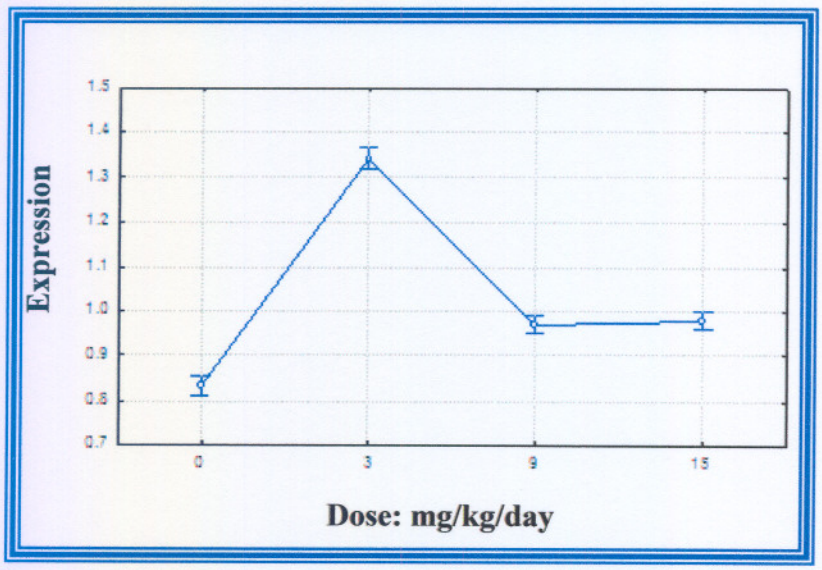


***Figure 4.28. MT-2 RNA expression in skeletal muscle at given rotenone dose concentrations.*** *Expression is indicated as the means (n=6). The vertical bars indicate the 95% confidence interval determined from the mean squared error $p < 0.05$.*

### 4.9.4 MT-2 expression in heart muscle

For MT-2 in heart muscle it was indicated that the given groups (0, 3, 9, 15 mg/kg/day) have approximately equal variance on the dependent variable. The Bartlett test for MT-2 in heart muscle tissue indicated *(p= 0.152196),* specifying that the variances in the data set are equal. Also, data for MT-2 in heart muscle comply with normal distribution as can be observed in Figure 4.29. A parametric test was performed on MT-2 data which indicated statistical significance if $p < 0.05$ and a post hoc test on unequal group sizes was performed to determine the difference of statistical significance between means for various dose groups as is represented in Table 4.11.

After statistical significance was established between various dose groups for MT-2, practical significance was calculated by means of effect size with the means squared error. Data which proved to be practically significant ($d \geq 0.8$) are represented in Table 4.11.

As can be observed in the statistical analysis for MT-2 expression in heart muscle displayed below, significant and practical expression changes occurred at the given rotenone concentrations. Statistically significant analysis occurred at all the given rotenone dose concentrations.

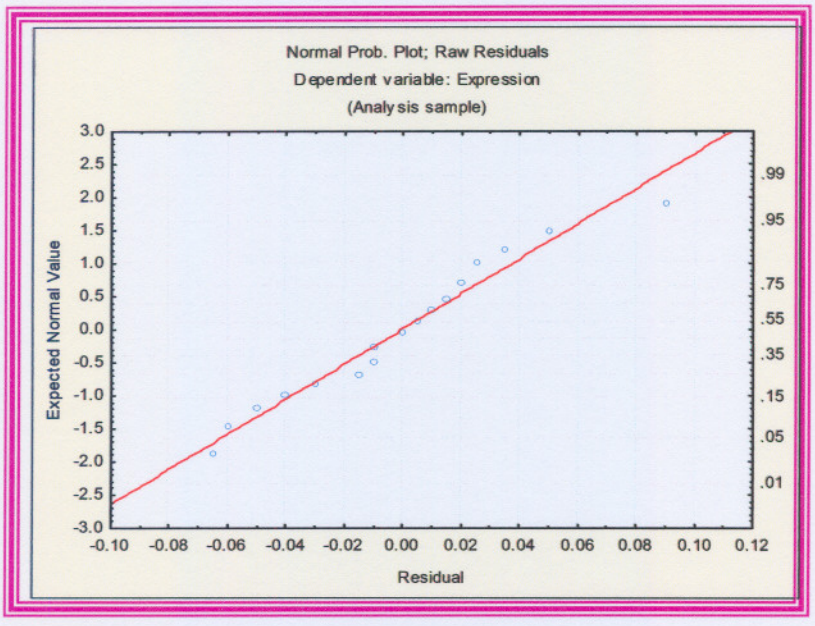


***Figure 4.29. Probability plot for MT-2 expression in heart muscle.*** *The appearance of the manner with which the data is spread in comparison to the red straight line indicates that the data for this particular tissue for MT-2 is normally distributed and does thus comply with the assumptions of ANOVA.*

Table 4.11 summarises the statistical outcome of the analysis of MT-2 expression in heart muscle tissue. In this particular case the ANOVA parametric test and unequal post hoc test was performed on the data set. This table also indicates the presence of statistical significance between the dose groups as well as the biological worth of the significant data (practical significant).

**Table 4.11 ANOVA and unequal post hoc results of MT-2 RNA expression in heart muscle.**

| **MT-2 Heart muscle: Statistical significance ($p < 0.05$)** | | | | | **SS dose groups: mg/kg/day** | **Practical significance ($d$ = *effect size*)** |
|---|---|---|---|---|---|---|
| **Dose: mg/kg/day** | **0** | **3** | **9** | **15** | | |
| **0** | | 0.000435 | 0.000181 | 0.000181 | 0 and 3 | 3.28266 |
| **3** | 0.000435 | | 0.000181 | 0.000181 | 0 and 9 | 12.7367 |
| **9** | 0.000181 | 0.000181 | | 0.000181 | 0 and 15 | 27.9683 |
| **15** | 0.000181 | 0.000181 | 0.000181 | | 3 and 9 | 9.45406 |
| | - | - | - | - | 3 and 15 | 24.6856 |
| | - | - | - | - | 9 and 15 | 15.2315 |

*This table indicates $p < 0.05$ (in red), thus statistical significance amongst the means for MT-2 expression in heart muscle tissue was present. SS = Statistical significance.*

The mean values and the 95% confidence intervals are graphically displayed in Figure 4.30. For MT-2 expression in heart muscle the statistically and practically significant values were determined in all the given dose groups. The trend and level of increase observed in heart muscle was similar to liver tissue where an initial increase at 3 mg/kg/day was experienced and further significantly increased at 9 and again at 15 mg/kg/day that was also more than a two-fold increase in expression.

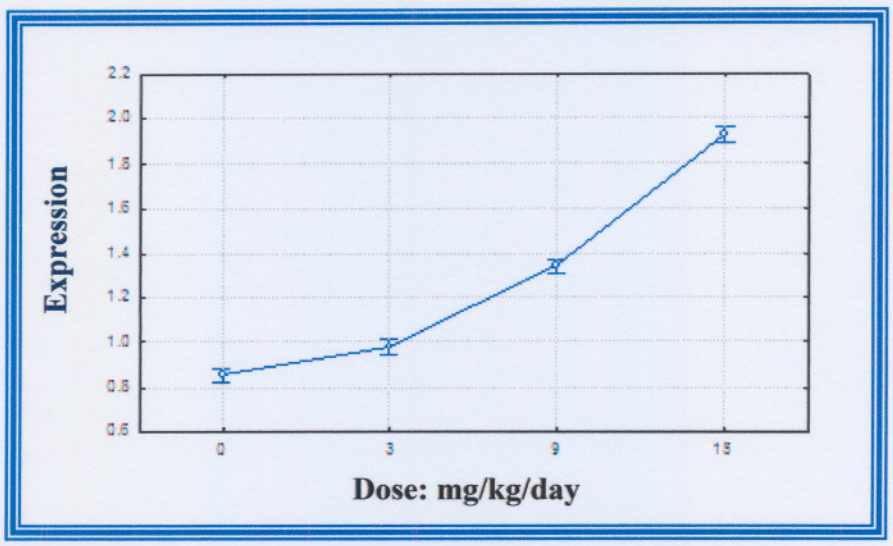


***Figure 4.30. MT-2 RNA expression in heart muscle at given rotenone dose concentrations.*** *Expression is indicated as the means (n=6). The vertical bars indicate the 95% confidence interval determined from the mean squared error p <0.05.*

## 4.10 MT-3 expression in rotenone-treated rat tissues

Table 4.12 gives a summary of the expression ratios of MT-3 in the various rotenone-treated rat tissues. The various statistical analyses of the data are further discussed in the following sections. As mentioned before, MT-3 expression could not be detected in either skeletal or heart muscle. This is as expected since MT-3 is a brain-specific isoform. It was, however, surprising to be able to clearly detect expression in the liver. Raw data generated from the real-time PCR analysis is displayed in Appendix B of this dissertation.

**Table 4.12 MT-3 RNA expression ratios in tissues of rats treated with rotenone**

| Tissue | [Rotenone] mg/kg/day | Mean | Expression ratio | SD |
|---|---|---|---|---|
| **Brain** | 0 | 1.9933 | 1.00 | 0.043205 |
| | 3 | 2.35 | 1.18 | 0.027386 |
| | 9 | 2.59 | 1.30 | 0.014142 |
| | 15 | 3.62 | 1.82 | 0.02 |
| **Liver** | 0 | 1.1217 | 1.00 | 0.042622 |
| | 3 | 1.32 | 1.18 | 0.022361 |
| | 9 | 1.5 | 1.34 | 0.021909 |
| | 15 | 1.6 | 1.43 | 0.023664 |
| **Heart muscle** | 0 | N/D | N/D | N/D |
| | 3 | N/D | N/D | N/D |
| | 9 | N/D | N/D | N/D |
| | 15 | N/D | N/D | N/D |
| **Skeletal muscle** | 0 | N/D | N/D | N/D |
| | 3 | N/D | N/D | N/D |
| | 9 | N/D | N/D | N/D |
| | 15 | N/D | N/D | N/D |

*Expression ratio calculated relative to the baseline (control) group. Mean = six samples done in triplicate before normalising it relative to the control group. N/D = Not detected*

### 4.10.1 MT-3 expression in brain tissue

For MT-3 in the brain it was indicated that the given dose groups (0, 3, 9, 15 mg/kg/day) have approximately equal variance for the dependent variable. Bartlett test for MT-3 in brain tissue indicated $p = 0.1$, specifying that the variances in the data set are equal. Also, data for MT-3 in the brain comply with normal distribution as can be observed in Figure 4.31. A parametric test was performed on MT-3 data which indicated statistical significance if $p < 0.05$ and a post hoc test on unequal group sizes was performed to determine the difference of statistically significant between means for various dose groups as it is represented in Table 4.13.

After statistically significant differences were established between the various dose groups for MT-3, practical significance was calculated by means of effect size with the means squared error. Data which proved to be practically significant ($d \geq 0.8$) are represented in Table 4.13.

As can be observed in the statistical analysis displayed below, statistically and practically significant expression changes occur for MT-3 expression in the brain at the given rotenone concentrations. Statistically significant analysis occurred at all the given rotenone dose concentrations.

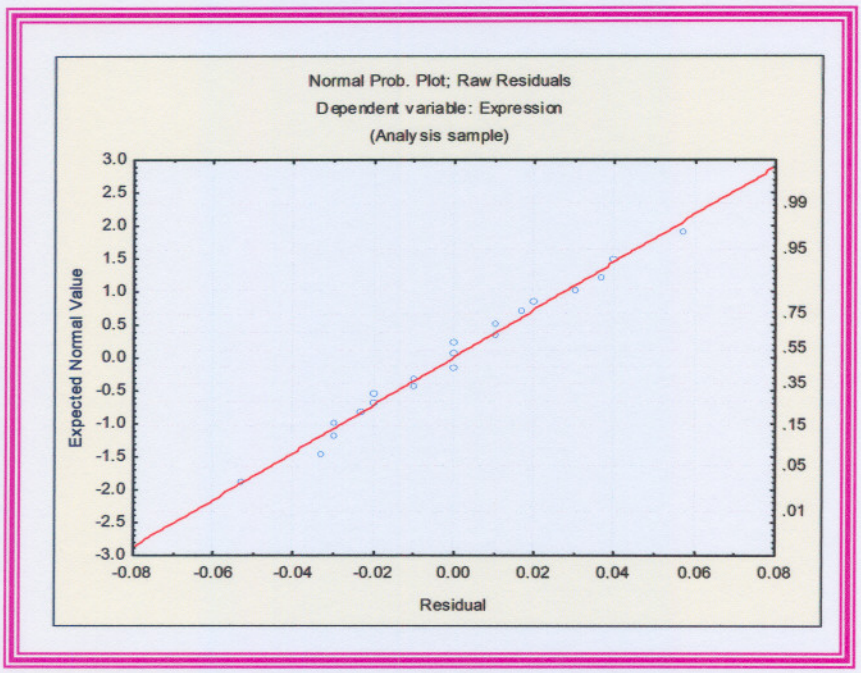


***Figure 4.31. Probability plot for MT-3 expression in the brain.*** *The appearance of the manner with which the data is spread in comparison to the red straight line indicates that the data for this particular tissue for MT-3 is normally distributed and does thus comply with the assumptions of ANOVA.*

Table 4.13 summarises the statistical outcome of MT-3 expression in brain tissue. In this particular case the ANOVA parametric test and unequal post hoc test was performed on the data set. This table also indicates the presence of statistical significance between the dose groups as well as the biological worth of the significant data (practical significant).

**Table 4.13 ANOVA and unequal post hoc results for the MT-3 RNA expression in the brain**

| MT-3 expression in the brain: Statistical significance ($p < 0.05$) | | | | | SS dose groups: mg/kg/day | Practical significance ($d$ = *effect size*) |
|---|---|---|---|---|---|---|
| **Dose: mg/kg/day** | **0** | **3** | **9** | **15** | | |
| **0** | | 0.000181 | 0.000181 | 0.000181 | 0 and 3 | 12.559 |
| **3** | 0.000181 | | 0.000181 | 0.000181 | 0 and 9 | 21.010 |
| **9** | 0.000181 | 0.000181 | | 0.000181 | 0 and 15 | 57.2781 |
| **15** | 0.000181 | 0.000181 | 0.000181 | | 3 and 9 | 2.66667 |
| | - | - | - | - | 3 and 15 | 8.4507 |
| | - | - | - | - | 9 and 15 | 36.2670 |

*This table indicates $p < 0.05$ (in red), thus statistical significance amongst the means for MT-3 expression in brain tissue was present. SS = Statistical significance.*

MT-3 expression in the brain presented with both practically and statistically significant values in all the given dose groups. The statistically significant results obtained and indicated in Table 4.13 are graphically displayed in Figure 4.32. The expression increased slightly but significantly at a rotenone dosage of 3 mg/kg/day and then significantly increased even more to an almost two-fold value at 15 mg/kg/day. This trend was similar to MT-2 in liver and heart muscle.

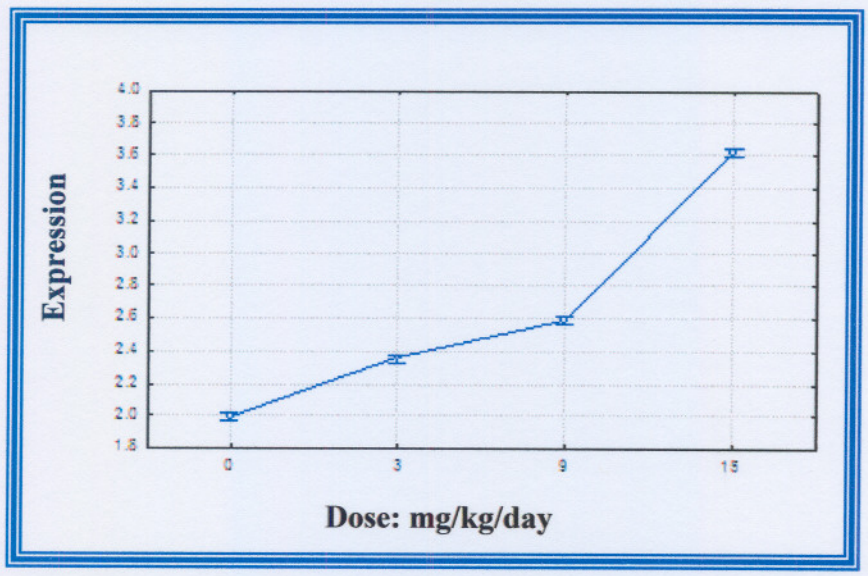


***Figure 4.32. MT-3 RNA expression in the brain at given rotenone dose concentrations.*** *Expression is indicated as the means (n=6). The vertical bars indicate the 95% confidence interval determined from the mean squared error $p < 0.05$.*

### 4.10.2 MT-3 expression in liver tissue

For MT-3 in the liver it was indicated that the given groups (0, 3, 9, 15 mg/kg/day) have approximately equal variance for the dependent variable. The Bartlett test for MT-3 in liver tissue indicated *(p= 0.37),* specifying that the variances in the data set are equal. Also, data for MT-3 in the liver comply with the assumption of a normal distribution as can be observed in Figure 4.33 A parametric test was performed on MT-3 data which indicated statistical significance if $p < 0.05$ and a post hoc test on unequal group sizes was performed to indicate the difference of statistical significance between means for various dose groups as it is represented in Table 4.14.

After statistical significance was established between various dose groups for MT-3, practical significance was calculated by means of effect size with the means squared error. Data which proved to be practically significant ($d \geq 0.8$) are represented in Table 4.14.

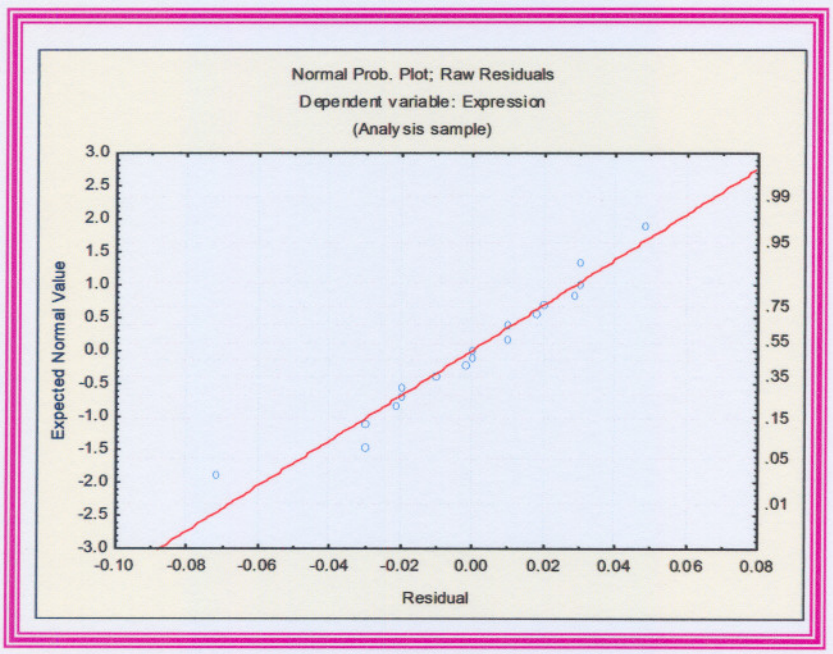


***Figure 4.33. Probability plot for MT-3 expression in the liver.*** *The appearance of the manner with which the data is spread in comparison to the red straight line indicates that the data for this particular tissue for MT-3 is normally distributed and does thus comply with the assumptions of ANOVA.*

Table 4.14 summarises the statistical outcome of MT-3 expression in liver tissue. In this particular case the ANOVA parametric test and unequal post hoc test was performed on the data set. This table also indicates the presence of statistical significance between the dose groups as well as the biological worth of the significant data (practical significant).

**Table 4.14 ANOVA and unequal post hoc results for MT-3 RNA expression in the liver.**

| **MT-3 expression in the liver: Statistical significance ($p < 0.05$)** | | | | | **SS dose groups: mg/kg/day** | **Practical significance ($d$ = *effect size*)** |
|---|---|---|---|---|---|---|
| **Dose mg/kg/day** | **0** | **3** | **9** | **15** | | |
| **0** | | **0.000181** | **0.000181** | **0.000181** | 0 and 3 | 6.76791 |
| **3** | **0.000181** | | **0.000181** | **0.000181** | 0 and 9 | 12.91126 |
| **9** | **0.000181** | **0.000181** | | **0.000225** | 0 and 15 | 5.18201 |
| **15** | **0.000181** | **0.000181** | **0.000225** | | 3 and 9 | 6.13795 |
| | - | - | - | - | 3 and 15 | 9.54792 |
| | - | - | - | - | 9 and 15 | 3.40997 |

*This table indicates $p < 0.05$ (in red), thus statistical significance amongst the means for MT-3 expression in liver tissue was present. SS = Statistical significance.*

The mean values and the 95% confidence intervals are graphically displayed in Figure 4.34. MT-3 expression in the liver indicated practically and statistically significant values in all the given dose groups. Although the normalised expression levels were not as high as in brain tissue, the responsiveness to rotenone treatment was similar in that the expression increased dose-dependently and significantly from 0 to 15 mg/kg/day to a level almost twice as high as baseline levels.

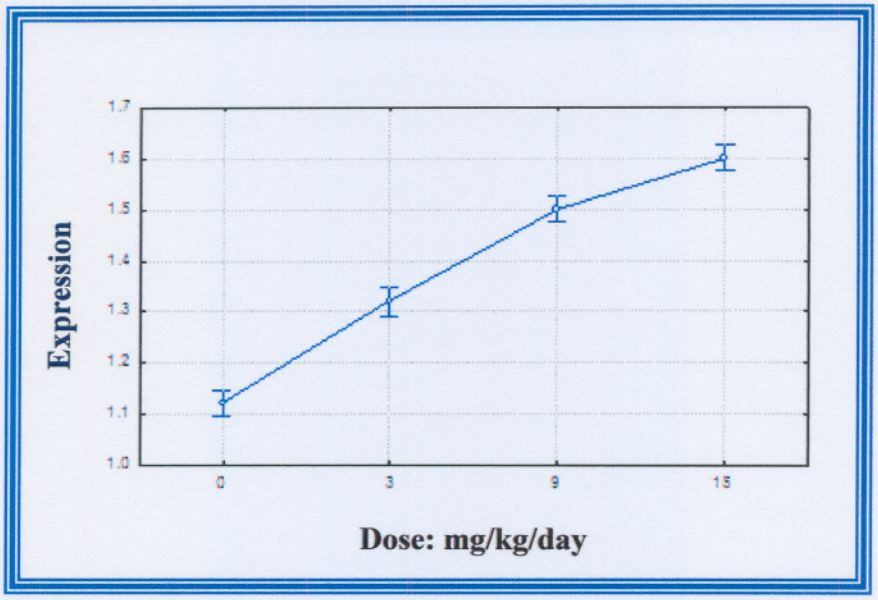


***Figure 4.34. MT-3 RNA expression in the liver at given rotenone dose concentrations.*** *Expression is indicated as the means (n=6). The vertical bars indicate the 95% confidence interval determined from the mean squared error $p < 0.05$.*

## 4.11 Correlation data

The tissues isolated from rotenone-treated rats used in the PhD study performed by Alessandrini (2006) were used to determine some biochemical parameters that could theoretically be compared to MT expression. A comparison of complex I activities as presented by Alessandrini was made with MT expression. Unfortunately limited data for complex I activity were available from Alessandrini's study to perform a proper correlation test. The mean values for complex I activities are given in Appendix C, as provided by Alessandrini. Even though both Spearman and Pearson correlation were performed on the available data, no definite and statistical significance could be calculated. Scatter plots were utilised (results not shown) for the different MT isoforms, and illustrated that data sets were too widely spread over the plots, and did thus not give appropriate indication of correlation.

## 4.12 Discussion

Using real-time PCR the expression of the three MT isoforms that are known to occur in rats could be quantified relative to a reference gene. From this it was clear that the

expression of the three isoforms were not similar in all tissues. MT-1 expression could be detected in all the tissues except for skeletal muscle. When observing the analysis for MT-1 expression in the brain it evidently indicates the statistically and practically significant changes in expression with treatment of rotenone occurred mainly after the highest dosage. This pattern was not similar in liver and heart muscle tissue where the most significant increase was already after the lowest dosage. From this it may be concluded that the responsiveness of MT-1 in the brain as compared to liver and heart muscle is not the same, assuming that the level of inhibition were similar in the three tissues. In light of the complex I activity from rotenone treatment, the pattern of inhibition is not the same. For example, in brain complex I activity decreases almost two- fold from 0 to 3 mg/kg/day, whereas in liver the inhibition of complex I activity to rotenone appears to be much less. Real-time results indicate that MT-1 expression, however, increases much faster in the liver than in the brain tissue. An accurate correlation analysis that may be done at a later stage will provide a better interpretation of the correlation between MT-1 expression and complex I activity.

MT-2 is regarded as the most abundant isoform in mammals (Coyle *et al.*, 2002). This is also clear from this study. The expression could be detected in all tissues and was relatively high. Although the expression levels of MT-2 were not the same as with MT-1, it was apparent that the pattern of MT-2 induction was visually similar to that in the liver and heart muscle. The MT-2 expression increased dose-dependently in the liver and heart muscle but not in the brain and skeletal muscle. The fold increase in expression in these afore-mentioned tissues was also similar, at just more than two-fold.

MT-3 expression, as expected (Palmitter, 1998) was most abundant in brain tissue. It was also detected in liver tissue. The fold increase in brain tissue was significant after rotenone treatment to levels almost twice as high as baseline levels. The expression increase in liver was much less. The trend in these tissues was similar to that of MT-1.

The significance of the MT expression pattern detected in this study cannot be concluded from the data generated. This will require functional studies. The correlation of the expression patterns with biochemical data generated by Alessandrini (2006) will be of great value to get better insight into the meaning of the expression.

What can be deduced from the data is that the MT-1 to MT-3 expression is induced by rotenone treatment as was shown for MT-2 in the *in vitro* study of Reinecke *et al.* (2006). Secondly it can be deduced that the responsiveness of the various isoforms are different. It may then be deduced that the regulation of these genes are different. Information on the promoter regions of the three isoforms in rats is not available. This would be very useful to compare the *cis*-acting elements in the promoters of these genes in rats.

# Chapter Five

# Conclusion

## 5.1 Introduction

From the literature discussion in Chapter Two it was concluded that complex I deficiency leads to a cascade of events, such as oxidative stress, which ultimately stimulates the expression of genes such as metallothioneins, to restore homeostasis (Reinecke *et al.*, 2006). A consequence of complex I deficiency is the formation of ROS, which has a deleterious effect on the mitochondrion and consequently causes the induction of apoptosis (Wallace, 1999). As discussed in the literature, MTs are scavengers of ROS which can be over expressed when a mitochondrial deficiency occurs (van der Westhuizen *et al.*, 2003; Thomas *et al.*, 1986; Ghoshal & Samson, 2001). Most of the previous studies examined the interaction of oxidative stress and investigated the effect of MT expression against oxidative stress conditions. Unanswered questions noted in the literature has lead to the hypothesis of this study which is that an induced complex I deficiency will lead to an increase of MT RNA expression *in vivo*. The objective of this study was therefore to investigate the different MT-isoform expression in different tissues isolated from rats treated with various concentrations of the complex I inhibitor, rotenone.

The strategy for this investigation was outlined in Figure 2.10 and the methodology was described in detail in Chapter Three. A benefit of making use of PCR based techniques was mainly that it allowed for the differentiation between different MT isoforms. Real-time PCR techniques provide simple and fast analysis and importantly, quantitative measurement. Disadvantages of this technique are that it is very expensive and requires much repetition to test specificity and reproducibility. Other techniques to consider for future studies would be performing and making use of hybridisation techniques due to its specific analysis where probes only bind to specific sequences in contrast to SYBR® Green which binds to dsDNA whether it be amplified, specifically or non-specifically.

## 5.2 Expression of MTs in rotenone-treated rats

In Figure 5.1 a diagrammatic summary is given for the results discussed in Chapter Four. In addition to a statistical evaluation of the RNA expression data, the practical significance of the MT isoform expression in the rotenone-treated tissues was also calculated to determine if the expression of these MT isoforms had any biological worth. MT expression in various tissue types treated with various rotenone concentrations indicated that MT-1 expression increased significantly in brain, liver and heart muscle. In these tissues MT expression increased as the rotenone dose concentrations increased, although the responsiveness of MT-1 RNA expression in the brain compared to the liver and heart muscle was not the same. MT-1 expression increased much faster in the liver than it did in the brain. MT-2 RNA expression was detected in all the tissues, and the expression values for this isoform were relatively high. Expression of MT-2 increased significantly in all the given tissues as the dose concentrations of rotenone increased. The expression of MT-2 increased dose-dependently in both the liver and heart muscle tissues and not in the brain and skeletal muscle. Expression of the brain specific isoform, MT-3, was also detected in the liver. The expression increased significantly in both the brain and liver tissue as complex I activity decreased due to the rotenone treatment.

There are numerous compounds such as rotonoids, MPTP and piercidins that are effective inhibitors of complex I (Esposti, 1998). Complex I deficiency will lead to a decrease in ATP production and an increase in ROS, a mostly harmful component participating in the initiation of apoptosis (Reinecke *et al.*, 2006). Many agents that induce oxidative stress can induce MT expression (Hamer, 1986). Common enhancers or transcriptional regulators may influence the expression of MTs, however, direct expression and regulation of MTs can also be related to the intracellular environment of each cell type, such as heavy metals or an increase in ROS. The ROS sensitive, antioxidant response element (ARE) mediates MT RNA expression in response to ROS (Davies & Cousins, 2000). This is likely to be the reason for the increased expression in rotenone-treated rats, although no evidence exists for this statement. Another possible explanation for the increase in MT expression in the complex I deficient tissues might be that MTs play an important role in the homeostatic control of these tissues, as possible fluctuations in the metabolism of the various tissues

occur. MT expression may possibly play a role in the detoxification of this whole process and, in particular, the scavenging of ROS (van der Westhuizen *et al.,* 2003; Reinecke *et al.,* 2006). Even though no significant results for correlation in MT expression and complex I activity was generated in this investigation, it is speculated that a negative correlation between these two parameters will be demonstrated. For the general comparisons of MT expression, complex I activity and other related biochemical parameters the study of Alessandrini (2006) should be reviewed.

Results obtained from Reinecke *et al.* (2006) in an *in vitro* study done on rotenone-treated HeLa cells have indicated no induction of MT-1 expression. That study determined elevated expression of MT-2A which correlates with the results on MT-2 expression obtained in this study. According to Uchida *et al.* (1991), deficient MT-3 expression in the brain, specifically neuronal cells might be a probable cause for seizures. As mentioned before the MT-3 expression in the study presented here increased in the induced complex I deficient brain tissue. The induction of MT-3 expression has been reported in a number of experimental models of brain injury (Hidalgo *et al.,* 2001*).* These models either included physically or chemically induced brain injury. In the investigation presented here, it was demonstrated that by increasing the dose concentration of rotenone, an increase in MT-2 and MT-3 expression occurred in the brain. As reviewed by Hidalgo *et al.* (2001), MT-3 expression in injured brain cells is often down-regulated initially after which it returns to its original levels. A possible reason for this observation might be because of the different biological properties of MT-3, or even that the differences in MT-expression might be linked to different tissues and different cellular properties.

In Figure 5.1 a diagrammatic summary is given for the obtained results described in Chapter Four.

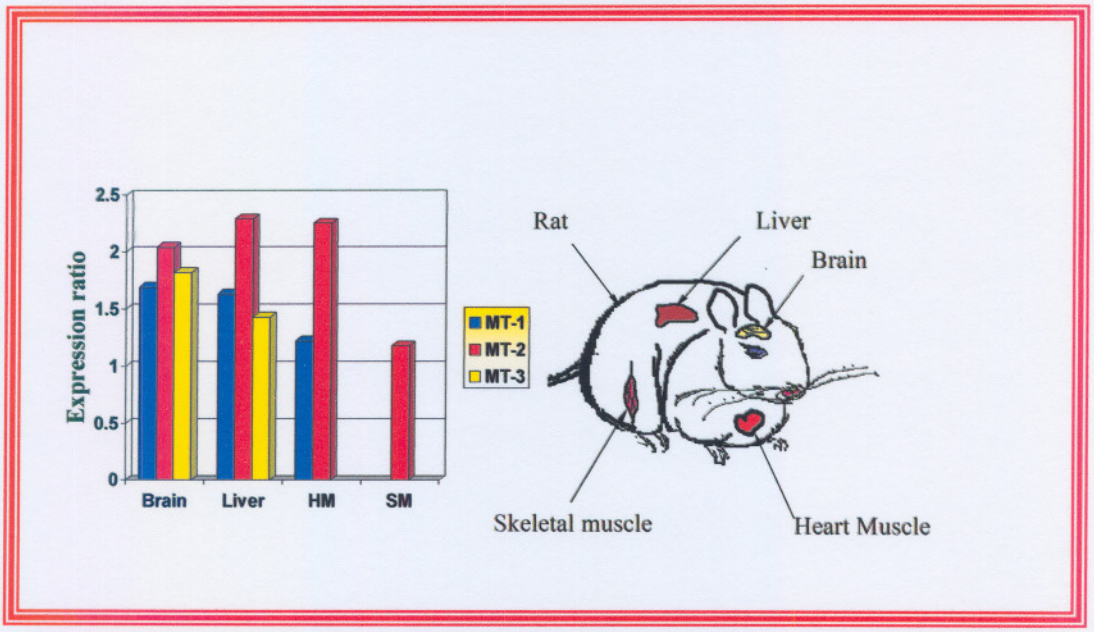


***Figure 5.1. A diagrammatic presentation of experimental outline and design of a rat with various tissues that represent the species and tissue used in this study.*** *The data sheet indicates the relative fold of expression from 0 mg/kg/day to 15 mg/kg/day, where 0 mg/kg/day were denoted as 1. The amount of specific MT isoform expression in various tissues which are discussed more critically in Sections 4.7 to 4.12. MT-1 RNA expression = blue, MT-2 RNA expression = red, MT-3 RNA expression = yellow.*

## 5.3 Conclusions

The results from this study supported the proposed hypothesis that treatment of rats with rotenone, increases MT RNA expression. This induction of expression is likely to be a result of inhibition of complex I activity due to the activity of rotenone and subsequent increase of free radicals that can induce MT expression. Although functional studies are required, the associated antioxidant properties of MTs in general may point to a protective response. In this study a clear observation, that expression patterns (responsiveness) in rotenone-treated tissues are different between the three isoforms was noted. To evaluate the different expression patterns of the MT isoforms, investigation of the promoter regions and further expression studies would be necessary. This would be of importance as currently no functional distinctions can be made between the isoforms.

The fact that different MT isoforms are concentrated in particular tissues or cell-types in the body, suggests that they may have distinct tissue or cell-dependent roles. Furthermore, the cell specific expression of MT isoforms indicates that they may not only have different biological functions but that the isoforms may be expressed according to the specific needs in different cell types. The over expression of MTs may contribute to a protected effect on the pathology of disease, although this still needs to be established. Furthermore, the results of this study show that the expression of the various MT isoforms in rotenone-treated rat tissues is not expressed in a similar way to the induced deficiency, which may point to a differential regulation and response of the three MT isoforms to such a deficiency.

The results of this investigation have addressed the problem statement and proved to support the hypothesis as outlined in Chapter Two. Future research may pursue MT expression to be used as biomarkers in tissues of mammals which are exposed to a contaminated environment and/or high metal exposure. Other studies to consider are to measure MT isoform expression in tumor cells and oxidative stress models and, in particular, to determine if the various isoforms have defined functional roles. Thus, will MT expression facilitate tumor cell growth by acting as a zinc donor to various transcription factors. A concern in these studies may be that, as MT inhibits the process of apoptosis, that MT expression may resist any oncogenic drug treatment.

Current research is shifting towards the clarification of the physiological functions of MTs. Studies focussing on the mechanism of the regulation of MT expression and the intracellular localisation of MT is increasing. Another approach that needs to be considered is to correlate MT protein levels with RNA expression levels. This can be done with immunological techniques, such as ELISA. This would give useful information because post transcriptional processes could alter the level of MT protein expression. This would be required to better evaluate the responsiveness of MT expression during rotenone treatment or other interventions associated with MT expression and function.

# References


1. Alessandrini, M. 2006. Evaluation of possible therapeutic intervention strategies for mitochondrial Complex I deficiency. Ph.D. thesis
2. Alphey, L. 1997. DNA sequencing from experimental methods to bioinformatics. *BIOS Scientific Publishers, Ltd. Oxford, UK.*
3. Anderson S., Bankier, A.T., Barrell, B.G., de Bruijn, M.H.L., Coulson, A.R., Drouin, J., Eperon, I.C., Nierlich, D.P., Roe, B.A., Sanger, F., Schreier, P.H., Smith, A.J.H., Staden, R., Young, I.G. 1981. Sequence and organization of the human mitochondrial genome. Nature. 290: 457-465.
4. Andrews, G.K. 2000. Regulation of metallothionein gene expression by oxidative stress and metal ions. *Biochem. Pharmacol.* 59: 95-104.
5. Aschner, M., Cherian, M.G., Klaassen, C.D., Palmiter, R.D., Erickson, J.C., and Bush, A.I. 1997. Metallothioneins in brain: The role in physiology and pathology. *Toxicology and Applied Pharmacology.* 142: 229-242.
6. Bauman, J.W., Lui, J., Lui, P., and Klaassen, C.D. 1991. Increase in metallothionein produced by chemicals that induce oxidative stress. *Toxicology and Applied Pharmacology.* 110: 347-354.
7. Bindoff, L. 1999. Treatment of mitochondrial disorders: practical and theoretical issues. *European Journal of Paediatric Neurology.* 3:201-208.
8. Binz, P.A., and Kägi, J.H.R. 1999. Classification of metallothionein. http://www.biochem.unizh.ch/mtpage/classif.html.
9. Bittel, D., Dalton, T.P., Samson, S., Geclamu, L., and Andrews, G.K. 1998. The DNA binding activity of metal response element-binding transcription factor-1 is activated *in vivo* and *in vitro* by zinc, but not by other transition metals. *The Journal of Biological Chemistry.* 273: 7127-7133.
10. Bogenhagen, D., and Clayton, D.A., 1974. The number of Mitochondrial Deoxyribonucleic Acid Genomes in Mouse L and Human HeLa Cells:

Quantitative isolation of mitochondrial deoxyribonucleic acid. *The Journal of Biological Chemistry.* 294(24): 7991-7995.

11. Bustin, S.A. 2000. Absolute quantification of mRNA using real-time reverse transcription polymerase chain reaction assays. *Journal of Molecular Endocrinology.* 25: 169-193.
12. Cadenas, E., and Davies, K.J.A. 2000. Mitochondrial free radical generation, oxidative stress and aging. *Free Radical Biology and Medicine.* 29(3/4): 222-230.
13. Carelli, V., Ross-Cisneros, F.N., Sadun, A.A. 2004. Mitochondrial dysfunction as a cause of optic neuropathies. *Progress in Retinal and Eye Research.* 23(1): 53-89.
14. Carrasco, J., Hernandez, J., Bluethmann, H. and Hidalgo, J. 1998. Interleukin-6 and tumor necrosis factor-alpha type 1 receptor deficient mice reveal a role of IL-6 and TNF-alpha on brain metallothionein-I and –III regulation. *Mol. Brain Res.* 57: 221-234.
15. Chabonon, H., Nury, D., Mickleburgh, I., Burtle, B and Hesketh, J. 2004. Characterization of the *cis*-acting element directing perinuclear localization of the Metallothionein-1 mRNA. *Biochemical Society Transactions.* 32: part 5.
16. Chance, B., Sies, H., and Boveris, A. 1979. Hydroperoxide metabolism in mammalian organs. *Phys. Rev.* 59: 527-605.
17. Chassaigne, H., and Lobinski, R. 1998. Polymorphism and identification of Metallothionein isoforms by reversed-phase HPLC with on-line ion-spray mass spectrometric detection. *Analytical Chemistry.* 70: 2536-2543.
18. Chen, S.H., Lin, C.Y., Cho, C.S., Lo, C.Z., and Hsiung, C.A. 2003. Primer Design Assistant (PDA): a web-based primer design tool. *Nucleic Acids Research.* Vol.31. 13: 3751-3754.
19. Chinnery, P.F. 2002. Inheritance of mitochondrial disorders. *Mitochondrion.* 2: 149-155.
20. Choudhuri, S., Kramer, K.K., Berman, N.E.J., Dalton, T.P., Andrews, G.K., and Klaassen, C.D. 1995. Constitutive expression of metallothionein genes in mouse brain. *Toxicology and Applied Pharmacology.* 131: 144-154.

21. Coyle, P., Philcox, J.C., Carey, L.C., Rofe, A.M. 2002. Metallothionein: The multipurpose protein. *Cellular and Molecular Life Sciences.* 59: 001-21.

22. Cunningham, M.L., Solimanb, M.S., Badrb, M.Z., Matthews, H.B. 1995. Rotenone, an anticarcinogen, inhibits cellular proliferation but not peroxisome proliferation in mouse liver. *Cancer Letters.* 95: 93-97.

23. Dalton, T.P., Bittel, D., and Andrews, G.K. 1997. Reversible activation of the mouse metal response element-binding transcription factor-1 DNA binding involves zinc interactions with the zinc-finger domain. *Mol. Cell. Biol.* 17: 2781-2789.

24. Dalton, T.P., Shertzer, H.G., and Alvaro, P. 1999. Regulation of gene expression by reactive oxygen. *Pharmacol. Toxicol.* 39: 67-101.

25. Davies, S.R., and Cousins, R.J. 2000. Metallothionein expression in animals: A physiological perspective on function. *J. Nutr.* 130: 1085-1088.

26. De, S.K., Mcaster, M.T. and Andrews, G.K. 1990. Endotoxin induction of murine metallothionein gene expression. *The Journal of Biological Chemistry.* 265: 15267-15274.

27. DiMauro, S. 2004. Mitochondrial diseases. *Biochimica et Biophysica Acta,* 1658: 80-88.

28. Ellis, S.M., and Steyn, H.S. 2003. Practical significance (effect sizes) versus or in combination with statistical significance (p-values). *Management Dynamics.* 12(4): 51-53.

29. Esposti, M.D. 1998. Inhibitors of NADH-Ubiquinone reductase: an overview. *Biochimica et Biophysica Acta*, 1364:222-235.

30. Fearnley, I. M., and Walker, J. E. 1992 Conservation of sequences of subunits of mitochondrial complex I and their relationships with other proteins. *Biochimica et Biophysica Acta,* 1140: 105-134

31. Frey, T.G., and Mannella, C.A. 2000. The internal structure of mitochondria. *Trends in Biochemical Science.* 25(7): 319-324.

32. Ghoshal, K., and Samson, T.J. 2001. Regulation of metallothionein gene expression. *Progress in Nucleic Acid Research and Molecular Biology.* 66: 358.

33. Giacconi, R., Cipriano, C., Muzzioli, M., Gasparini, N., Orlando, F. and Mocchegiani, E. 2003. Interrelationships among brain. *Mech. Ageing Dev.* 124: 371-378.

34. Gray, M.W. 1993. Origin and evolution of organelle genomes. *Current Opinion in Genetics and Development.* 3: 884-890.

35. Greenamyre, J.T., Sherer T.B., Betarbet R., Panov A.V. 2003. Complex I and Parkinson's disease. *IUBMB Life.* 52: 135-141.

36. Grigorieff, N. 1998. Three-dimensional structure of bovine NADH:ubiquinone oxidoreductase (complex I) at 22 A in ice. *Journal of Molecular Biology.* 277(5): 1033-46.

37. Grigorieff, N. 1999. Structure of the respiratory NADH:ubiquonone oxidoreductase (complex I). *Current Position in Structural Biology.* 9: 476-483.

38. Haase, H. and Maret, W. 2004. A differential assay for the reduced and oxidized states of metallothionein and thionein. *Analytical Biochemistry.* 333: 19-26.

39. Hamer, D.H. 1986. Metallothionein. *Annu. Rev. Biochem.* 55: 913-951.

40. Haq, F., Mahoney, M., Koropatnick, J. 2003. Signalling events for metallothionein induction. *Mutation Research.* 533: 211-226.

41. Hidalgo, J., Aschner, M., Zatta, P., Vasak, M. 2001. Roles of the metallothionein family of proteins in the central nervous system. *Brain Res Bull.* 55: 133–145.

42. Hirst, J., Carrol, J., Fearnley, I.M., Shannon, R.J., and Walker, J. E. 2003. The nuclear encoded subunits of complex I from bovine heart mitochondria. *Biochimica et Biophysica Acta*, 1604: 135-150.

43. Hunziker, P.E., Wan, M., Heuchel, R., Radtke, F., Kägi, J.H. 1995. Regulation of metallothionein gene expression in Cd- or Zn-adapted RK-13 cells. *Experentia.* 51: 606-11.

44. Jacob, S.T., Ghoshal, K., Sheridan, J.F. 1999. Induction of Metallothionein by stress and its molecular mechanisms. *Gene expression.* 7: 301-310.

45. Kägi, J. H. R., Vasak, M., Lerch, K., Gilg, D.E.O., Hunziker, P., Bernhard, W.R., Good, M. 1984. Structure of mammalian metallothionein. *Environ. Health Perspect.* 54: 93-103.

46. Kägi, J.H.R. 1991. Overview of metallothioneins. *In Methods in Enzymology.* 205: 614.

47. Kägi, J.H.R., and Vallee, B.L. 1960. Metallothionein: a cadmium- and zinc- containing protein from equine renal cortex. *The Journal of Biological Chemistry.* 235: 3460-3465.

48. Kägi, J.H.R., Himmelhoch, S.R., Whanger, P.D., Bethune, J.L., Vallee, B.L. 1974. Equine Hepatic and Renal metallothioneins. *Journal of Biological Chemistry.* 249(11): 3537-3542.

49. Kägi, J.H.R., Nordberg, M., 1979. Metallothionein. Basel: Birkhauser Verlag.

50. Karin, M., Eddy, R.L., Henry, W.M., Haley, L.L., Byers, M.G., Shows, T.B. 1984. Human metallothionein genes are clustered on chromosome 16. *Proceedings of the National Academy of Sciences of the United States of America.* 81: 5494-5498.

51. Kerner, J., and Hoppel, C. 2000. Fatty acid import into mitochondria. *Biochemica et Biophysica Acta.* 1486: 1-17.

52. Klaassen, C.D., Choudhuri, S. 2000. Use of genetically altered animal models in understanding the role of metallothionein in cadmium toxicity. *Pure Appl. Chem.* 72(6): 1023-1026.

53. Koh, J.Y., Suh, S.W., Gwag, B.J., He, Y.Y., Hsu, C.Y., and Choi, D.W. 1996. The role of zinc in selective neuronal death after transient global cerebral ischemia. *Science.* 272: 1013-1016.

54. Kojima, S., Shimada, A., Morita, T., Yamano, Y. and Umemura, T. 1999. Localization of metallothioneins-I and –II and MT-III in the brain of aged dog. *J. Vet. Med. Sci.* 61: 343-349.

55. Kojima, Y., Otsuka, S., and Yamanaka, T. 1988. *Bioactive Molecules. Elsevier. Tokyo,* 539.

56. Koropatnick, J., and Leibrandt, M.E.I. 1995. Effects of metals on gene expression. *Handbook of Experimental Pharmacology, Toxicology of metals, Biochemical Aspects (R.A. Goyer and M.G. Cherian, Eds.).* 115: 91-120. Springer Verlag, New York.

57. Levadoux-Martin, M., Mahon P., Beattie J.H., Wallace H.M. and Hesketh J.E. 1999. Cell-cycle-dependent nuclear import of metallothionein requires

its mRNA to be associated with the perinuclear cytoskeleton. *Journal of Biological Chemistry*, 274: 34961-34966.

58. Li, T.Y., Kraker, A.J., Shaw, C.F., Petering, D.H. 1980. Ligand substitution reactions of metallothionein with EDTA and apo-carbonic anhydrase. *Proceedings of the National Academy of Sciences of the United States of America.* 77: 6334-6338.

59. Liu, Y., Fiskum, G., Schubert, D. 2002. Generation of reactive oxygen species by the mitochondrial electron transport chain. *Journal of Neurochemistry.* 80: 780-787.

60. Loeffen, J.L.C.M., Smeitink, J.A.M., Trijbels, J.M.F., Janssen, A.J.M., Triepels, R.H., Senger, R.C.A. and Van Den Heuvel, L.P. 2000. Isolated Complex I Deficiency in Children: Clinical, Biochemical and Genetic Aspects. *Human Mutation*, 15: 123-134.

61. Maniatis, T., Fritsch, E.F., Sambrook, J. 1982. *Molecular cloning: a laboratory manual. NY: Cold Spring Harbor Laboratory Press.* 249-251, A468.

62. Mannella, C.A., 2000. Our changing views of mitochondria. J. *Bioenerg. Biomembr.* 32: 1-4.

63. Maret, W. and Vallee, B.L. 1998. Thiolate ligands in metallothionen confer redox activity on zinc clusters. *Proceedings of the National Academy of Sciences of the United States of America.* 95: 3478-3482.

64. Mathews, C.K. and Van Holde, K.E. 2000. *Biochemistry 3rd edition.* Benjamin/Cummings Publishing Company. USA.

65. Mayes, P.A., Murray, R.K., Granner, D.K., Rodwell, V.W. 2000. *Harper's Biochemistry, 25th edition.* Appelton and Lange.

66. Mitchell, P. 1961. Coupling of phosphorylation to electron and hydrogen transfer by chemiosmotic type of mechanism. *Nature.* 191: 144-148.

67. Mitchell, P. 1979. Keilin's respiratory chain concept and its chemiosmotic consequences. *Science.* 206: 1148-1158.

68. Mocchegiani, E., Giacconi, R., Cipriano, C., Gasparini, N., Orlando, F., Stecconi, R., Muzzioli, M., Isani, G. and Carpene, E. 2002. Metallothioneins (I + II) and thyroid-thymus axis efficiency in old mice: role of corticosterone and zinc supply. *Mech. Ageing Dev.* 123: 675-694.

69. Mocchegiani, E., Giacconi, R., Fattoretti, P., Casoli, T., Cipriano, C., Muti, E., Malavolta, M., DiStefano, G. and Bertoni-Freddari, C. 2004. Metallothionein isoforms (I + II and III) and interleukin-6 in the hippocampus of old rats: may their concomitant increments lead to neurodegeneration? *Brain Research Bulletin.* Vol 63(2): 133-142.

70. Moffat, P., and Denizeau, F. 1997. Metallothionein in physiopathological processes. *Drug. Metab. Review.* 29: 261-307.

71. Morgan-Hughes, J.A., Darveniza, P., Landon, D.N., Land, J.M. and Clark, J.B. 1979. A mitochondrial myopathy with a deficiency of respiratory chain NADH-CoQ reductase activity. *Journal of Neurological Science.* 43: 27-46.

72. Morin, C. 2000. [Web:] http://members.aol.com/christofmorin/index.html.

73. Mullis:http://www.britannica.com/ebc/article9375591?query=Mullis%2C%201986andct

74. Munnich, A., and Rustin, P. 1996. Clinical spectrum and diagnosis of mitochondrial disorders. *Am. J. Med. Genet.* 106: 4-17.

75. Nielson, K.B., Atkin, C.L., Winge, D.R. 1985. Distinct metal-binding configurations in Metallothionein. *The Journal of Biological Chemistry.* 260: 5342-5350.

76. Nordberg and Kojima. MT-page Classification. http://www.biochem.unizh.ch/mtpage/classif.html.

77. Nordberg, M., and Nordberg, G.F., 2000. Toxicological aspects of metallothionein. *Cell. Mol. Biol.* 46: 451–463.

78. Olivier, Y. 2004. Analysis of metallothionein expression levels in NADH:ubiquinone oxidoreductase deficiency. Potchefstroom: North-West University. (Dissertation – M.Sc).

79. Ono, S., Koropatnick, D.J., and Cherian, M.G. 1997. Regional brain distribution of metallothionein, zinc and copper in toxic milk mutant transgenic mice. *Toxicology.* 124: 1-10.

80. Palmitter, R.D., Findley, S.D., Whitemore, T.E. and Durnam, D.M. 1992. A brain-specific member of the metallothionein gene family. *Proceedings of the National Academy of Sciences of the United States of America.* 89: 6333-6337.

81. Passarella, S., Atlante, A., Valenti, D., De Bari, L. 2003. The role of mitochondrial transport in energy metabolism. *Mitochondrion.* 2: 319-343.

82. Penkowa, M., Giralt, M., Carrasco, J. and Hidalgo, J. 2000. Zinc or copper deficiency-induced impaired inflammatory response to brain trauma may be caused by the concomitant metallothionein changes. *J. Neurotrauma* 18: 447-463.

83. Perkins, G., and Frey, T.G. 2000. Recent structural insight into mitochondria gained by microscopy. *Micron: The International Research and Review Journal of Microscopy,* 31: 97-111.

84. Pfaffl, M.W., Horgan, G.W., Dempfle, L. 2002. Relative expression software tool (REST©) for group-wise comparison and statistical analysis of relative expression results in real-time PCR. *Nucleic Acids Research.* 30(9): 2-10.

85. Pulkes, T., and Hanna, M.G. 2001. Human mitochondrial diseases. *Advanced Drug Delivery Reviews.* 49(1-2): 27-43.

86. Quesada, A.R., Byrnes, R.W., Krezoski, S.O. and Petering, D.H. 1996. Direct reaction of $H_2O_2$ with sulfhydryl groups in HL-60 cells: zinc-metallothionein and other sites. *Arch. Biochem. Biophys.* 334: 241-250.

87. Quiafe, C.J., Findley, S.D., Erickson, J.C., Froelick, G.J., Kelly, E.J., Zambrowicz, B.P., Palmiter, R.D. 1994. Induction of a new metallothionein isoforms (MT-IV) occurs during differentiation of stratified squamous epithelia. *Biochemistry.* 33: 7250-7259.

88. Raha, S., and Robinson, B.H. 2001. Mitochondria, oxygen free radicals, and apoptosis. *American Journal of Medical Genetics.* 106: 62-70.

89. Rautenbach, G.S. 2004. Differentiated tissue response to rotenone induced complex I deficiency in rats. Potchefstroom: North-West University. (Dissertation – M.Sc).

90. Reinecke, F., Levanets, O., Olivier, Y., Louw, R., Semete, B., Grobler, A., Hidalgo, J., Smeitink, J.A.M., Olckers, A., van der Westhuizen, F.H. (2006) Metallothionein-2A expression is inducible and protects against ROS-mediated cell death in rotenone treated HeLa cells. In print. *Biochemical Journal.* 395: 405-415.

91. Richards, M.P. Characterization of the metal composition of metallothionein isoforms using reversed-phase high-performance liquid chromatography with atomic absorption spectrophotometric detection. 1989. *J. Chromatogr.* 482: 87-97.

92. Robinson, B.H. 1998. Human Complex I deficiency: Clinical spectrum and involvement of oxygen free radicals in the pathogenicity of the defect. *Biochimica et Biophysica Acta*, 1364: 271-286.

93. Ruitenbeek, W., Wendel, U., Trijbels, F., Sengers, R. 1996. Mitochondrial energy metabolism. *In* Blau, N., Duran, M., Blaskovics, M.E., *ed.* Physician's Guide to the Laborotory Diagnosis of Metabolic diseases. *Chapman and Hall Medical.* 391: 404-405.

94. Sanger, F., Nicklen, S., Coulson, A.R. 1977. DNA sequencing with chain-terminating inhibitors. *Proceedings of the National Academy of Sciences of the United States.* 74(12): 5463-5467.

95. Santon, A., Albergoni, V., Sturniolo, G.C. and Irato, P. 2004. Evaluation of MT expression and detection of apoptotic cells in LEC rat kidneys. *Biochemica et Biophysica Acta.* 1688: 223-231.

96. Sato, M. and Kondoh, M. 2002. Recent studies on metallothionein: protection against toxity of heavy metals and oxygen free radicals. *J. Exp. Med.* 196: 9-22.

97. Sato, M., and Bremmer, I. 1993. Oxygen free radicals and metallothionein. *Free Radical Biology and Medicine.* 14: 325-337.

98. Scheffler, I.E. 2001. A century of mitochondrial research: achievements and perspectives. *Mitochondrion.* 1: 3-31.

99. Smeitink, J., van den Heuvel, L. 1999. Human mitochondrial complex I in health and disease. *Am. J. Hum. Genet.* 64: 1505-1510.

100. Smeitink, J., van den Heuvel, L., and DiMauro, S. 2001. The genetics and pathology of oxidative phosphorylation. *Nat. Rev. Genet.* 2: 342-352.

101. Smeitink, J.A.M., Van Den Heuvel, L.W.P.J., Koopman, W.J.H., Nijtmans, L.G.J. 2004. Cell biological consequences of mitochondrial NADH:Ubiquinone oxidoreductase deficiency. *Current Neurovascular Research.* 1(1): 1-12.

102. STATISTICA, StatSoft, Inc. 2004. Version 7.1. www.statsoft.com.

103. Stennard, F.A., Holloway, A.F., Hamilton, J., and West, A.K., 1994. Characterization of six additional human metallothionein genes. *Biochemica et Biophysica Acta.* 1218: 357-365.

104. Steyn, A.G.W., Smit, C.F, and Du Toit, S.H.C. 1998. *Moderne Statistiek vir die Praktyk.* J.L. van Schaik: Pretoria.

105. Suzuki, K.T., Rui, M., Ueda, J., and Ozawa, T. 1999. Metallothionein IV, in: C.D. Klaassen (Ed.), Role of Metallothionein in the Cytotoxity of Copper in the Liver of LEC rats. *Birkhäuser Verlag, Basel.* 397-402.

106. Taanman, J.W. 1999. The mitochondrial genome: structure, transcription, translation and replication. *Biochimica et Biophysica Acta*, 1410: 103-123.

107. Thein, S.L., and Wallace, R.B. 1986. The use of synthetic oligonucleotides as specific hybridization probes in the diagnosis of genetic disorders. *Human genetic diseases: a practical approach. Davies, K.E., ed.* Oxford: IRL Press, 33-50.

108. Thomas, J.P., Bachowski, G.J., and Girotti, A.W. 1986. Inhibition of cell membrane lipid peroxidation by cadmium- and zinc-metallothioneins. *Biochemica et Biophysica Acta.* 884: 448-461.

109. Triepels, R.H., Van den Heuvel, L.P., Trijbels, J.J. and Smeitink, J.A. 2001. Respiratory chain complex I deficiency. *American Journal of Medical Genetics.* 106: 37-45.

110. Uchida, Y., Takio, K., Titani, K., Ihara, Y., and Tomonaga, M. 1991. The growth inhibitory factor that is deficient in the Alzheimer's disease brain is a 68 amino acid metallothionein-like protein. *Neuron.* 7: 337-347.

111. Udom, A.O., and Brady, F.O., (1980). Reactivation *in vitro* of Zinc-Requiring Apo-Enzymes by Rat Liver Zinc-Thionein. *Biochemical Journal.* 187: 329-335.

112. Vallee, B.L. 1995. The function of metallothionein. *Neurochem. Int.* 27: 23-33.

113. van der Westhuizen, FH., van den Heuvel, L.P., Smeets, R., Veltman, J.A., Pfundt, R., Geurts van Kessel, A., Ursing, B., and Smeitink, J. 2003. Human mitochondrial complex I deficiency: investigating transcriptional responses by microarry. *Neuropediatrics.* 34: 14-22.

114. Vandescompele, J., De Preter, K., Pattyn, F., Poppe, B., van Roy, N., De Paepe, A., and Spelman, F. 2002. Accurate normalization of real-time

quantitative RT-PCR data by geometric averaging of multiple internal control genes. *Genome Biology.* 3: 34.1-34.11.

115. Vašák, M., Wörgotter, E., Wagener, G., Kägi, J.H.R. and Wüthrich, K. 1987. Metal co-ordination in rat liver metallothionein-2 prepared with or without reconstitution of the metal clusters, and comparison with rabbit liver metallothionein-2. *J. Mol. Biol.* 196(3): 711-719.

116. Voet, D. and Voet, J.G. 1995. *Biochemistry. 2nd Edition.* New York : Wiley. 6p.

117. von Kleist-Retzow, J., Vial, E., Chantiel-Groussard, K., Rötg, A., Munnich, A., Rustin, P., Taanman, J. 1999. Biochemical, genetic and immunoblot analyses of 17 patients with an isolated cytochrome *c* oxidase deficiency. *Biochimica et Biophysica Acta.* 1455: 35-44.

118. Wakeyama, H., Takeshige, K., Takayanagi, R., and Minakami, S. 1982. Superoxide- forming NADPH oxidase preparation of pig polymorphnuclear leukocytes. *Biochemical Journal,* 205 (3): 593-601.

119. Walker, J.E., Arizmendi, J.M., Dupuis, A. 1992. Sequences of 20 subunits of NADH:ubiquinone oxidoreductase from bovine heart mitochondria. Application of a novel strategy for sequencing proteins using the polymerase chain reaction. *J. Mol. Biol.* 226: 1051-1072.

120. Wallace, D.C., 1999. Mitochondrial disease in man and mouse. *Science.* 283:1482-1488

121. Wilson, K., and Walker, J. 2000. *Practical Biochemistry.* Principles and techniques, 5th edition.

122. Woo, E.S., Monks, A., Watkins., S.C., Wang, A.S. and Lazo, L.S. 1997. Diversity of metallothionein content and subcellular localization in the National Cancer Institute tumor panel. *Cancer Chemother. Pharmacol.* 41: 61-68.

123. Yang, Y., Maret, W. and Vallee, B.L. 2001. Differential fluorescence labeling of cysteinyl clusters uncovers high tissue levels of thionein. *Proceedings of the National Academy of Sciences of the United States of America.* 98: 5556-5559.

124. Ye, B., Maret, B., and Vallee, L. 2001. Zinc metallothionein import into liver mitochondria modulates respiration. *Proceedings of the National Academy of Sciences of the United States of America.* 98: 2317-2322.

125. Zhou, Z., Ding, H., Qin, F., Lui, L., and Cheng, S. 2003. Effect of $Zn_7$-metallothionein on oxidative stress in liver of rats with severe thermal injury. *Acta Pharmacol Sin.* 24: 764-770.

# Appendix A

## Photographic representations of agarose gels

In section 4.2 the gel representations was set at a contrast of 77% and a brightness of 77% to indicate whether smearing of secondary annealing was visible on the photo. In this section of the appendix the same representations are illustrated, with no adjustments made. Text indicated in bold type represents the optimised conditions subsequently used in this study.

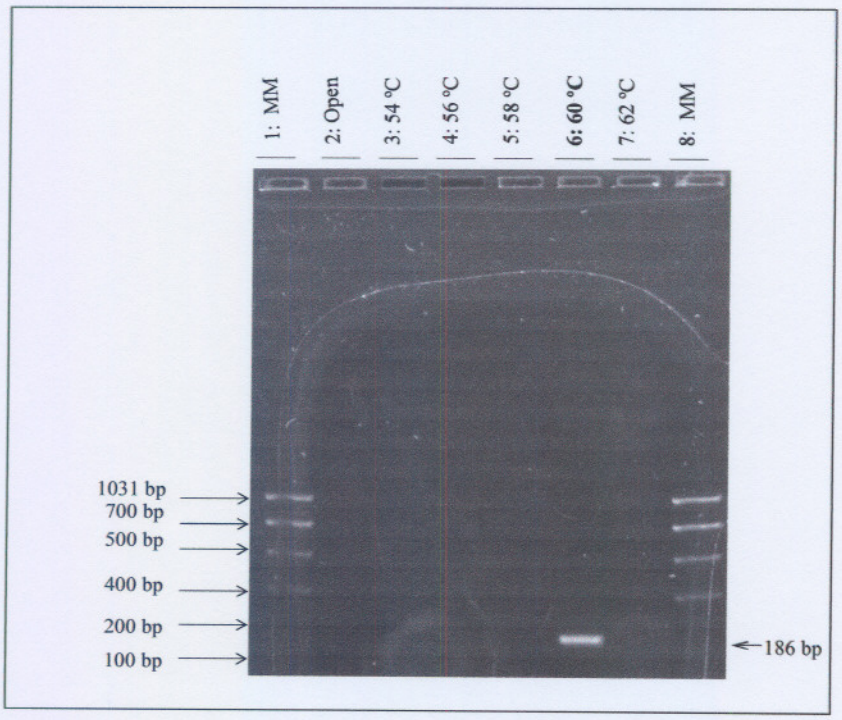


***Figure A.1. Optimisation of $T_a$ for MT-1 PCR.*** *This figure shows a photographic representation of a 1% agarose gel with EtBr staining, where 10 µl of five PCR reactions for MT-1 at different $T_a$ were loaded. The reactions were loaded as indicated above. The fragment sizes (bp) are indicated with arrows.*

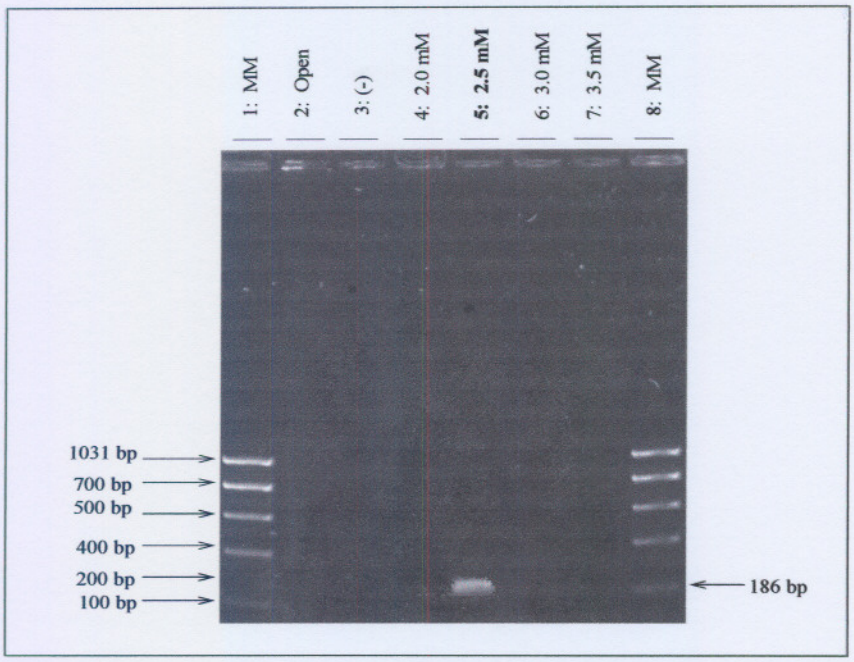


***Figure A.2. Optimisation of $MgCl_2$ concentration for MT-1 PCR.*** *This figure shows a photographic representation of a 1% agarose gel with EtBr staining, where 10 µl of five PCR reactions for MT-1 at different $MgCl_2$ concentrations were loaded. The reactions were loaded as indicated above. The fragment sizes (bp) are indicated with arrows.*

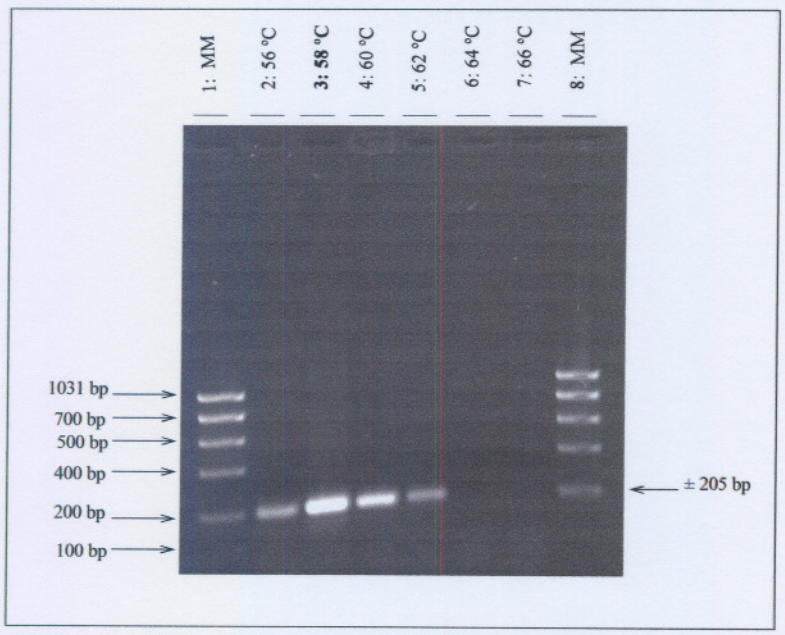


***Figure A.3. Optimisation of $T_a$ for MT-2 PCR.*** *This figure shows a photographic representation of a 1% agarose gel with EtBr staining, where 10 µl of six PCR reactions for MT-2 at different $T_a$ were loaded. The reactions were loaded as indicated above. The fragment sizes (bp) are indicated with arrows.*

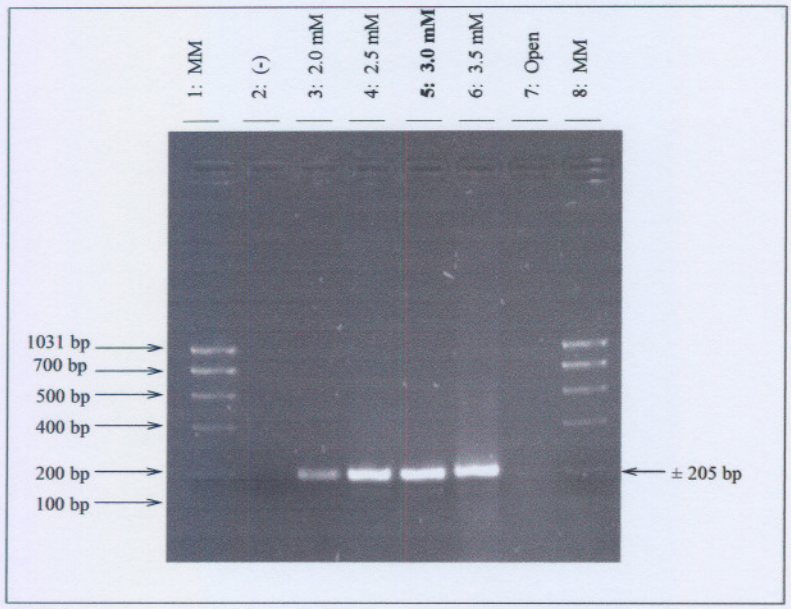


***Figure A.4. Optimisation of $MgCl_2$ concentration for MT-2 PCR.*** *This figure shows a photographic representation of a 1% agarose gel with EtBr staining, where 10 µl of five PCR reactions for MT-2 at different $MgCl_2$ concentrations were loaded. The reactions were loaded as indicated above. The fragment sizes (bp) are indicated with arrows.*

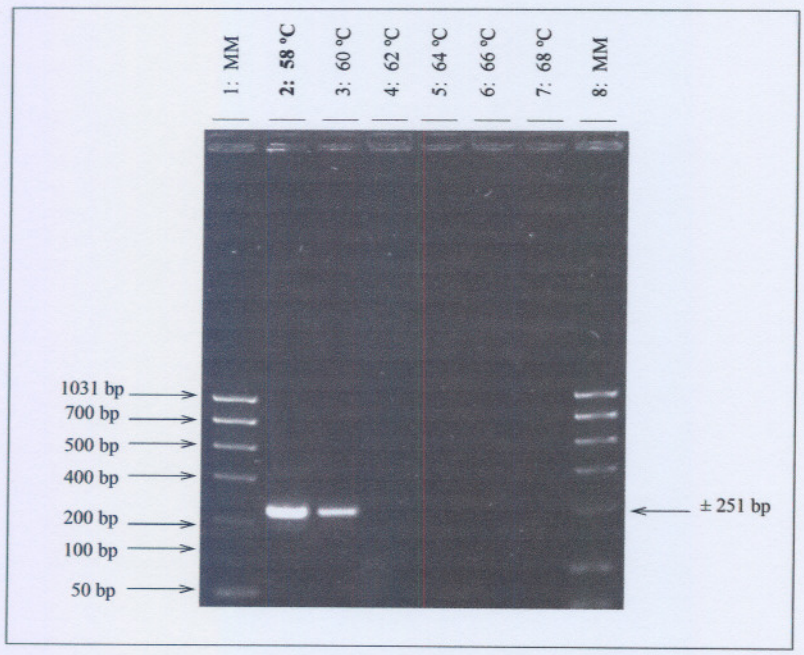


***Figure A.5. Optimisation of $T_a$ for MT-3 PCR.*** *This figure shows a photographic representation of a 1% agarose gel with EtBr staining, where 10 µl of six PCR reactions for MT-3 at different $T_a$ were loaded. The reactions were loaded as indicated above. The fragment sizes (bp) are indicated with arrows.*

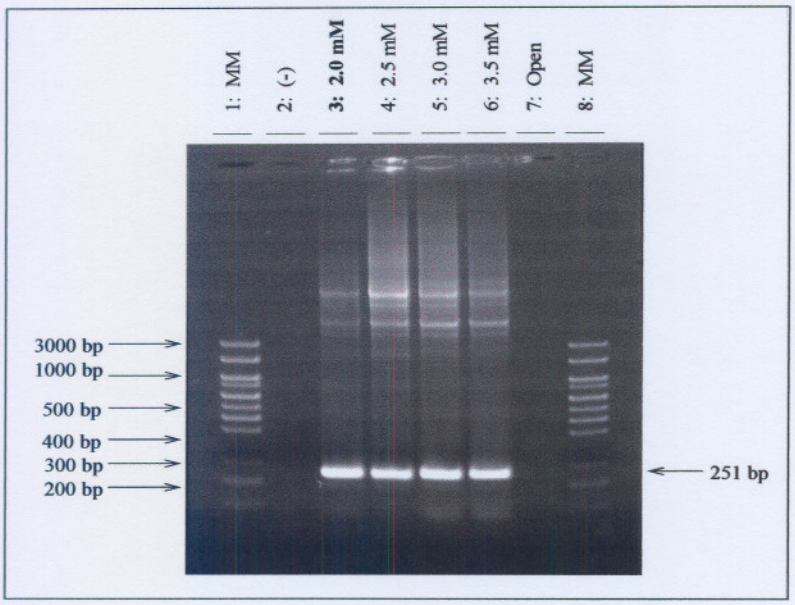


***Figure A.6. Optimisation of $MgCl_2$ concentration of MT-3 PCR.*** *This figure shows a photographic representation of a 1% agarose gel with EtBr staining, where 10 µl of five PCR reactions for MT-3 at different $MgCl_2$ concentrations were loaded. The reactions were loaded as indicated above. The fragment sizes (bp) are indicated with arrows.*

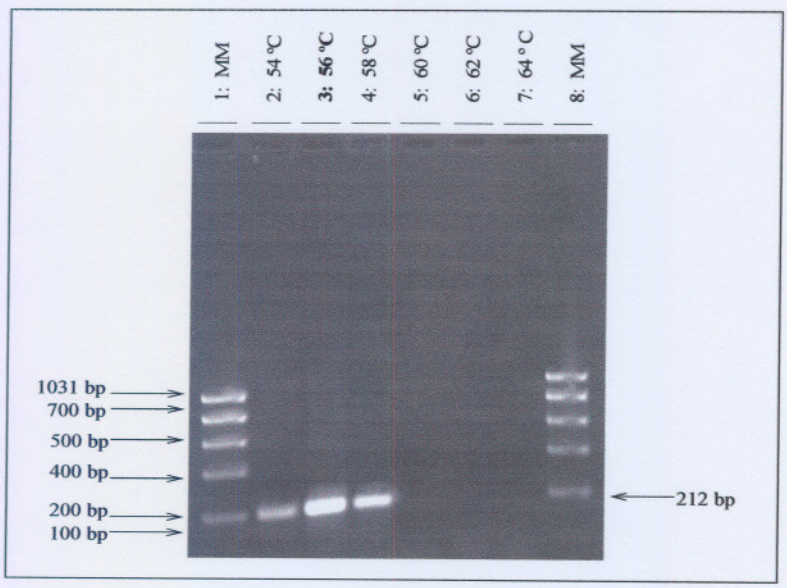


***Figure A.7. Optimisation of $T_a$ for β2MG PCR.*** *This figure shows a photographic representation of a 1% agarose gel with EtBr staining, where 10 µl of six PCR reactions for β2MG at different $T_a$ were loaded. The reactions were loaded as indicated above. The fragment sizes (bp) are indicated with arrows.*

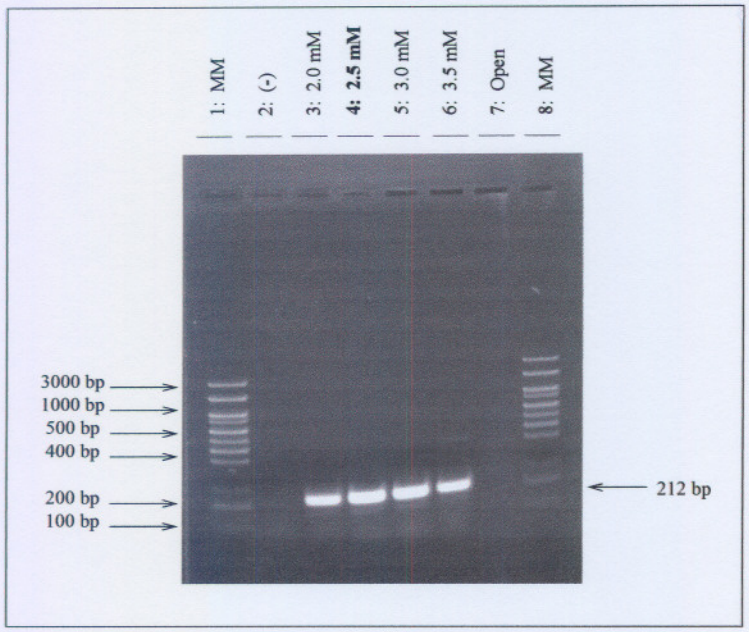


***Figure A.8. Optimisation of $MgCl_2$ concentration for β-2MG PCR.*** *This figure shows a photographic representation of a 1% agarose gel with EtBr staining, where 10 µl of five PCR reactions for β-2MG at different $MgCl_2$ concentrations were loaded. The reactions were loaded as indicated above. The fragment sizes (bp) are indicated with arrows.*

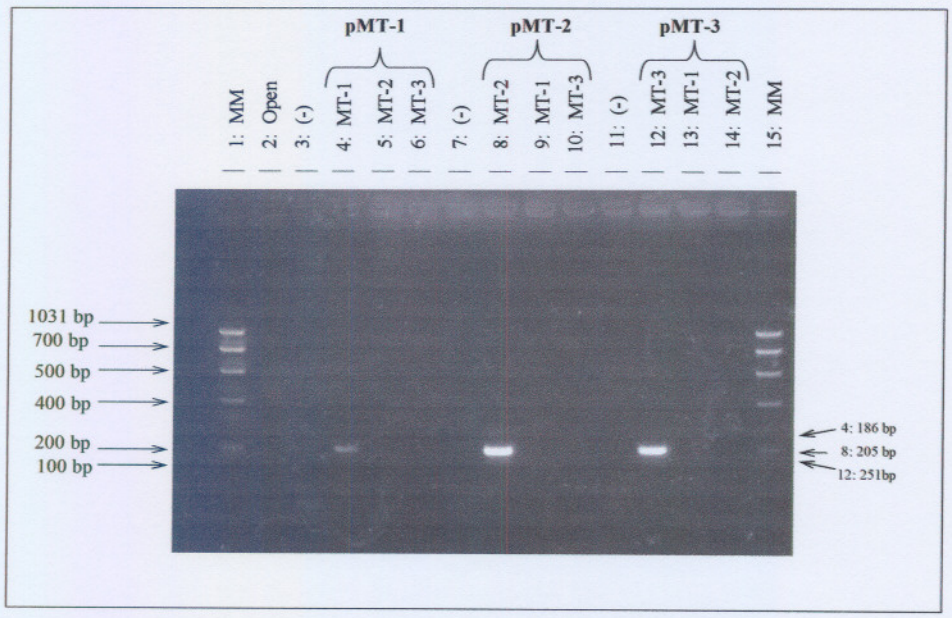


***Figure A.9. MT isoform specificity for pMT-1, pMT-2 and pMT-3.*** *This figure shows a photographic representation of a 1% agarose midi gel with EtBr staining, where 15 µl of twelve PCR reactions for pMT-1 to pMT-3 at optimal PCR reactions were loaded. The reactions were loaded as indicated above. The fragment sizes (bp) are indicated with arrows.*

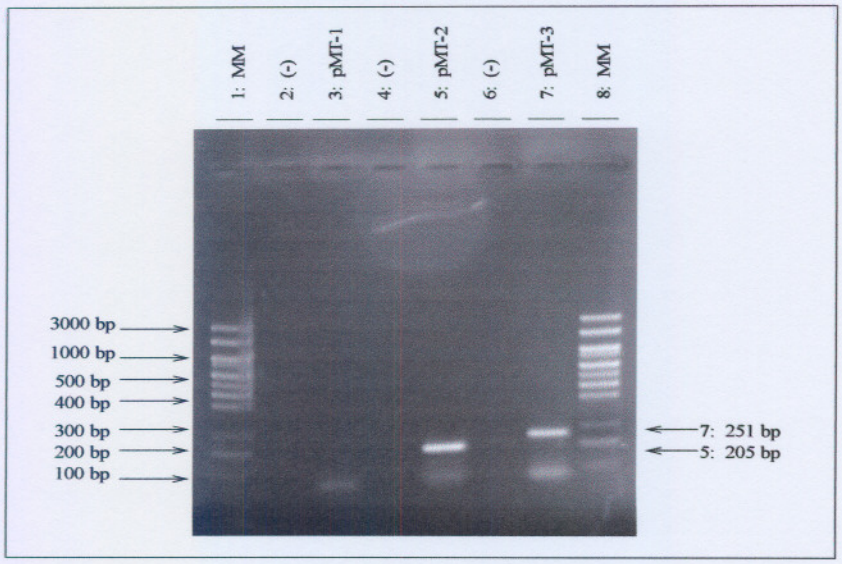


***Figure A.10. MT isoform specificity for pMT-1, pMT-2 and pMT-3.*** *This figure shows a photographic representation of a 1% agarose mini gel with EtBr staining, where 10 µl of six PCR reaction conditions for pMT-1 to pMT-3 at optimal PCR reactions were loaded. The reactions were loaded as indicated above. The fragment sizes (bp) are indicated with arrows.*

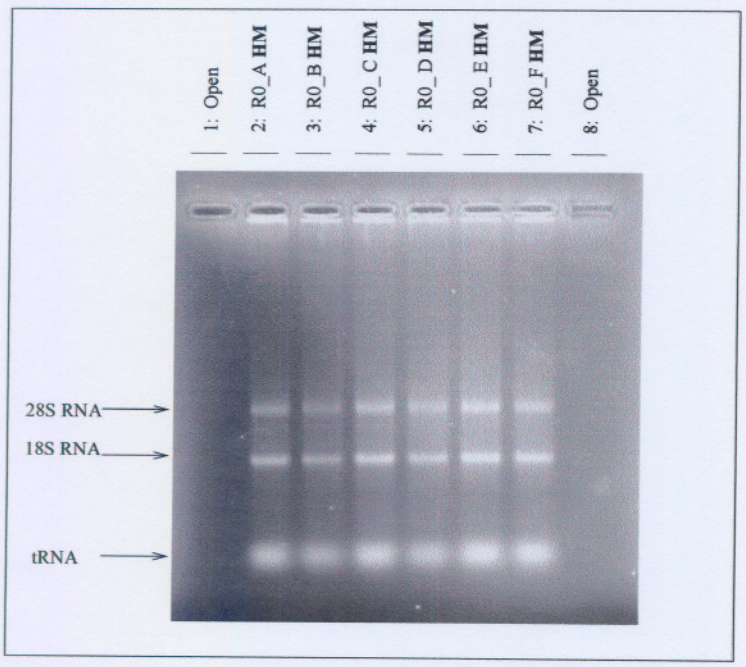


***Figure A.11. Integrity analysis of isolated RNA samples.*** *This figure shows a photographic representation of a 1% agarose gel with EtBr staining where 10 µl of 3 µg RNA from six rats obtained from heart muscle of the control group. The arrows indicate where the 28S, 18S and tRNA is situated.*

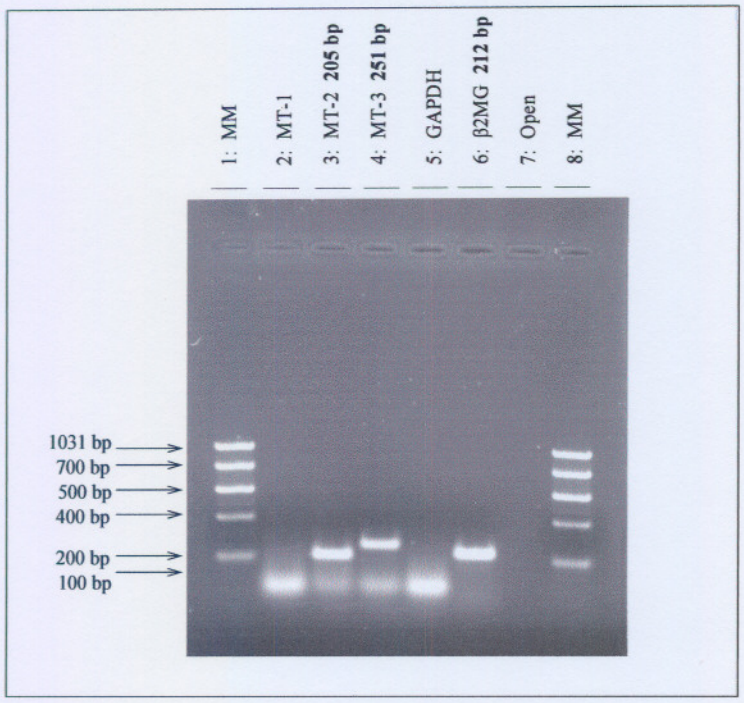


***Figure A.12. PCR amplification of cDNA prepared from the RNA sample R0_A Br.*** *This figure shows a photographic representation of a 1% agarose gel with EtBr staining, where 10 µl of five PCR reactions for MT-1 to MT-3 and the housekeeping genes GAPDH and β2MG at optimal PCR reactions were loaded. The reactions were loaded as indicated above. The fragment sizes (bp) are indicated with arrows.*

# Appendix B

## Real time PCR

Table B1 to B3 consist of the raw expression data generated from the real-time PCR analyses. The expression values indicated in these tables were normalised to the housekeeping gene expression in the same sample, which was calculated as described in Equation 3.5. The values are the averages of triplicate analyses.

**Table B.1. Real-time PCR expression data for MT-1**

| | | Metallothionein-1 | | | |
|---|---|---|---|---|---|
| Rat nr | Dose | Expression Brain | Expression Liver | Expression SM | Expression HM |
| 1 | 0 | 0.6 | 1.02 | N/D | 0.78 |
| 2 | 0 | 0.57 | 1.13 | N/D | 0.81 |
| 3 | 0 | 0.61 | 1.09 | N/D | 0.77 |
| 4 | 0 | 0.6 | 1.07 | N/D | 0.79 |
| 5 | 0 | 0.58 | 1.1 | N/D | 0.82 |
| 6 | 0 | 0.62 | 1.12 | N/D | 0.8 |
| **SD** | **0** | **0.018619** | **0.039707** | **N/D** | **0.018708** |
| **Mean** | **0** | **0.59667** | **1.0883** | **N/D** | **0.795** |
| 1 | 3 | 0.56 | 1.46 | N/D | 0.89 |
| 2 | 3 | 0.65 | 1.47 | N/D | 0.95 |
| 3 | 3 | 0.87 | 1.65 | N/D | 0.97 |
| 4 | 3 | 0.62 | 1.55 | N/D | 1.01 |
| 5 | 3 | 0.6 | 1.67 | N/D | 0.98 |
| **SD** | **3** | **0.121861** | **0.09798** | **N/D** | **0.044721** |
| **Mean** | **3** | **0.66** | **1.56** | **N/D** | **0.96** |
| 1 | 9 | 0.65 | 1.71 | N/D | 0.98 |
| 2 | 9 | 0.73 | 1.66 | N/D | 1 |
| 3 | 9 | 0.59 | 1.68 | N/D | 0.95 |
| 4 | 9 | 0.77 | 1.66 | N/D | 0.89 |
| 5 | 9 | 0.6 | 1.59 | N/D | 1.05 |
| 6 | 9 | 0.68 | 1.72 | N/D | 0.95 |
| **SD** | **9** | **0.071274** | **0.046476** | **N/D** | **0.054037** |
| **Mean** | **9** | **0.67** | **1.67** | **N/D** | **0.97** |
| 1 | 15 | 1.01 | 1.69 | N/D | 0.95 |
| 2 | 15 | 0.99 | 1.8 | N/D | 0.93 |
| 3 | 15 | 0.98 | 1.78 | N/D | 1.07 |
| 4 | 15 | 1.07 | 1.77 | N/D | 0.86 |
| 5 | 15 | 0.99 | 1.76 | N/D | 1.03 |
| 6 | 15 | 1.02 | 1.82 | N/D | 0.98 |
| **SD** | **15** | **0.032863** | **0.044721** | **N/D** | **0.074565** |
| **Mean** | **15** | **1.01** | **1.77** | **N/D** | **0.97** |

*SM = skeletal muscle, HM = heart muscle, SD = standard deviation, N/D = not detected.*

**Table B.2. Real-time PCR expression data for MT-2**

| | | Metallothionein-2 | | | |
|---|---|---|---|---|---|
| Rat nr | Dose | Expression Brain | Expression Liver | Expression SM | Expression HM |
| 1 | 0 | 1.1 | 2 | 0.77 | 0.88 |
| 2 | 0 | 1.2 | 2.04 | 0.81 | 0.84 |
| 3 | 0 | 1.25 | 2.2 | 0.88 | 0.87 |
| 4 | 0 | 1.19 | 2.24 | 0.84 | 0.79 |
| 5 | 0 | 1.17 | 2.26 | 0.85 | 0.89 |
| 6 | 0 | 1.28 | 2.24 | 0.85 | 0.86 |
| **SD** | **0** | **0.063061** | **0.113431** | **0.038297** | **0.036194** |
| **Mean** | **0** | **1.1983** | **2.1633** | **0.83333** | **0.855** |
| 1 | 3 | 2.43 | 2.97 | 1.35 | 0.92 |
| 2 | 3 | 1.78 | 3.04 | 1.33 | 0.93 |
| 3 | 3 | 2.33 | 3.01 | 1.31 | 0.98 |
| 4 | 3 | 2.22 | 3 | 1.34 | 1 |
| 5 | 3 | 2.49 | 2.98 | 1.37 | 1.07 |
| **SD** | **3** | **0.282046** | **0.027386** | **0.022361** | **0.060415** |
| **Mean** | **3** | **2.25** | **3** | **1.34** | **0.98** |
| 1 | 9 | 2.41 | 4.12 | 0.99 | 1.39 |
| 2 | 9 | 2.32 | 4.17 | 0.97 | 1.3 |
| 3 | 9 | 2.31 | 4.13 | 0.95 | 1.33 |
| 4 | 9 | 2.6 | 4.16 | 0.97 | 1.35 |
| 5 | 9 | 2.25 | 4.15 | 0.96 | 1.34 |
| 6 | 9 | 2.33 | 4.11 | 0.98 | 1.33 |
| **SD** | **9** | **0.123774** | **0.023664** | **0.014142** | **0.029665** |
| **Mean** | **9** | **2.37** | **4.14** | **0.97** | **1.34** |
| 1 | 15 | 2.51 | 4.97 | 0.99 | 1.91 |
| 2 | 15 | 2.44 | 4.92 | 0.98 | 1.89 |
| 3 | 15 | 2.45 | 4.93 | 0.97 | 1.93 |
| 4 | 15 | 2.39 | 4.95 | 0.98 | 1.94 |
| 5 | 15 | 2.47 | 4.96 | 0.96 | 1.91 |
| 6 | 15 | 2.38 | 4.97 | 1 | 1.94 |
| **SD** | **15** | **0.04899** | **0.020976** | **0.014142** | **0.02** |
| **Mean** | **15** | **2.44** | **4.95** | **0.98** | **1.92** |

*SM = skeletal muscle, HM = heart muscle, SD = standard deviation, N/D = not detected.*

**Table B.3. Real-time PCR expression data for MT-3**

| | | Metallothionein-3 | | | |
|---|---|---|---|---|---|
| Rat nr | Dose | Expression Brain | Expression Liver | Expression SM | Expression HM |
| 1 | 0 | 2.01 | 1.1 | N/D | N/D |
| 2 | 0 | 1.97 | 1.05 | N/D | N/D |
| 3 | 0 | 1.94 | 1.15 | N/D | N/D |
| 4 | 0 | 1.96 | 1.12 | N/D | N/D |
| 5 | 0 | 2.05 | 1.14 | N/D | N/D |
| 6 | 0 | 2.03 | 1.17 | N/D | N/D |
| **SD** | **0** | **0.043205** | **0.042622** | **N/D** | **N/D** |
| **Mean** | **0** | **1.9933** | **1.1217** | **N/D** | **N/D** |
| 1 | 3 | 2.33 | 1.31 | N/D | N/D |
| 2 | 3 | 2.32 | 1.33 | N/D | N/D |
| 3 | 3 | 2.39 | 1.32 | N/D | N/D |
| 4 | 3 | 2.36 | 1.35 | N/D | N/D |
| 5 | 3 | 2.35 | 1.29 | N/D | N/D |
| **SD** | **3** | **0.027386** | **0.022361** | **N/D** | **N/D** |
| **Mean** | **3** | **2.35** | **1.32** | **N/D** | **N/D** |
| 1 | 9 | 2.6 | 1.51 | N/D | N/D |
| 2 | 9 | 2.57 | 1.47 | N/D | N/D |
| 3 | 9 | 2.59 | 1.5 | N/D | N/D |
| 4 | 9 | 2.58 | 1.51 | N/D | N/D |
| 5 | 9 | 2.59 | 1.48 | N/D | N/D |
| 6 | 9 | 2.61 | 1.53 | N/D | N/D |
| **SD** | **9** | **0.014142** | **0.021909** | **N/D** | **N/D** |
| **Mean** | **9** | **2.59** | **1.5** | **N/D** | **N/D** |
| 1 | 15 | 3.63 | 1.57 | N/D | N/D |
| 2 | 15 | 3.62 | 1.58 | N/D | N/D |
| 3 | 15 | 3.62 | 1.62 | N/D | N/D |
| 4 | 15 | 3.65 | 1.59 | N/D | N/D |
| 5 | 15 | 3.59 | 1.61 | N/D | N/D |
| 6 | 15 | 3.61 | 1.63 | N/D | N/D |
| **SD** | **15** | **0.02** | **0.023664** | **N/D** | **N/D** |
| **Mean** | **15** | **3.62** | **1.6** | **N/D** | **N/D** |

*SM = skeletal muscle, HM = heart muscle, SD = standard deviation, N/D = not detected.*

# Appendix C

## Complex I activity

Table C.1 summarises results of complex I activity in rotenone-treated rat tissues, performed by Alessandrini (2006). Complex I activities (nmol.min$^{-1}$) are expressed in terms of units citrate synthase.

**Table C.1. Complex I activity measurements in brain, heart muscle, liver, and skeletal muscle.**

| Dose group | Tissue | | | | | | | |
|---|---|---|---|---|---|---|---|---|
| | Brain | | Heart muscle | | Liver | | Skeletal muscle | |
| | Mean | SD | Mean | SD | Mean | SD | Mean | SD |
| NX | 2.1009 | 0.4314 | 6.6736 | 1.9926 | 20.9906 | 11.4025 | 4.9524 | 1.9617 |
| VX | 1.9856 | 0.4190 | 6.3285 | 2.7003 | 9.0458 | 1.8103 | 3.4686 | 1.1131 |
| R3X | 1.2246 | 0.1780 | 3.6550 | 0.8723 | 16.6375 | 7.7500 | 3.4366 | 1.3122 |
| R6X | 1.3036 | 0.2555 | 5.0425 | 2.3630 | 8.0874 | 6.1928 | 2.5917 | 2.1097 |
| R9X | 1.5957 | 0.5455 | 2.4783 | 0.7439 | 7.1150 | 2.0022 | 2.6095 | 1.4254 |
| R12X | 1.1951 | 0.4048 | 1.8018 | 0.3488 | 12.0068 | 6.0481 | 2.6241 | 1.3076 |
| R15X | 1.2416 | 0.4733 | 1.2182 | 0.6901 | 6.1108 | 3.7289 | 2.9537 | 1.3238 |

*All rat dose groups were dosed every morning for a period of 14 days, after which they were sacrificed via decapitation on day 15. The treatments included: NX = nothing, VX = vehicle, SD = standard deviation, R3X = 3 mg.kg$^{-1}$, R6X = 6 mg.kg$^{-1}$, R9X = 9 mg.kg$^{-1}$, R12X = 12 mg.kg$^{-1}$, R15X = 15 mg.kg$^{-1}$. Brain, heart muscle and liver activities are expressed in nmol.min$^{-1}$.UCS, while skeletal muscle is in μmol.min$^{-1}$.UCS.*